

University of Nevada, Reno

**Theory of the ac Stark Effect on the Atomic Hyperfine
Structure and Applications to Microwave Atomic Clocks**

A dissertation submitted in partial fulfillment of the
requirements for the degree of Doctor of Philosophy in
Physics

by

Kyle Beloy

Dr. Andrei Derevianko/Dissertation Advisor

August, 2009

Abstract

Microwave atomic clocks are based on the intrinsic hyperfine energy interval in the ground state of an atom. In the presence of an oscillating electric field, the atomic system—namely, the hyperfine interval—becomes perturbed (the ac Stark effect). For the atomic sample in a clock, such a perturbation leads to an undesired shift in the clock frequency and, ultimately, to an inaccuracy in the measurement of time. Here a consistent perturbation formalism is presented for the theory of the ac Stark effect on the atomic hyperfine structure. By further implementing relativistic atomic many-body theory, this formalism is then utilized for two specific microwave atomic clock applications: a high-accuracy calculation of the blackbody radiation shift in the ^{133}Cs primary frequency standard and a proposal for microwave clocks based on atoms in an engineered optical lattice.

Preface

Much of the content of this dissertation was published in the following scientific journal articles with a focus on atomic clocks:

- Micromagic clock: microwave clock based on atoms in an engineered optical lattice. K. Beloy, A. Derevianko, V. A. Dzuba, and V. V. Flambaum, *Phys. Rev. Lett.* 102, 120801 (2009)
- ac Stark shift of the Cs microwave atomic clock transitions. P. Rosenbusch, S. Ghezali, V. A. Dzuba, V. V. Flambaum, K. Beloy, and A. Derevianko, *Phys. Rev. A* 79, 013404 (2009)
- High-accuracy calculation of the blackbody radiation shift in the ^{133}Cs primary frequency standard. K. Beloy, U. I. Safronova, and A. Derevianko, *Phys. Rev. Lett.* 97, 040801 (2006)

These journal articles reflect only a fraction of the research undertaken during my career as a graduate student. For a more complete overview of the various research I have partaken in during this time, the reader is referred to the following supplemental list of scientific journal articles:

- Precision determination of electroweak coupling from atomic parity violation and implications for particle physics. S. G. Porsev, K. Beloy, and A. Derevianko, *Phys. Rev. Lett.* 102, 181601 (2009)
- Calculation of Stark-induced absorption on the $6s6p\ ^3P_1 - 6s^2\ ^1S_0$ transition in Hg. K. Beloy, V. A. Dzuba, and A. Derevianko, *Phys. Rev. A* 79, 042503 (2009)

- Second-order effects on the hyperfine structure of P states of alkali-metal atoms. K. Beloy and A. Derevianko, *Phys. Rev. A* 78, 032519 (2008)
- Convergence of all-order many-body methods: coupled-cluster study for Li. A. Derevianko, S. G. Porsev, and K. Beloy, *Phys. Rev. A* 78, 010503(R) (2008)
- Nuclear magnetic octupole moment and the hyperfine structure of the $5D$ states of the Ba^+ ion. K. Beloy, A. Derevianko, V. A. Dzuba, G. T. Howell, B. B. Blinov, and E. N. Fortson, *Phys. Rev. A* 77, 052503 (2008)
- Application of the dual-kinetic-balance sets in the relativistic many-body problem of atomic structure. K. Beloy and A. Derevianko, *Comp. Phys. Comm.* 179 310 (2008)
- Hyperfine structure of the metastable 3P_2 state of alkaline-earth atoms as an accurate probe of nuclear magnetic octupole moments. K. Beloy, A. Derevianko, and W. R. Johnson, *Phys. Rev. A* 77, 012512 (2008)

Table of Contents

Abstract	i
Preface	ii
List of Tables	vii
List of Figures	ix
1 Introduction	1
1.1 Applications of Atomic Clocks	1
1.2 A Brief Review of Atomic Timekeeping	2
1.3 Atomic Fountain Clocks	5
1.4 Optical Lattice Clocks	7
1.5 Dissertation Structure	9
2 The Hyperfine Structure	11
2.1 Eigenstates of the Electronic Hamiltonian	11
2.2 The Hyperfine Interaction	13
3 The ac Stark Effect	18
3.1 The Interaction with an Electromagnetic Plane Wave	18

3.2	The Total Perturbation and the Hyperfine Clock Shift	21
3.3	The Second-Order ac Stark Shift	24
3.4	The Third-Order ac Stark Shift	31
3.5	The ac Stark Shift Summarized	36
3.6	The 1D Optical Lattice Trap	38
4	High-Accuracy Calculation of the Blackbody Radiation Shift in the	
	¹³³Cs Primary Frequency Standard	42
4.1	Introduction	42
4.2	Problem Set-Up	43
4.3	Results and Discussion	49
5	Micromagic Clock: Microwave Clock Based on Atoms in an Engi-	
	neered Optical Lattice	56
5.1	Introduction	56
5.2	Problem Set-Up	57
5.3	Results and Discussion	62
6	Conclusion	70
	Bibliography	72
A	Atomic Units	79
A.1	Definitions	79
A.2	Atomic Unit Conversion Table	81
B	Angular Momentum and Spinor Spherical Harmonics	82
B.1	Brief Review of Angular Momentum Theory	82
B.2	Orbital and Spin-1/2 Angular Momentum	86

B.3	Spinor Spherical Harmonics and C -Tensor Matrix Elements	87
C	Irreducible Spherical Tensor Operators	92
C.1	Definitions	92
C.2	Coupling Spherical Tensors	93
C.3	Wigner-Eckart Theorem	94
C.4	Additional Notational Conventions and Additional Expressions Specific to Vectors	96
D	Floquet Perturbation Theory	99
D.1	Foundations and the Floquet Perturbation Expansion	99
D.2	A Perturbation with Static and Harmonic Time-Dependent Parts . .	103
D.3	Additional Comments: Degeneracy, Resonance, and Applicability . .	107
E	Atomic Structure Theory	109
E.1	Slater Determinant Wavefunctions	109
E.2	Variations of the Slater Determinant	111
E.3	Matrix Elements Between Slater Determinant Wavefunctions	112
E.4	The Hartree-Fock Method	115
E.5	The Dirac Equation	117
E.6	The Dirac-Hartree-Fock Approximation	121
E.7	Non-Locality and Asymptotic Behavior of the DHF Potential	125
E.8	Single-Valence Systems and the V^{N-1} DHF Potential	128
E.9	Beyond the V^{N-1} DHF Approximation: Correlation Corrections . . .	132
E.10	Matrix Elements of the Electric Dipole and Hyperfine Interaction Operators	135
F	Finite Basis Sets Composed of B-Splines	140

F.1	Introducing B-Splines	140
F.2	Finite Basis Set Solutions to the Radial Dirac Equation	144
F.3	B-spline Basis Sets for the Radial Dirac Wavefunctions	148
F.4	Quasi-Completeness of the B-spline Basis Sets	151
G	The Zeeman Effect and the Quantizing Magnetic Field	155
G.1	The Zeeman Effect	155
G.2	The Quantizing Magnetic Field	159

List of Tables

2.1	Nuclear spin and magnetic dipole moments for isotopes ^{133}Cs , ^{27}Al , and $^{69,71}\text{Ga}$	17
4.1	Values of the scalar Stark coefficient k_s for ^{133}Cs reported by various groups	54
5.1	Comparison of the theoretical and experimental ac frequency shifts for the clock transition in Cs	62
A.1	Atomic unit conversion table	81
B.1	Conventional spectroscopic notation for the angular quantum number κ	88

List of Figures

2.1	Hyperfine structure of the ^{133}Cs ground state	16
3.1	Diagrammatical representation of an energy contribution of the type $\delta E^{(2,2)}$	22
3.2	Diagrammatical representation of $\delta E_n^{(0,2)}$	24
3.3	Representation of the electromagnetic plane wave geometrical parameters	30
3.4	Diagrammatical representations of the “top”, “center”, “bottom”, and “normalization” contributions to $\delta E_n^{(1,2)}$	33
3.5	Illustration of a 1D optical lattice trap	40
4.1	Values of the scalar Stark coefficient k_s for ^{133}Cs reported by various groups	55
5.1	Differential polarizability of the Cs clock transition as a function of laser frequency	63
5.2	Third-order polarizabilities and differential polarizability for the Al μMagic clock levels as a function of lattice laser frequency	67

Chapter 1

Introduction

1.1 Applications of Atomic Clocks

Atomic clocks provide the most precise measurements of time. The most accurate atomic clocks are capable of realizing the International System (SI) base unit for time, the second, to a fractional uncertainty on the order of 10^{-16} , making time the most accurately measured physical quantity [44]. For this reason, the definitions of three other SI base units—the meter, candela, and ampere—also depend on the second [81]. As an example, the meter is defined in terms of the length traveled by light in a vacuum during a given fraction of a second.

Along with their key role in precision metrology, atomic clocks also provide physicists with several opportunities to study the basic laws of the universe. These include, for example, tests of Einstein’s theory of general relativity [47, 26], studies of fundamental symmetries between matter and anti-matter [13], and searches for possible variations in the fundamental constants of nature [26, 24]. As a specific illustration, atomic clocks have been used to set a constraint on the variation of the fine structure constant of $\dot{\alpha}/\alpha < 1.3 \times 10^{-16} \text{ yr}^{-1}$ [26]. Future generations of atomic clocks

will undoubtedly open new avenues of scientific exploration and place more stringent bounds on existing results.

Aside from their applications in the sciences, atomic clocks have had a profound effect on society as well. Atomic clocks operating onboard satellites and in ground stations constitute an integral part of the U.S. Global Positioning System (GPS), providing accurate positioning, navigating, and timing services for various military and civilian needs. GPS is routinely used to synchronize financial and communication (cellular telephone, internet, etc.) networks, monitor and diagnose irregularities in electrical power grids, and enhance emergency services [52]. Several atomic clocks operating around the world also contribute to the realization of Universal Coordinated Time (UTC) [4].

1.2 A Brief Review of Atomic Timekeeping

The 20th Century saw the resonators used for primary frequency standards progress from pendulums to quartz crystals to atoms [44]. Predating the first standards based on atoms, a working clock based on the 23.8 GHz inversion transition in ammonia molecules was developed in 1948 at the U.S. National Bureau of Standards (NBS) (NBS changed its name to the National Institute of Standards and Technology (NIST) in 1988). The ammonia clock reached an estimated fractional uncertainty of 2×10^{-8} [7]. Despite not surpassing the accuracy of the best quartz frequency standards of that time ($\sim 10^{-9}$) [73], the ammonia clock marked an important advancement in precision metrology and paved the way for further advancements using atoms. Shortly after the development of the ammonia clock, it became evident that atomic beam techniques provided more promise as the next generation of primary frequency standards. This ushered in the era of cesium atomic clocks, which have served as the U.S. national

primary frequency standard from 1959 to present day [44].

Prior to the 13th General Conference on Weights and Measures (CGPM) in 1967, the SI second was defined in terms of *ephemeris* time, specifically the fraction $1/31,556,925.9747$ of the tropical year 1900. Though this definition was closely connected to the historical meaning of the second, it was an impractical definition for precision metrology (the tropical year is an inconvenient quantity to measure accurately; furthermore, the explicit reference to the tropical year 1900 is necessary as the Earth’s orbital motion about the Sun is not precisely that of a stable resonator) [4]. By the end of the 1950’s, the hyperfine transition of cesium had been measured to high precision by atomic beam techniques, the accuracy being limited by the difficulty in measuring ephemeris time itself [50]. Motivated by this advancement in atomic beam measurements, along with the inherent stability of atoms as resonators, the 13th CGPM redefined the SI second with the statement [81]

The second is the duration of 9,192,631,770 periods of the radiation corresponding to the transition between the two hyperfine levels of the ground state of the cesium 133 atom.

With this new definition for the SI second, the cesium clocks were no longer subject to inaccuracy in determining ephemeris time, effectively making the realization of the second (that is, the “new second”) more accurate. In 1997, this definition was amended to include the clarifying sentence

This definition refers to a cesium atom at rest at a temperature of 0 K.

It is worth noting that the frequency corresponding to the hyperfine transition of cesium (9,192,631,770 Hz) lies in the microwave region of the electromagnetic spectrum.

From 1959 through 1998, seven cesium beam clocks had served as the U.S. national primary frequency standard at NBS/NIST; the last of these these beam clocks, NIST-

7, reached a fractional uncertainty of 5×10^{-15} before being retired. From 1998 to present day, NIST-F1, a cesium atomic fountain clock, has served as the U.S. national primary frequency standard. A general description of cesium atomic fountain clocks is presented in Section 1.3. Presently, NIST-F1 is estimated to have a fractional uncertainty of 4×10^{-16} , with other cesium fountain clocks operating throughout the world having similar or slightly worse uncertainties. NIST-F2, a cesium fountain clock currently being developed to succeed NIST-F1, employs a number of design improvements and is expected to reach an accuracy below the 10^{-16} level [44].

The advent of the femtosecond laser frequency comb as well as several advances in cooling and trapping of neutral atoms and ions in recent years has opened up the possibility to use optical ($\sim 10^{15}$ Hz) transitions rather than microwave transitions for frequency standards. Optical frequencies are ~ 5 orders of magnitude larger than microwave frequencies; this, in principle, indicates a potential for improvement in clock precision and stability of roughly the same order [19]. Theoretical and experimental efforts for next-generation optical frequency standards are primarily focused on two general set-ups: single ions in radio frequency (RF) Paul traps [20, 49, 70, 21, 57, 66, 65, 17] and neutral atoms confined in optical lattices [37, 79, 77, 6, 15, 45, 78, 80].

Single trapped ions can be laser-cooled to their lowest vibrational state, highly suppressing undesired Doppler effects. Furthermore, there is essentially a limitless bound on interrogation time for the ion confined in an RF Paul trap. The compactness relative to a fountain or beam also allows for much better control of environmental effects. Using a single ion avoids detrimentally strong ion-ion interactions; however, such a set-up inevitably suffers from a low signal-to-noise ratio. Despite this, single ion clocks based on Hg^+ and Al^+ have already been demonstrated with *systematic* fractional uncertainties below 10^{-16} [65]. Thus, just as the overall accuracy of the

cesium clocks were at one time limited by the inaccuracy in realizing the second as defined by ephemeris time, the overall accuracy of these ion clocks are currently limited by the inaccuracy in realizing the second as defined in terms of the cesium atom.

Clocks based on neutral atoms confined in optical lattices share the previously mentioned benefits of the ion clocks (i.e., suppression of Doppler effects, long interrogation times, and control of environment), but with the additional advantage that millions of atoms may be trapped and interrogated simultaneously, substantially improving the measurement statistics. The fundamental disadvantage of optical lattice clocks, however, is that the confining lattice lasers may cause significant shifts in the atomic structure, diminishing their accuracy. An optical lattice clock using ^{87}Sr has already been demonstrated with a systematic fractional uncertainty of 1.5×10^{-16} [45]; like the Hg^+ and Al^+ ion clocks, the overall accuracy of this clock is also limited by the inaccuracy in the direct measurement of the cesium standard. Optical lattice clocks will be considered in more detail in Section 1.4.

It is likely that one of these two described arrangements employing optical frequencies will serve as the next-generation of primary frequency standards, inevitably leading to another redefinition of the SI second. Whether this definition is to be based on ions or neutral atoms, of course, remains to be seen.

1.3 Atomic Fountain Clocks

In this section, a brief description of atomic fountain clocks is presented. Here specifications are given for the NIST-F1 cesium fountain clock following from Refs. [11, 33, 28, 59, 32, 44]. Other fountain clocks operate using the same basic principles as NIST-F1.

To begin the process, a sample of $\sim 10^8$ cesium atoms are laser cooled in an optical molasses. This incorporates six lasers slightly red-detuned from an atomic transition. The beams intersect at the atomic sample, with one pair of lasers in the vertical direction and two other pairs orthogonal in the horizontal plane. A frequency differential in the vertical lasers is used to impart momentum to the atoms. With a temperature below $1 \mu\text{K}$ and an upward velocity of $\sim 4 \text{ m/s}$, the lasers are turned off and the atomic cloud, being subject to gravity, begins a ballistic flight. From here the atomic cloud undergoes a state-selection process, ensuring all of the atoms are in the same hyperfine state. The atomic cloud then passes through a microwave cavity; the effect of this microwave cavity is to place the atoms in a coherent superposition of the two hyperfine states. The atomic cloud continues upward until it reaches its apogee and subsequently begins to fall downward. A portion of the atomic cloud passes once again through the microwave cavity in its descent (due to thermal expansion, only $\sim 10\%$ of the atoms pass through the microwave cavity a second time and subsequently remain to be considered). The two pulses of microwave radiation experienced by these atoms constitute a variant of Ramsey's separated oscillatory field method of interferometry [62]. For the final step, a measurement is performed to determine the relative population of atoms in the two hyperfine states. The entire process described here takes on the order of 1 s. Over the course of many cycles, the frequency in the microwave cavity is fine-tuned such that the excitation probability is maximized. A count of 9,192,631,770 oscillations corresponding to the (optimal) radiation in the microwave cavity, adjusted appropriately for a number of systematic corrections, may then be interpreted as the second.

Currently, the leading uncertainty in NIST-F1 is due to the thermal (i.e., black-body) radiation (BBR) from the clock's surroundings, which are regulated at a temperature of 320 K for operational purposes. This effect was first considered in 1982

[29], prior to the first operational fountain clocks, and prompted the eventual amendment to the definition of the SI second specifying a cesium atom at a temperature of 0 K (i.e., in the absence of BBR). The second largest uncertainty behind the BBR uncertainty arises due to (spin-exchange) collisions between atoms. These two effects, along with some shifts associated with the microwave power level, account for the majority of the uncertainty in NIST-F1. Prior to the latest uncertainty analysis report [28], the second order Zeeman shift also provided a significant contribution to the overall uncertainty. As discussed in Ref. [28], this has since been reduced substantially and is now small in comparison to the aforementioned uncertainties.

Design improvements for NIST-F2 include a cryogenically cooled chamber (at 77 K) and a multiple-launch process involving as many as ten separate atomic clouds per cycle. These two enhancements will largely suppress the blackbody radiation and collision associated uncertainties, respectively.

1.4 Optical Lattice Clocks

Optical lattice clocks are based on the principle that neutral atoms may be trapped by means of the ac Stark effect. The ac Stark effect is given a detailed presentation in Chapter 3; for this section, a brief qualitative discussion in the context of trapping will be sufficient.

An atom subject to an oscillating electric field experiences an ac Stark shift in its energy that is, to the lowest order, quadratic in the field amplitude. This energy shift may be positive or negative and depends on the particular atomic state being considered and the frequency of the oscillating electric field. An interesting scenario arises when considering an atom in a *standing wave* for which the wavelength is much larger than the characteristic size of the atom. In this case, the amplitude of the

oscillating field experienced by the atom depends on its particular location within the standing wave, vanishing at the nodes of the standing wave and being maximum at the antinodes. Consequently, the atom is attracted to either the nodes or anti-nodes of the standing wave, whichever location minimizes its energy via the ac Stark shift. In practice, this concept is demonstrated by trapping atoms in a standing wave formed by two laser beams of similar frequency and polarization directed at each other. This 1D example has intuitive extensions to 2D or 3D. The periodicity of intensity minima and maxima arising from such a laser configuration is suggested in the term “optical lattice.”

With atoms trapped in an optical lattice, a narrow transition frequency, such as the $^1S_0 \rightarrow ^3P_0$ transition in alkali metal atoms, may be probed by a separate laser. This narrow transition frequency may then serve as the reference frequency for an optical lattice clock. However, both atomic energy levels (e.g., 1S_0 and 3P_0 levels) are ac Stark shifted by the trapping lasers. Generally, the perturbation is not precisely identical for each level. The relative difference between Stark shifts corresponds to an overall shift in the transition frequency and ultimately leads to an inaccuracy in the clock. However, the ac Stark shift for each level may depend differently on the frequency (i.e., wavelength) of the lattice lasers; this opens up the possibility of finding a suitable wavelength for which the levels are indeed shifted identically, canceling the effect of the lattice lasers on the clock frequency. Such a wavelength is referred to as a “magic wavelength.”

With the leading ac Stark shift vanishing at the magic wavelength, other effects which might ultimately limit the accuracy of optical lattice clocks include heating from the lattice lasers, perturbations fourth order in the lattice field (hyperpolarizability), and—as with the fountain clocks—BBR, collisional, and second order Zeeman shifts. In regard to the latter effects, the optical lattice scheme has some notable advantages

compared to the fountain (or beam). Firstly, the localization of the atoms should allow for better control of the environment and, thus, the BBR and Zeeman effects. Secondly, the optical lattice clock can, in principle, be prepared in 3D with no more than a single-atom occupancy for any given lattice site [36]; such a set-up would essentially eliminate collisional shifts. These prospective advantages are largely yet to be realized.

Another possibly significant clock shift was recently identified by Taichenachev *et al.* [78]. This shift, due to magnetic dipole ($M1$) and electric quadrupole ($E2$) perturbations to the vibrational levels of the trapped atoms, was estimated (a rigorous calculation is yet to be done) to be fractionally as large as 10^{-16} for the ^{87}Sr optical lattice clock. Whether this clock shift may be suppressed by clever engineering of the optical lattice is still an open question.

1.5 Dissertation Structure

The remainder of this dissertation is as follows. Chapter 2 provides a discussion of the atomic hyperfine structure. The theory developed therein is pertinent to all following Chapters. In Chapter 3 the theory of the ac Stark effect is developed using Floquet perturbation theory. In this treatment, the hyperfine interaction is treated perturbatively and on equal footing as the interaction with the electric field. Explicit expressions are given for the two leading orders, being zeroth (second) order in the hyperfine interaction (electric field) and first (second) order in the hyperfine interaction (electric field), respectively. The connection to the trapping potential of the optical lattice follows. The expressions formulated in Chapter 3 set the foundation for the two chapters following. Chapters 4 and 5 present the results of original research undertaken throughout the preparation of this dissertation. In Chapter 4, a high-

accuracy calculation of the BBR shift in the cesium primary frequency standard is presented. Chapter 5 provides a proposal for lattice clocks based on the (microwave) hyperfine transition of aluminum and gallium atoms. The conclusions of this research have been previously presented in scientific journal articles, Refs. [10, 67, 9]. Final concluding remarks will then be given in Chapter 6. This dissertation also includes several appendices containing useful supplementary information.

Unless specified otherwise, atomic units will be used throughout the remainder of the dissertation. A description of atomic units, along with several useful conversions, is presented in Appendix A.

Chapter 2

The Hyperfine Structure

2.1 Eigenstates of the Electronic Hamiltonian

The original research presented in Chapters 4 and 5 focuses on atomic clocks which are based on microwave frequencies. In particular, this incorporates radiation tuned to the hyperfine energy splitting in the ground state of the atom. Thus it is appropriate to begin with a discussion of atomic hyperfine structure.

Consider the electronic Hamiltonian, H_{elec} , describing the interaction of the atomic electrons with each other as well as with the nuclear charge. The operator \mathbf{J} , representing the total angular momentum of the electrons, commutes with H_{elec} . Thus the eigenstates of H_{elec} can be taken as angular momentum eigenstates (see Appendix B) satisfying

$$H_{\text{elec}}|\gamma JM_J\rangle = E_{\gamma J}|\gamma JM_J\rangle,$$

where γ encapsulates all remaining electronic quantum numbers beyond the angular momentum quantum numbers J and M_J needed to specify the state. Note that the energy $E_{\gamma J}$ cannot depend on a particular M_J -state; consequently the level $E_{\gamma J}$ is

$(2J + 1)$ -fold degenerate.

The operator representing the spin angular momentum of a nucleus is \mathbf{I} and has associated angular momentum eigenstates $|IM_I\rangle$. A nucleus may be regarded as a composition of electric and magnetic multipole moments. With k representing the multipolarity ($k = 0, 1, 2, \dots$ corresponding to monopole, dipole, quadrupole, \dots), angular momentum considerations limit the allowed multipole moments to $k \leq 2I$. Furthermore, parity considerations limit allowed electric multipole moments to even k and magnetic multipole moments to odd k . As a specific example, the nucleus of the stable ^{69}Ga isotope has nuclear spin $I = 3/2$; thus it is allowed electric monopole (i.e., the nuclear charge), magnetic dipole, electric quadrupole, and magnetic octupole moments.

The electronic Hamiltonian, which describes interactions of the electrons with only the nuclear charge, commutes with the angular momentum operator \mathbf{I} . Thus, the proper eigenstates of H_{elec} for the entire atomic (nuclear + electronic) system are built from angular momentum eigenstates of both \mathbf{I} and \mathbf{J} and satisfy

$$H_{\text{elec}}|IM_I, \gamma JM_J\rangle = E_{\gamma J}|IM_I, \gamma JM_J\rangle.$$

As is often the case, when interested only in operators that act exclusively within the electronic subspace it becomes unnecessary (and burdensome) to explicitly specify the nuclear quantum numbers I and M_I . However, it is noticed here that with the additional consideration of the nuclear substates (as given by M_I), the level $E_{\gamma J}$ is realized to be $(2I + 1) \times (2J + 1)$ -fold degenerate.

As H_{elec} commutes individually with with \mathbf{I} and \mathbf{J} , it certainly commutes with the operator $\mathbf{F} = \mathbf{I} + \mathbf{J}$, representing the total angular momentum of the system. Thus the eigenstates of H_{elec} can alternatively be taken as angular momentum eigenstates

of \mathbf{F} . Such eigenstates are linear combinations of the states $|IM_I, \gamma JM_J\rangle$, and are given explicitly by

$$|\gamma I J F M_F\rangle = \sum_{M_I M_J} C_{IM_I J M_J}^{F M_F} |IM_I, \gamma JM_J\rangle, \quad (2.1)$$

where the $C_{IM_I J M_J}^{F M_F}$ represent the conventional Clebsch-Gordon coefficients [83] (in expressions to follow, the subscript on M_F will be dropped; it is included here for consistency). The allowed values of F follow from the triangular selection rule of the Clebsch-Gordon coefficients, namely $|I - J| \leq F \leq I + J$. The level $E_{\gamma J}$ does not depend on the quantum numbers F or M_F ; considering all possible combinations of F and M_F one would find that the level $E_{\gamma J}$ is, of course, still $(2I + 1) \times (2J + 1)$ -fold degenerate.

2.2 The Hyperfine Interaction

The total Hamiltonian describing the atomic system is the electronic Hamiltonian H_{elec} supplemented by the hyperfine interaction V_{hfi}

$$H = H_{\text{elec}} + V_{\text{hfi}},$$

where V_{hfi} describes the interaction of the atomic electrons with the higher electric and magnetic multipole moments of the nucleus (i.e., those with multipolarity $k > 0$).

The hyperfine interaction may be written in the form¹ [71]

$$V_{\text{hfi}} = \sum_{k=1} T_k^{(\text{nuc})} \cdot T_k^{(\text{elec})}, \quad (2.2)$$

where $T_k^{(\text{nuc})}$ and $T_k^{(\text{elec})}$ are rank- k spherical tensor operators (see Appendix C) acting exclusively in the nuclear and electronic subspaces, respectively, and $T_k^{(\text{nuc})} \cdot T_k^{(\text{elec})}$ is their scalar product. The operator $T_k^{(\text{nuc})}$ is associated with the nuclear multipole moment of multipolarity k ; the nuclear dipole moment is considered explicitly below.

In practical applications, the hyperfine interaction V_{hfi} is typically taken as a perturbation to the electronic Hamiltonian. As V_{hfi} is a scalar operator (it is composed of the scalar products $T_k^{(\text{nuc})} \cdot T_k^{(\text{elec})}$), it commutes with the total angular momentum operator \mathbf{F} , and thus the total Hamiltonian H also commutes with \mathbf{F} (this conclusion can also be drawn from physical insight: absent from external fields, the total atomic system cannot have any directional preference in space). The eigenstates of the total Hamiltonian can therefore be taken as angular momentum eigenstates of \mathbf{F} . In common perturbation theory language, the “good” zeroth order states are the coupled states $|\gamma I J F M\rangle$ given by Eq. (2.1). The hyperfine interaction splits the $(2I + 1) \times (2J + 1)$ -fold degenerate level $E_{\gamma J}$ into $2X + 1$ distinct levels associated with each allowed value of F , where $X = \min(I, J)$ (in particular, for $J = 1/2$ and $I \geq 1/2$ there are $2X + 1 = 2$ allowed values of F given by $F = I \pm 1/2$). Each of these levels is still $(2F + 1)$ -fold degenerate as the choice of quantization axis is arbitrary. In the context of perturbation theory, with $E_{\gamma J}$ being the level of interest, the $(2I + 1) \times (2J + 1)$ -dimensional space spanned by the unperturbed

¹Note that the summation starts at $k = 1$, corresponding to the dipole interaction. One can, in principle, write the monopole interaction as $T_0^{(\text{nuc})} \cdot T_0^{(\text{elec})}$. This is nothing more than the Coulomb interaction ($\sum_q = -Z/r_q$) which is already incorporated into H_{elec} . However, as $T_0^{(\text{nuc})}$ and $T_0^{(\text{elec})}$ are both scalars, it is apparent in this form that \mathbf{I} and \mathbf{J} do indeed commute with this part of H_{elec} .

eigenstates $|\gamma I J F M\rangle$ is referred to as the *model space*.² A representation of the hyperfine structure of the ground state of the ^{133}Cs atom is presented in Figure 2.1

The interactions of the electrons with the nuclear multipole moments is dominated by the interaction with the nuclear charge, which is treated non-perturbatively within H_{elec} . Similarly, the interaction of the electrons with the magnetic dipole moment typically dominates over the interactions with the remaining multipole moments. Thus for several applications, retaining only the $k = 1$ term of Eq. (2.2) provides a sufficient description of the atomic hyperfine structure. This approximation will be taken for the remainder of the dissertation; making the associations $\boldsymbol{\mu} = T_{k=1}^{(\text{nuc})}$ and $\boldsymbol{\mathcal{T}} = T_{k=1}^{(\text{elec})}$ ($\boldsymbol{\mu}$ and $\boldsymbol{\mathcal{T}}$ being vector operators), the hyperfine interaction is now written

$$V_{\text{hfi}} = \boldsymbol{\mu} \cdot \boldsymbol{\mathcal{T}}. \quad (2.3)$$

The nuclear magnetic dipole moment $\bar{\mu}$ is conventionally defined as the expectation value of the z -component of $\boldsymbol{\mu}$, μ_z , for the “stretched” nuclear state³

$$\bar{\mu} \equiv \langle I, M_I = I | \mu_z | I, M_I = I \rangle = \begin{pmatrix} I & 1 & I \\ -I & 0 & I \end{pmatrix} \langle I || \boldsymbol{\mu} || I \rangle,$$

where the last equality follows from the Wigner-Eckart theorem, Eq. (C.4). The dipole

²Throughout this dissertation it will be assumed that the energy level $E_{\gamma,J}$ (defining the model space) is not degenerate with any level $E_{\gamma',J}$ for which $\gamma' \neq \gamma$ (such that the model space does not have to be extended to include these states); one consequence of this assumption is that the model space has definite parity.

³From Eq. (2.2) and the commutation relations for spherical tensor operators (Appendix C), it is evident that V_{hfi} does not commute with \mathbf{I} (or \mathbf{J} for that matter). Strictly speaking, perturbation theory allows intermediate states involving excited nuclear states; consequently off-diagonal states such as $\langle \gamma'_I I' M'_I | T_k^{(\text{nuc})} | \gamma_I I M_I \rangle$ appear in the general theory. However, the energy scale for nuclear excitations is far larger than the energy scale for electronic excitations and such terms are insignificant in atomic perturbation theory. This justifies treating the nucleus as a fundamental particle with intrinsic nuclear moments associated with the reduced matrix elements $\langle I || T_k^{(\text{nuc})} || I \rangle$.

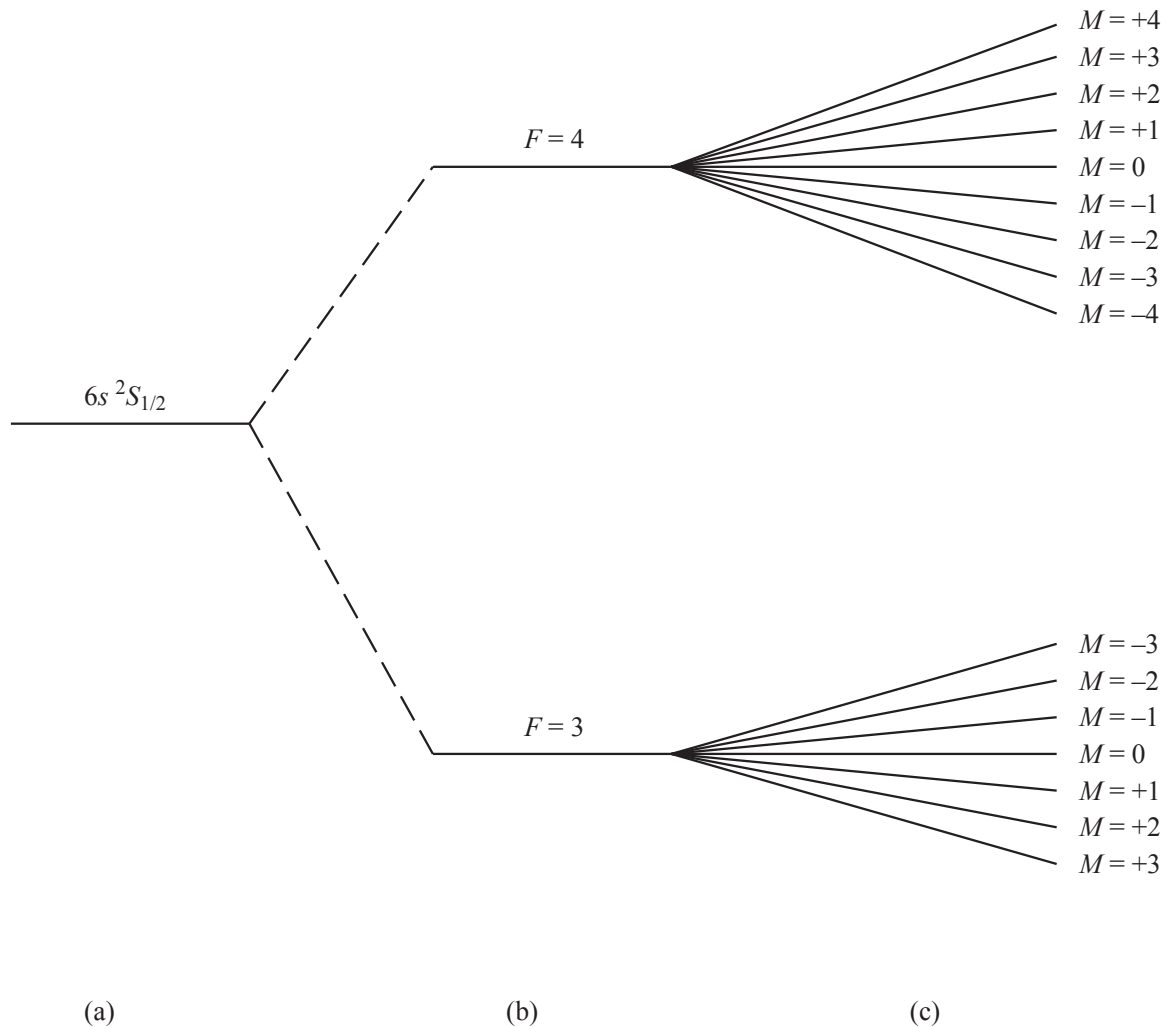


Figure 2.1: Hyperfine structure of the ^{133}Cs ground state ($I = 7/2$, $J = 1/2$). (a) In the absence of the hyperfine interaction the ground level is $(2I+1) \times (2J+1) = 16$ -fold degenerate. (b) With the hyperfine interaction “turned on”, the level is split into two hyperfine levels with $F = 4$ and $F = 3$. The $F = 4$ level is $(2F+1) = 9$ -fold degenerate, whereas the $F = 3$ level is $(2F+1) = 7$ -fold degenerate. (c) The degeneracy in the hyperfine levels may be lifted by application of an external magnetic field (here assumed in the z -direction).

Table 2.1: Nuclear spin and magnetic dipole moments for isotopes ^{133}Cs , ^{27}Al , and $^{69,71}\text{Ga}$. All values are taken from Ref. [75].

Isotope	I	$\bar{\mu}/\mu_{\text{N}} = g_I I$
^{133}Cs	7/2	2.5829128(15)
^{27}Al	5/2	3.6415069(7)
^{69}Ga	3/2	2.01659(5)
^{71}Ga	3/2	2.56227(2)

moment may also be expressed in terms of the dimensionless nuclear gyromagnetic ratio, g_I ,

$$\bar{\mu} = g_I I \mu_{\text{N}}.$$

Here μ_{N} is the nuclear magneton $\mu_{\text{N}} = e\hbar/(2m_p c = \alpha/2m_p)$, where $\alpha \simeq 1/137$ is the fine structure constant and $m_p \simeq 1836$ a.u. is the proton mass. With an explicit evaluation of the 3- j symbol above, the reduced matrix element may be seen to be related to g_I and μ_{N} by

$$\langle I || \boldsymbol{\mu} || I \rangle = \sqrt{I(I+1)(2I+1)} g_I \mu_{\text{N}}. \quad (2.4)$$

Nuclear dipole moments have been accurately measured for all isotopes being considered in this dissertation; these are presented in Table 2.1.

An explicit expression for the vector operator $\boldsymbol{\mathcal{T}}$ acting on the electron coordinates is reserved for Section E.10 of the Appendix. An expression for the corresponding single-particle matrix elements between Dirac spinors is also provided therein.

Chapter 3

The ac Stark Effect

3.1 The Interaction with an Electromagnetic Plane Wave

An atom's energy levels and corresponding eigenfunctions are perturbed under the influence of an oscillating electric field; this is referred to as the ac Stark effect. The underlying theory describing clock shifts due to blackbody radiation (Chapter 4) or optical lattice fields (Chapter 5) is built upon the ac Stark effect. The expressions derived in this chapter provide the foundations for the following two chapters.

The discussion begins with an expression for the electric field associated with a general plane electromagnetic wave (see, for example, Ref. [30])

$$\mathcal{E}(\mathbf{r}, t) = \frac{1}{2} \mathcal{E} \hat{\boldsymbol{\epsilon}} e^{-i(\omega t - \mathbf{k} \cdot \mathbf{r})} + \text{c.c.}, \quad (3.1)$$

where c.c. represents the complex conjugate of the preceding term. Here $\hat{\boldsymbol{\epsilon}}$ is the complex polarization vector and \mathbf{k} is the (real) wave vector. The magnitude of wave vector is proportional to the angular frequency, $k = \omega/c$, with c being the speed of

light. The amplitude \mathcal{E} can in general be complex, though its complex phase can just be associated with a time delay. Such a time delay has no physical significance for the problem at hand, and it is thus assumed that \mathcal{E} is real. The (time-averaged) Poynting vector associated with this plane electromagnetic wave is

$$\mathbf{S} = \frac{c}{8\pi} \mathcal{E}^2 \hat{\mathbf{k}}.$$

The intensity is simply $|\mathbf{S}|$.

Being a unit vector, the polarization vector satisfies

$$\hat{\boldsymbol{\epsilon}}^* \cdot \hat{\boldsymbol{\epsilon}} = 1.$$

The polarization vector and the wave vector are orthogonal—i.e., $\hat{\boldsymbol{\epsilon}} \cdot \mathbf{k} = 0$. Consequently, the vector product $\hat{\boldsymbol{\epsilon}}^* \times \hat{\boldsymbol{\epsilon}}$ necessarily points in the direction of \mathbf{k} . Specifically,

$$\hat{\boldsymbol{\epsilon}}^* \times \hat{\boldsymbol{\epsilon}} = i\mathcal{A}\hat{\mathbf{k}},$$

where the real proportionality constant \mathcal{A} is termed the *degree of circular polarization*. It is plainly seen that the degree of circular polarization is limited by $|\mathcal{A}| \leq 1$. In particular, $\mathcal{A} = 0$ corresponds to linear polarization, $\mathcal{A} = 1$ ($\mathcal{A} = -1$) corresponds to right-(left-)circular polarization, and the intermediate values correspond to appropriate intermediate elliptical polarizations.¹ Clearly a polarization vector which is real ($\hat{\boldsymbol{\epsilon}}^* = \hat{\boldsymbol{\epsilon}}$) necessarily corresponds to $\mathcal{A} = 0$ (i.e., linear polarization).

¹The degree of circular polarization is related to the eccentricity e of the corresponding ellipse by

$$|\mathcal{A}| = \frac{2\sqrt{1-e^2}}{2-e^2}.$$

Along with the electric field, a plane electromagnetic wave also has a complementary magnetic field. A complete description of the interaction of an atom with this plane electromagnetic wave involves a decomposition into electric and magnetic multipolar interactions. For neutral atoms there is no electric monopole moment. Furthermore, for wavelengths ($= 2\pi c/\omega$) much larger than the characteristic size of the atom ($\sim a_B$), the atom effectively “sees” a uniform oscillating field and the higher multipolar (multipolarity $k > 1$) effects become negligible. Furthermore, considering only intensities which have an appreciable effect on the system, the electric dipole interaction dominates over the magnetic dipole interaction. Thus, in the long-wavelength regime (the regime to which this work is limited) the interaction of an atom with the plane electromagnetic wave, Eq. (3.1), is sufficiently described by the electric dipole interaction alone.

With the atom assumed to be at the origin, the long-wavelength approximation is implemented by taking $e^{\pm i\mathbf{k}\cdot\mathbf{r}} \simeq 1$ in Eq. (3.1), such that the atom effectively “sees” the uniform oscillating electric field

$$\bar{\mathcal{E}}(t) = \frac{1}{2}\mathcal{E}\hat{\epsilon}e^{-i\omega t} + \text{c.c.} \quad (3.2)$$

The interaction of the atom with this field is given by

$$V_{E1} = -\bar{\mathcal{E}}(t) \cdot \mathbf{D},$$

where \mathbf{D} is the electric dipole operator

$$\mathbf{D} = -\sum_{q=1}^N \mathbf{r}_q.$$

Here \mathbf{r} is the position vector and the summation q is over all atomic electrons. This

interaction can be cast in the form

$$V_{E1} = V_- e^{-i\omega t} + V_+ e^{+i\omega t},$$

where

$$V_- = -\frac{\mathcal{E}}{2} (\hat{\boldsymbol{\epsilon}} \cdot \mathbf{D}), \quad V_+ = -\frac{\mathcal{E}}{2} (\hat{\boldsymbol{\epsilon}}^* \cdot \mathbf{D}). \quad (3.3)$$

Note that \mathbf{D} is a Hermitian operator and $V_-^\dagger = V_+$. An expression for the matrix elements of \mathbf{r} between Dirac spinors is provided in Section E.10.

3.2 The Total Perturbation and the Hyperfine Clock Shift

The total Hamiltonian describing the atomic system in the presence of the plane electromagnetic wave, Eq. (3.1), is given by

$$\begin{aligned} H &= H_{\text{elec}} + V_{\text{hfi}} + V_{E1} \\ &= H_{\text{elec}} + V_{\text{hfi}} + V_- e^{-i\omega t} + V_+ e^{+i\omega t}. \end{aligned}$$

It should be noted that in the second line here all of the time-dependence is written out explicitly—that is, H_{elec} , V_{hfi} , V_- , and V_+ are all time-independent operators. With the eigenstates $|\gamma I J F M\rangle$ and energies $E_{\gamma J}$ of the electronic Hamiltonian H_{elec} assumed to be known, the remaining interaction $V_{\text{hfi}} + V_- e^{-i\omega t} + V_+ e^{+i\omega t}$ can be treated effectively as a perturbation. This perturbation is precisely of the form of Eq. (D.5) of Appendix D, wherein the appropriate Floquet perturbation expressions are subsequently developed.

The mean energy shift δE can be decomposed into contributions from the various

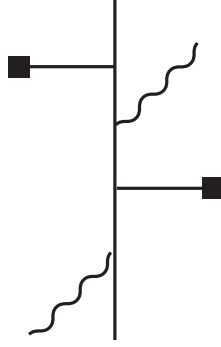


Figure 3.1: Diagrammatical representation of an energy contribution of the type $\delta E^{(2,2)}$. The capped solid lines each represent the interaction of the electrons with the nuclear magnetic dipole (V_{hfi}) and the wavy lines each represent the interaction of the electrons with a photon of the external field (V_{E1}).

orders of perturbation theory in the usual way—namely, $\delta E = \delta E^{(1)} + \delta E^{(2)} + \dots$. One may further decompose each $\delta E^{(l)}$ into terms $\delta E^{(m,n)}$ (with $m + n = l$) which represent contributions which are m -th order in the the perturbation V_{hfi} and n -th order in the perturbation V_{E1} (i.e., V_{\pm}). As an example, the second order energy shift can be decomposed as

$$\delta E^{(2)} = \delta E^{(2,0)} + \delta E^{(0,2)} + \delta E^{(1,1)},$$

where $\delta E^{(2,0)}$ represents terms second-order in V_{hfi} , $\delta E^{(0,2)}$ represents terms second-order in V_{E1} , and $\delta E^{(1,1)}$ represents terms first-order in both V_{hfi} and V_{E1} . A diagrammatical representation of an energy contribution of the type $\delta E^{(2,2)}$ —i.e., second order in V_{hfi} and second order in V_{E1} —is given in Figure 3.1.

For the microwave atomic clocks, the clock frequency ν is defined in terms of the hyperfine energy splitting for the ground state of the atom in the absence of external

fields. Using the notation introduced above, this is

$$\begin{aligned}\nu &= \frac{1}{2\pi} \left[\left(E_2 + \sum_m \delta E_2^{(m,0)} \right) - \left(E_1 + \sum_m \delta E_1^{(m,0)} \right) \right] \\ &= \frac{1}{2\pi} \left[\sum_m \delta E_2^{(m,0)} - \sum_m \delta E_1^{(m,0)} \right],\end{aligned}\tag{3.4}$$

where subscripts 2 and 1 label the upper and lower hyperfine levels, respectively (it is assumed that $J = 1/2$ or $I = 1/2$ such that there are only two hyperfine levels). The factor of $1/2\pi$ here is the proportionality constant between frequency and angular frequency (i.e., energy for atomic units). The second equality in this expression is realized by noting that the states 2 and 1 are part of the same hyperfine manifold and thus their unperturbed energies are degenerate ($E_2 = E_1$). When the additional perturbation V_{E_1} is “turned on”, the splitting between the hyperfine levels now becomes

$$\nu + \delta\nu = \frac{1}{2\pi} \left[\sum_{mn} \delta E_2^{(m,n)} - \sum_{mn} \delta E_1^{(m,n)} \right].\tag{3.5}$$

The physical quantity to be considered for this work is $\delta\nu$. To this end, it is apparent from comparing Eq. (3.4) and Eq. (3.5) that it suffices to only consider explicitly the terms $\delta E^{(m,n)}$ with $n > 0$ —that is, terms that depend explicitly on the perturbation V_{E_1} . This conclusion could certainly have been drawn from intuition; however, the notation introduced here will aid in providing a consistent formalism for the hyperfine Stark effect.

The following two sections provide derivations for the second and third order ac Stark shifts. These sections are heavy in technical detail; summarized results of these sections are given in Section 3.5.

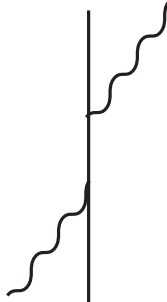


Figure 3.2: Diagrammatical representation of $\delta E_n^{(0,2)}$. There are two photon interactions but no hyperfine interaction.

3.3 The Second-Order ac Stark Shift

Again it is mentioned that the perturbation $V_{\text{hfi}} + V_- e^{-i\omega t} + V_+ e^{+i\omega t}$ is precisely of the form of Eq. (D.5). With the associations $V_s \rightarrow V_{\text{hfi}}$ and $\mathcal{E}_{nq}^{(l)} \rightarrow \delta E_n^{(l)}$, the subsequent Floquet perturbation expressions, Eqs. (D.6), are thus applicable to this system. From the Floquet perturbation formalism, it can be determined that the energy shift of arbitrary order only contains terms in which V_{E1} contributes in even orders (i.e., $\delta E^{(m,n)} = 0$ if n is odd).² Thus the problem begins with the second order energy shift, in which the pertinent terms are all given by $\delta E_n^{(0,2)}$. A diagrammatical representation of this energy shift is given in Figure 3.2.

²In the related static problem (the static Stark effect), it is also found that the corresponding static perturbation V_{E1} only contributes in even orders, assuming a model space of definite parity. This follows from the fact that the hyperfine interaction is an even parity operator whereas the dipole operator is an odd parity operator—i.e., $\mathcal{P}V_{\text{hfi}}\mathcal{P}^\dagger = V_{\text{hfi}}$ and $\mathcal{P}\mathbf{D}\mathcal{P}^\dagger = -\mathbf{D}$. The former can only connect states of like parity, whereas the latter can only connect states of opposite parity. The Floquet formalism, however, never makes this assumption; the shifts associated with odd powers of a general harmonic perturbation simply time-average to zero. For this particular problem, the Floquet perturbation expressions should reduce to the correct static perturbation expressions in the limit $\omega \rightarrow 0$. To complete the connection one should assume a real polarization vector and make the appropriate rms substitution $\mathcal{E} \rightarrow \mathcal{E}\sqrt{2}$.

Taken directly from Eqs. (D.6), the shift $\delta E_n^{(0,2)}$ is

$$\delta E_n^{(0,2)} = \sum_{n'} \frac{\langle n|V_+|n'\rangle\langle n'|V_-|n\rangle}{E_n - E_{n'} + \omega} + \sum_{n'} \frac{\langle n|V_-|n'\rangle\langle n'|V_+|n\rangle}{E_n - E_{n'} - \omega},$$

or explicitly specifying the quantum numbers (i.e., $|n\rangle = |\gamma I J F M\rangle$)

$$\begin{aligned} \delta E_{\gamma I J F M}^{(0,2)} &= \sum_{\gamma' J' F' M'} \frac{\langle \gamma I J F M|V_+|\gamma' I J' F' M'\rangle\langle \gamma' I J' F' M'|V_-|\gamma I J F M\rangle}{E_{\gamma J} - E_{\gamma' J'} + \omega} \\ &+ \sum_{\gamma' J' F' M'} \frac{\langle \gamma I J F M|V_-|\gamma' I J' F' M'\rangle\langle \gamma' I J' F' M'|V_+|\gamma I J F M\rangle}{E_{\gamma J} - E_{\gamma' J'} - \omega}. \end{aligned}$$

The summations here exclude states which lie within the degenerate model space, $(\gamma' J') = (\gamma J)$; this will be implicit in similar expressions to follow. This energy shift may be regarded as the expectation value of an operator $H_{\gamma J}^{(0,2)}$ for the unperturbed state

$$\delta E_{\gamma I J F M}^{(0,2)} = \langle \gamma I J F M|H_{\gamma J}^{(0,2)}|\gamma I J F M\rangle. \quad (3.6)$$

With the explicit form of V_{\pm} , Eqs. (3.3), $H_{\gamma J}^{(0,2)}$ may be expressed as

$$H_{\gamma J}^{(0,2)} = \left(\frac{\mathcal{E}}{2}\right)^2 (\hat{\epsilon}^* \cdot \mathbf{D}) R_{\gamma J}^{(+)} (\hat{\epsilon} \cdot \mathbf{D}) + \left(\frac{\mathcal{E}}{2}\right)^2 (\hat{\epsilon} \cdot \mathbf{D}) R_{\gamma J}^{(-)} (\hat{\epsilon}^* \cdot \mathbf{D}), \quad (3.7)$$

where $R_{\gamma J}^{(\pm)}$ are the frequency-dependent resolvent operators, given by

$$\begin{aligned} R_{\gamma J}^{(\pm)} &= \sum_{\gamma' J' F' M'} \frac{|\gamma' I J' F' M'\rangle\langle \gamma' I J' F' M'|}{E_{\gamma J} - E_{\gamma' J'} \pm \omega} \\ &= \sum_{\gamma' J' M'_I M'_J} \frac{|I M'_I, \gamma' J' M'_J\rangle\langle I M'_I, \gamma' J' M'_J|}{E_{\gamma J} - E_{\gamma' J'} \pm \omega} \\ &= \sum_{\gamma' J' M'_J} \frac{|\gamma' J' M'_J\rangle\langle \gamma' J' M'_J|}{E_{\gamma J} - E_{\gamma' J'} \pm \omega}. \end{aligned}$$

The second equality (which changes to the alternative coupling scheme $|IM'_I, \gamma' J' M'_J\rangle$) holds due to the fact that the denominators are independent of F' and M' . The last equality follows from the closure relation $\sum_{M'_I} |IM'_I\rangle\langle IM'_I| = 1$ in the nuclear subspace; consequently the resolvent operators act completely within the electronic subspace. In the next section, the frequency-independent resolvent operator $R_{\gamma J}^{(0)}$ will also be used

$$R_{\gamma J}^{(0)} = \sum_{\gamma' J' M'_J} \frac{|\gamma' J' M'_J\rangle\langle\gamma' J' M'_J|}{E_{\gamma J} - E_{\gamma' J'}}.$$

From the commutation relations for spherical tensor operators, Eq. (C.1), the resolvent operators are seen to be scalar operators. Furthermore, it is easy to see that they are Hermitian.

Attention will initially be directed to the first term of Eq. (3.7) without the prefactor. Following from Eq. (C.3) of Appendix C, this group of spherical tensors may be recoupled to isolate the polarization vectors from the operators which act in the atomic space

$$(\hat{\boldsymbol{\epsilon}}^* \cdot \mathbf{D}) R_{\gamma J}^{(+)} (\hat{\boldsymbol{\epsilon}} \cdot \mathbf{D}) = \sum_{K=0,1,2} (-1)^K \{\hat{\boldsymbol{\epsilon}}^* \otimes \hat{\boldsymbol{\epsilon}}\}_K \cdot \left\{ \mathbf{D} \otimes R_{\gamma J}^{(+)} \mathbf{D} \right\}_K.$$

Here the $\{\dots\}_K$ represent spherical tensors of rank K (see Appendix C for definitions and notations). The allowed values of K are limited by the triangular selection rule; as the composite tensors $\{\dots\}_K$ here involve the coupling of two rank-1 tensors, K is consequently limited by $0 \leq K \leq 2$. The second term of Eq. (3.7) may be recoupled in a similar fashion. Also making use of the relation $\{\hat{\boldsymbol{\epsilon}} \otimes \hat{\boldsymbol{\epsilon}}^*\}_K = (-1)^K \{\hat{\boldsymbol{\epsilon}}^* \otimes \hat{\boldsymbol{\epsilon}}\}_K$,

the operator $H_{\gamma J}^{(0,2)}$ may now be written

$$H_{\gamma J}^{(0,2)} = \left(\frac{\mathcal{E}}{2}\right)^2 \sum_{K=0,1,2} (-1)^K \{\hat{\boldsymbol{\varepsilon}}^* \otimes \hat{\boldsymbol{\varepsilon}}\}_K \cdot \left(\left\{ \mathbf{D} \otimes R_{\gamma J}^{(+)} \mathbf{D} \right\}_K + (-1)^K \left\{ \mathbf{D} \otimes R_{\gamma J}^{(-)} \mathbf{D} \right\}_K \right). \quad (3.8)$$

Using the Wigner-Eckart theorem, Eq. (C.4), matrix elements of the rank- k tensor acting in the atomic space may be expressed in terms of corresponding reduced matrix elements,

$$\begin{aligned} & \langle \gamma I J F' M' | \left(\left\{ \mathbf{D} \otimes R_{\gamma J}^{(+)} \mathbf{D} \right\}_{KQ} + (-1)^K \left\{ \mathbf{D} \otimes R_{\gamma J}^{(-)} \mathbf{D} \right\}_{KQ} \right) | \gamma I J F M \rangle \\ &= (-1)^{F'-M'} \begin{pmatrix} F' & K & F \\ -M' & Q & M \end{pmatrix} \\ & \times \langle \gamma I J F' || \left(\left\{ \mathbf{D} \otimes R_{\gamma J}^{(+)} \mathbf{D} \right\}_K + (-1)^K \left\{ \mathbf{D} \otimes R_{\gamma J}^{(-)} \mathbf{D} \right\}_K \right) || \gamma I J F \rangle. \quad (3.9) \end{aligned}$$

The diagonal reduced matrix elements (i.e., $F' = F$) define the second order ‘‘reduced’’ polarizabilities $\alpha_{\gamma I J F; K}^{(2)}$,

$$\alpha_{\gamma I J F; K}^{(2)} = \langle \gamma I J F || \left(\left\{ \mathbf{D} \otimes R_{\gamma J}^{(+)} \mathbf{D} \right\}_K + (-1)^K \left\{ \mathbf{D} \otimes R_{\gamma J}^{(-)} \mathbf{D} \right\}_K \right) || \gamma I J F \rangle. \quad (3.10)$$

Angular reduction may be performed on the right-hand side of this expression with

the help of formulas from Appendix C,

$$\begin{aligned}
\alpha_{\gamma I J F; K}^{(2)} &= (-1)^{I-J+F} (2F+1) \sqrt{(2K+1)} \begin{Bmatrix} F & K & F \\ J & I & J \end{Bmatrix} \\
&\times \sum_{\gamma' J'} \begin{Bmatrix} J & K & J \\ 1 & J' & 1 \end{Bmatrix} \langle \gamma J \| \mathbf{D} \| \gamma' J' \rangle \langle \gamma' J' \| \mathbf{D} \| \gamma J \rangle \\
&\times \left[\frac{1}{E_{\gamma J} - E_{\gamma' J'} + \omega} + \frac{(-1)^K}{E_{\gamma J} - E_{\gamma' J'} - \omega} \right]. \tag{3.11}
\end{aligned}$$

For the remainder of this section the quantum numbers $\gamma I J$ will be omitted for clarity.

The second order reduced polarizabilities are related to the conventional second order scalar $\alpha_F^{\text{S},(2)}$, axial $\alpha_F^{\text{a},(2)}$, and tensor $\alpha_F^{\text{T},(2)}$ polarizabilities [48] by

$$\begin{aligned}
\alpha_F^{\text{S},(2)} &= \frac{1}{\sqrt{3(2F+1)}} \alpha_{F;K=0}^{(2)}, \\
\alpha_F^{\text{a},(2)} &= -\sqrt{\frac{2F}{(2F+1)(F+1)}} \alpha_{F;K=1}^{(2)}, \\
\alpha_F^{\text{T},(2)} &= -\sqrt{\frac{2F(2F-1)}{3(2F+1)(F+1)(2F+3)}} \alpha_{F;K=2}^{(2)}. \tag{3.12}
\end{aligned}$$

It should be noted that the polarizabilities are—via the resolvent operators in Eq. (3.10)—frequency-dependent.

From Eqs. (3.6, 3.8, 3.9, 3.10), the energy shift can be written in terms of the reduced polarizabilities as

$$\delta E_{FM}^{(0,2)} = \left(\frac{\mathcal{E}}{2} \right)^2 \sum_{K=0,1,2} (-1)^K \{ \hat{\boldsymbol{\epsilon}}^* \otimes \hat{\boldsymbol{\epsilon}} \}_{K0} (-1)^{F-M} \begin{pmatrix} F & K & F \\ -M & 0 & M \end{pmatrix} \alpha_{F;K}^{(2)}. \tag{3.13}$$

The $Q = 0$ components are picked out of the scalar product due to the selection rule $M' + Q + M = 0$ associated with the 3- j symbol of Eq. (3.9). The attention will now

be turned to the polarization-dependent factors $\{\hat{\boldsymbol{\epsilon}}^* \otimes \hat{\boldsymbol{\epsilon}}\}_{K0}$. Employing Eqs. (C.5), these are evaluated to be

$$\begin{aligned}\{\hat{\boldsymbol{\epsilon}}^* \otimes \hat{\boldsymbol{\epsilon}}\}_{00} &= -\frac{1}{\sqrt{3}} (\hat{\boldsymbol{\epsilon}}^* \cdot \hat{\boldsymbol{\epsilon}}) = -\frac{1}{\sqrt{3}}, \\ \{\hat{\boldsymbol{\epsilon}}^* \otimes \hat{\boldsymbol{\epsilon}}\}_{10} &= \frac{i}{\sqrt{2}} (\hat{\boldsymbol{\epsilon}}^* \times \hat{\boldsymbol{\epsilon}}) \cdot \hat{\mathbf{e}}_z = -\frac{1}{\sqrt{2}} \mathcal{A}(\hat{\mathbf{k}} \cdot \hat{\mathbf{e}}_z), \\ \{\hat{\boldsymbol{\epsilon}}^* \otimes \hat{\boldsymbol{\epsilon}}\}_{20} &= \frac{1}{\sqrt{6}} [3(\hat{\boldsymbol{\epsilon}}^* \cdot \hat{\mathbf{e}}_z)(\hat{\boldsymbol{\epsilon}} \cdot \hat{\mathbf{e}}_z) - (\hat{\boldsymbol{\epsilon}}^* \cdot \hat{\boldsymbol{\epsilon}})] = \frac{1}{\sqrt{6}} [3|\hat{\boldsymbol{\epsilon}} \cdot \hat{\mathbf{e}}_z|^2 - 1].\end{aligned}$$

At this point it is useful to introduce the parameters θ_k and θ_p , satisfying

$$\begin{aligned}\cos\theta_k &= \hat{\mathbf{k}} \cdot \hat{\mathbf{e}}_z, \\ \cos^2\theta_p &= |\hat{\boldsymbol{\epsilon}} \cdot \hat{\mathbf{e}}_z|^2.\end{aligned}$$

It is apparent that the parameter θ_k may be regarded as the angle between the wave vector and the z -axis. Furthermore, for linear polarization the parameter θ_p may be regarded as the angle between the polarization direction and the z -axis. For a more general geometrical interpretation of θ_p , it is useful to further introduce the parameters θ_{maj} , θ_{min} , and φ . Geometrical representations of these parameters are given in Figure 3.3; these parameters satisfy³

$$\cos^2\theta_p = |\hat{\boldsymbol{\epsilon}} \cdot \hat{\mathbf{e}}_z|^2 = \cos^2\varphi \cos^2\theta_{\text{maj}} + \sin^2\varphi \cos^2\theta_{\text{min}}, \quad \mathcal{A} = \sin(2\varphi).$$

From here on the parameters θ_k , θ_p and \mathcal{A} will be used exclusively. From geometrical considerations it is found that θ_k and θ_p must satisfy the inequality $\cos^2\theta_k + \cos^2\theta_p \leq 1$.

³Furthermore, the complex polarization vector may be expressed as $\hat{\boldsymbol{\epsilon}} = e^{i\gamma}(\cos\varphi \hat{\boldsymbol{\epsilon}}_{\text{maj}} + i \sin\varphi \hat{\boldsymbol{\epsilon}}_{\text{min}})$, where γ is real and $\hat{\boldsymbol{\epsilon}}_{\text{maj}}$ and $\hat{\boldsymbol{\epsilon}}_{\text{min}}$ are real unit vectors defined in Figure 3.3. The convention $\hat{\boldsymbol{\epsilon}}_{\text{maj}} \times \hat{\boldsymbol{\epsilon}}_{\text{min}} = \hat{\mathbf{k}}$ is adopted here.

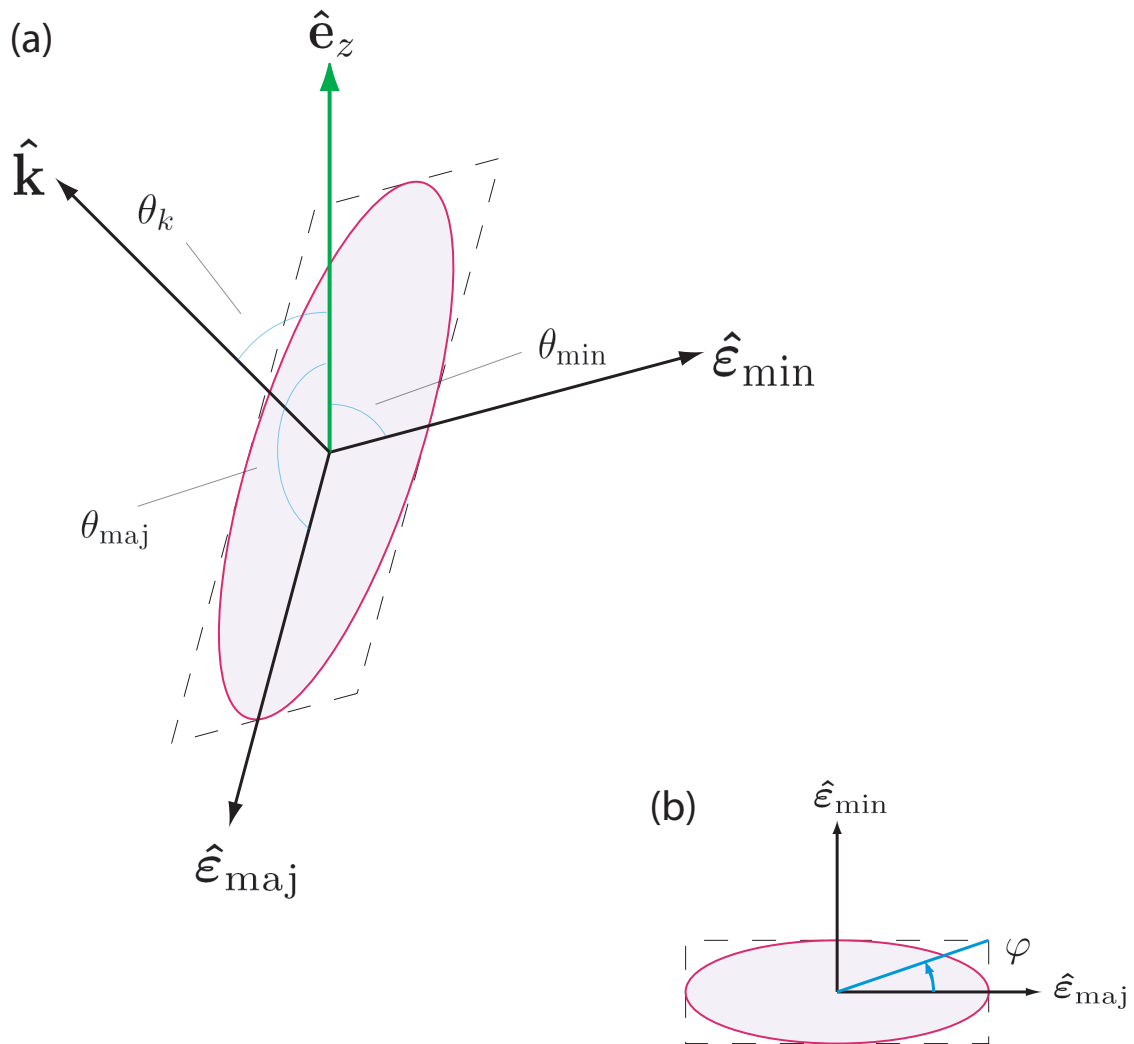


Figure 3.3: (Color online) Representation of the electromagnetic plane wave geometrical parameters. (a) The surface represents the ellipse swept out by the electric field vector in one period. Unit vector $\hat{\mathbf{e}}_{\text{maj}}$ ($\hat{\mathbf{e}}_{\text{min}}$) aligns with the semi-major (-minor) axis of the ellipse; $\hat{\mathbf{k}}$ is the unit wave vector. The vectors $\hat{\mathbf{e}}_{\text{maj}}$, $\hat{\mathbf{e}}_{\text{min}}$, and $\hat{\mathbf{k}}$ are mutually orthogonal, but may otherwise have an arbitrary orientation with respect to the z -axis ($\hat{\mathbf{e}}_z$). Parameters θ_{maj} , θ_{min} , and θ_k , are the angles between the respective unit vectors and the z -axis. (b) Parameter φ , represented here in the $\hat{\mathbf{e}}_{\text{maj}} - \hat{\mathbf{e}}_{\text{min}}$ plane, is directly related to the degree of circular polarization.

Using explicit expressions for the 3- j symbol appearing in Eq. (3.13), the second order energy shift expressed in terms of polarization parameters \mathcal{A} , θ_k , and θ_p and the second order polarizabilities $\alpha_F^{S,(2)}$, $\alpha_F^{a,(2)}$, and $\alpha_F^{T,(2)}$ is

$$\begin{aligned} \delta E_{FM}^{(0,2)} = & \\ & - \left(\frac{\mathcal{E}}{2} \right)^2 \left[\alpha_F^{S,(2)} + (\mathcal{A} \cos \theta_k) \frac{M}{2F} \alpha_F^{a,(2)} + \left(\frac{3 \cos^2 \theta_p - 1}{2} \right) \frac{3M^2 - F(F+1)}{F(2F-1)} \alpha_F^{T,(2)} \right]. \end{aligned} \quad (3.14)$$

It should be noted that the perturbative analysis above assumes F and M to be good quantum numbers. In practice this is assured with the application of a bias magnetic field; details are provided in Appendix G.

3.4 The Third-Order ac Stark Shift

Analysis of the third-order ac Stark shift proceeds in a similar manner as the second-order analysis. From Eqs. (D.6), the pertinent terms are found to be

$$\begin{aligned} \delta E_n^{(1,2)} = & \\ & \sum_{n'n''} \frac{\langle n | V_{\text{hfi}} | n'' \rangle \langle n'' | V_+ | n' \rangle \langle n' | V_- | n \rangle}{(E_n - E_{n''})(E_n - E_{n'} + \omega)} + \sum_{n'n''} \frac{\langle n | V_{\text{hfi}} | n'' \rangle \langle n'' | V_- | n' \rangle \langle n' | V_+ | n \rangle}{(E_n - E_{n''})(E_n - E_{n'} - \omega)} \\ & + \sum_{n'n''} \frac{\langle n | V_+ | n'' \rangle \langle n'' | V_{\text{hfi}} | n' \rangle \langle n' | V_- | n \rangle}{(E_n - E_{n''} + \omega)(E_n - E_{n'} + \omega)} + \sum_{n'n''} \frac{\langle n | V_- | n'' \rangle \langle n'' | V_{\text{hfi}} | n' \rangle \langle n' | V_+ | n \rangle}{(E_n - E_{n''} - \omega)(E_n - E_{n'} - \omega)} \\ & + \sum_{n'n''} \frac{\langle n | V_+ | n'' \rangle \langle n'' | V_- | n' \rangle \langle n' | V_{\text{hfi}} | n \rangle}{(E_n - E_{n''} + \omega)(E_n - E_{n'})} + \sum_{n'n''} \frac{\langle n | V_- | n'' \rangle \langle n'' | V_+ | n' \rangle \langle n' | V_{\text{hfi}} | n \rangle}{(E_n - E_{n''} - \omega)(E_n - E_{n'})} \\ & - \langle n | V_{\text{hfi}} | n \rangle \sum_{n'} \frac{\langle n | V_+ | n' \rangle \langle n' | V_- | n \rangle}{(E_n - E_{n'} + \omega)^2} - \langle n | V_{\text{hfi}} | n \rangle \sum_{n'} \frac{\langle n | V_- | n' \rangle \langle n' | V_+ | n \rangle}{(E_n - E_{n'} - \omega)^2}. \end{aligned} \quad (3.15)$$

The energy shift $\delta E_{\gamma J}^{(1,2)}$ (now with explicit quantum numbers $\gamma I J F M$) may be taken as the expectation value of the operator $H_{\gamma J}^{(1,2)}$. The operator $H_{\gamma J}^{(1,2)}$ may be decom-

posed into four operators—“top”, “center”, “bottom”, and “normalization”—such that the energy shift is written

$$\delta E_{\gamma J}^{(1,2)} = \langle \gamma I J F M | \left(H_{\gamma J}^{(1,2),\text{top}} + H_{\gamma J}^{(1,2),\text{cen}} + H_{\gamma J}^{(1,2),\text{bot}} + H_{\gamma J}^{(1,2),\text{nor}} \right) | \gamma I J F M \rangle,$$

where each of the four terms represents a line of the right-hand side of Eq. (3.15), in respective order. These operators may be written in the form

$$\begin{aligned} H_n^{(1,2),\text{top}} &= \left(\frac{\mathcal{E}}{2} \right)^2 \left[V_{\text{hfi}} R_{\gamma J}^{(0)} (\hat{\boldsymbol{\epsilon}}^* \cdot \mathbf{D}) R_{\gamma J}^{(+)} (\hat{\boldsymbol{\epsilon}} \cdot \mathbf{D}) + V_{\text{hfi}} R_{\gamma J}^{(0)} (\hat{\boldsymbol{\epsilon}} \cdot \mathbf{D}) R_{\gamma J}^{(-)} (\hat{\boldsymbol{\epsilon}}^* \cdot \mathbf{D}) \right], \\ H_{\gamma J}^{(1,2),\text{cen}} &= \left(\frac{\mathcal{E}}{2} \right)^2 \left[(\hat{\boldsymbol{\epsilon}}^* \cdot \mathbf{D}) R_{\gamma J}^{(+)} V_{\text{hfi}} R_{\gamma J}^{(+)} (\hat{\boldsymbol{\epsilon}} \cdot \mathbf{D}) + (\hat{\boldsymbol{\epsilon}} \cdot \mathbf{D}) R_{\gamma J}^{(-)} V_{\text{hfi}} R_{\gamma J}^{(-)} (\hat{\boldsymbol{\epsilon}}^* \cdot \mathbf{D}) \right], \\ H_{\gamma J}^{(1,2),\text{bot}} &= \left(\frac{\mathcal{E}}{2} \right)^2 \left[(\hat{\boldsymbol{\epsilon}}^* \cdot \mathbf{D}) R_{\gamma J}^{(+)} (\hat{\boldsymbol{\epsilon}} \cdot \mathbf{D}) R_{\gamma J}^{(0)} V_{\text{hfi}} + (\hat{\boldsymbol{\epsilon}} \cdot \mathbf{D}) R_{\gamma J}^{(-)} (\hat{\boldsymbol{\epsilon}}^* \cdot \mathbf{D}) R_{\gamma J}^{(0)} V_{\text{hfi}} \right], \\ H_{\gamma J}^{(1,2),\text{nor}} &= \left(\frac{\mathcal{E}}{2} \right)^2 \left[-V_{\text{hfi}} P_{\gamma J} (\hat{\boldsymbol{\epsilon}}^* \cdot \mathbf{D}) \left(R_{\gamma J}^{(+)} \right)^2 (\hat{\boldsymbol{\epsilon}} \cdot \mathbf{D}) \right. \\ &\quad \left. - V_{\text{hfi}} P_{\gamma J} (\hat{\boldsymbol{\epsilon}} \cdot \mathbf{D}) \left(R_{\gamma J}^{(-)} \right)^2 (\hat{\boldsymbol{\epsilon}}^* \cdot \mathbf{D}) \right], \end{aligned} \quad (3.16)$$

where $P_{\gamma J}$ is the projection operator for the model space, given by

$$P_{\gamma J} = \sum_{F' M'} |\gamma I J F' M'\rangle \langle \gamma I J F' M'| = \sum_{M_J} |\gamma J M_J\rangle \langle \gamma J M_J|.$$

The projection operator is a scalar operator and furthermore is Hermitian. Note that $H_{\gamma J}^{(1,2),\text{cen}}$ and $H_{\gamma J}^{(1,2),\text{nor}}$ are Hermitian operators, whereas $H_{\gamma J}^{(1,2),\text{top}}$ and $H_{\gamma J}^{(1,2),\text{bot}}$ are Hermitian conjugates of each other. Diagrammatical representations of each of the four terms are given in Figure 3.4.

Initially considering the top term, once again the polarization vectors may be

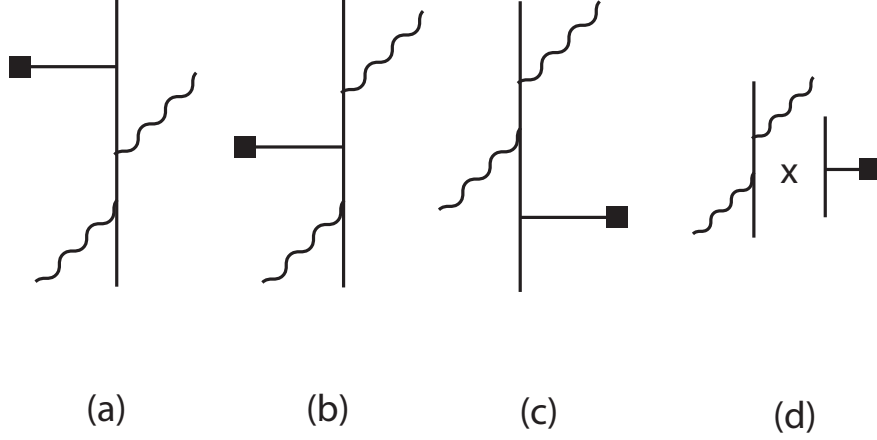


Figure 3.4: Diagrammatic representations of the (a) “top”, (b) “center”, (c) “bottom”, and (d) “normalization” contributions to $\delta E_n^{(1,2)}$. The names top, center, and bottom reflect the position of the hyperfine interaction with respect to the two photon interactions.

decoupled from the remaining operators acting in the atomic space

$$\begin{aligned}
 H_{\gamma J}^{(1,2),\text{top}} &= \left(\frac{\mathcal{E}}{2}\right)^2 \sum_{K=0,1,2} (-1)^K \{\hat{\boldsymbol{\varepsilon}}^* \otimes \hat{\boldsymbol{\varepsilon}}\}_K \\
 &\cdot \left(\left\{ V_{\text{hf}} R_{\gamma J}^{(0)} \mathbf{D} \otimes R_{\gamma J}^{(+)} \mathbf{D} \right\}_K + (-1)^K \left\{ V_{\text{hf}} R_{\gamma J}^{(0)} \mathbf{D} \otimes R_{\gamma J}^{(-)} \mathbf{D} \right\}_K \right).
 \end{aligned}$$

This has a similar form as Eq. (3.8) for the second order, the difference being only the second line of this expression. Analogous to the second order derivation, one may then define third-order reduced polarizabilities for the top term as

$$\begin{aligned}
 \alpha_{\gamma I J F; K}^{(3),\text{top}} &= \\
 &\langle \gamma I J F \| \left(\left\{ V_{\text{hf}} R_{\gamma J}^{(0)} \mathbf{D} \otimes R_{\gamma J}^{(+)} \mathbf{D} \right\}_K + (-1)^K \left\{ V_{\text{hf}} R_{\gamma J}^{(0)} \mathbf{D} \otimes R_{\gamma J}^{(-)} \mathbf{D} \right\}_K \right) \| \gamma I J F \rangle.
 \end{aligned}$$

Angular reduction of the right-hand side yields

$$\begin{aligned}
\alpha_{\gamma I J F; K}^{(3), \text{top}} &= (2F+1)\sqrt{(2K+1)}\sqrt{I(I+1)(2I+1)}g_I\mu_N \\
&\times \sum_{J'' J'} (-1)^{J+J''} \left\{ \begin{matrix} I & I & 1 \\ J & J'' & F \end{matrix} \right\} \left\{ \begin{matrix} K & J'' & J \\ I & F & F \end{matrix} \right\} \left\{ \begin{matrix} K & J'' & J \\ J' & 1 & 1 \end{matrix} \right\} \\
&\times \sum_{\gamma'' \gamma'} \frac{\langle \gamma J || \mathcal{T} || \gamma'' J'' \rangle \langle \gamma'' J'' || \mathbf{D} || \gamma' J' \rangle \langle \gamma' J' || \mathbf{D} || \gamma J \rangle}{(E_{\gamma J} - E_{\gamma'' J''})} \\
&\times \left[\frac{1}{(E_{\gamma J} - E_{\gamma' J'} + \omega)} + \frac{(-1)^K}{(E_{\gamma J} - E_{\gamma' J'} - \omega)} \right]. \tag{3.17}
\end{aligned}$$

Recoupling of the remaining three operators of Eq. (3.16) may be done in a similar manner, and corresponding reduced polarizabilities may be derived. The reduced polarizability for the center term is

$$\begin{aligned}
\alpha_{\gamma I J F; K}^{(3), \text{cen}} &= (2F+1)\sqrt{(2K+1)}\sqrt{I(I+1)(2I+1)}g_I\mu_N \\
&\times (-1)^{I-J-F+1} \sum_{J'' J'} \left\{ \begin{matrix} - & I & F & J \\ 1 & - & K & 1 \\ J' & 1 & - & J'' \\ J & I & F & - \end{matrix} \right\} \\
&\times \sum_{\gamma'' \gamma'} \langle \gamma J || \mathbf{D} || \gamma'' J'' \rangle \langle \gamma'' J'' || \mathcal{T} || \gamma' J' \rangle \langle \gamma' J' || \mathbf{D} || \gamma J \rangle \\
&\times \left[\frac{1}{(E_{\gamma J} - E_{\gamma'' J''} + \omega)(E_{\gamma J} - E_{\gamma' J'} + \omega)} \right. \\
&\quad \left. + \frac{(-1)^K}{(E_{\gamma J} - E_{\gamma'' J''} - \omega)(E_{\gamma J} - E_{\gamma' J'} - \omega)} \right], \tag{3.18}
\end{aligned}$$

where the term in curly braces is a 12- j symbol of the second kind (Appendix B; Ref. [83]). The reduced polarizability for the bottom term is simply

$$\alpha_{\gamma I J F; K}^{(3), \text{bot}} = \left(\alpha_{\gamma I J F; K}^{(3), \text{top}} \right)^*. \tag{3.19}$$

Finally, the reduced polarizability for the normalization term is

$$\begin{aligned}
\alpha_{\gamma I J F; K}^{(3), \text{nor}} &= (2F+1) \sqrt{(2K+1)} \sqrt{I(I+1)(2I+1)} g_{I\mu_N} \\
&\times (-1)^{2J+1} \begin{Bmatrix} I & I & 1 \\ J & J & F \end{Bmatrix} \begin{Bmatrix} K & J & J \\ I & F & F \end{Bmatrix} \langle \gamma J \| \mathbf{T} \| \gamma J \rangle \\
&\times \sum_{J'} \begin{Bmatrix} K & J & J \\ J' & 1 & 1 \end{Bmatrix} \sum_{\gamma'} \langle \gamma J \| \mathbf{D} \| \gamma' J' \rangle \langle \gamma' J' \| \mathbf{D} \| \gamma J \rangle \\
&\times \left[\frac{1}{(E_{\gamma J} - E_{\gamma' J'} + \omega)^2} + \frac{(-1)^K}{(E_{\gamma J} - E_{\gamma' J'} - \omega)^2} \right]. \tag{3.20}
\end{aligned}$$

The total third order reduced polarizability is

$$\alpha_{\gamma I J F; K}^{(3)} = \alpha_{\gamma I J F; K}^{(3), \text{top}} + \alpha_{\gamma I J F; K}^{(3), \text{cen}} + \alpha_{\gamma I J F; K}^{(3), \text{bot}} + \alpha_{\gamma I J F; K}^{(3), \text{nor}}. \tag{3.21}$$

Eqs. (3.12), which relate the second order reduced polarizabilities to the traditional second order polarizabilities, may be extended to the third order as well (taking $2 \rightarrow 3$ in those expressions). The third order energy shift may then be expressed in terms of polarization parameters \mathcal{A} , θ_k , and θ_p and the third order polarizabilities $\alpha_F^{\text{S},(3)}$, $\alpha_F^{\text{a},(3)}$, and $\alpha_F^{\text{T},(3)}$ as

$$\begin{aligned}
\delta E_{FM}^{(1,2)} &= \\
&- \left(\frac{\mathcal{E}}{2} \right)^2 \left[\alpha_F^{\text{S},(3)} + (\mathcal{A} \cos \theta_k) \frac{M}{2F} \alpha_F^{\text{a},(3)} + \left(\frac{3 \cos^2 \theta_p - 1}{2} \right) \frac{3M^2 - F(F+1)}{F(2F-1)} \alpha_F^{\text{T},(3)} \right].
\end{aligned}$$

This has precisely the same form as Eq. (3.14) for the second order, but with the appropriate third order polarizabilities in place of the second order polarizabilities.⁴

⁴It is rather straightforward to show that this may be generalized to all orders of $\delta E^{(n,2)}$. The corresponding operator $H^{(n,2)}$ contains terms of the form $(\dots)(\hat{\epsilon}^* \cdot \mathbf{D})(\dots)(\hat{\epsilon} \cdot \mathbf{D})(\dots)$, where

3.5 The ac Stark Shift Summarized

For the purposes of this research it is not necessary to proceed to an explicit analysis of fourth order perturbation theory. However, it is worth mentioning that beginning with the fourth order, terms which are higher than second order in V_{E1} start to appear. In particular, the terms fourth order in V_{E1} , $\delta E^{(n,4)}$, constitute the *hyperpolarizability* effects; these effects are small compared to the terms $\delta E^{(0,2)}$ and $\delta E^{(1,2)}$ analyzed in the previous two sections and need not be considered. For the remainder of the dissertation, δE is used with the understanding that only terms second order in V_{E1} are included (again terms zeroth order in V_{E1} are not of concern as they are not pertinent to hyperfine clock shifts). With this in mind, some of the main results of the previous sections are summarized here. The quantum numbers γIJ (corresponding to the model space) will be suppressed for clarity.

The energy shift may be written

$$\delta E_{FM}(\omega) = - \left(\frac{\mathcal{E}}{2} \right)^2 \left[\alpha_F^S(\omega) + (\mathcal{A} \cos \theta_k) \frac{M}{2F} \alpha_F^a(\omega) + \left(\frac{3 \cos^2 \theta_p - 1}{2} \right) \frac{3M^2 - F(F+1)}{F(2F-1)} \alpha_F^T(\omega) \right], \quad (3.22)$$

where dependence on the (angular) frequency of the plane electromagnetic wave is

(...) indicates some arbitrary combination of V_{hf} , resolvent, and projection operators. The (...) necessarily have scalar character, consequently such a term may always be recoupled as $\sum_K \{\hat{\mathbf{e}}^* \otimes \hat{\mathbf{e}}\}_K \cdot \{(\dots) \mathbf{D} \otimes (\dots) \mathbf{D}(\dots)\}_K$. As such, $\delta E^{(n,2)}$ can always be broken down into scalar, axial, and tensor parts with the respective polarization dependencies as seen for $\delta E^{(0,2)}$ and $\delta E^{(1,2)}$.

now made explicit. The parameters θ_k and θ_p satisfy

$$\begin{aligned}\cos\theta_k &= \hat{\mathbf{k}} \cdot \hat{\mathbf{e}}_z, \\ \cos^2\theta_p &= |\hat{\boldsymbol{\varepsilon}} \cdot \hat{\mathbf{e}}_z|^2.\end{aligned}$$

The scalar $\alpha_F^S(\omega)$, axial $\alpha_F^a(\omega)$, and tensor $\alpha_F^T(\omega)$ polarizabilities are related to the corresponding ‘‘reduced’’ polarizabilities $\alpha_{F;K}(\omega)$ by

$$\begin{aligned}\alpha_F^S(\omega) &= \frac{1}{\sqrt{3(2F+1)}}\alpha_{F;K=0}(\omega), \\ \alpha_F^a(\omega) &= -\sqrt{\frac{2F}{(2F+1)(F+1)}}\alpha_{F;K=1}(\omega), \\ \alpha_F^T(\omega) &= -\sqrt{\frac{2F(2F-1)}{3(2F+1)(F+1)(2F+3)}}\alpha_{F;K=2}(\omega).\end{aligned}\tag{3.23}$$

Eqs. (3.22, 3.23) may be taken on an order-by-order basis with the leading order being the second order. Explicit expressions for the second and third order reduced polarizabilities are given by Eqs. (3.11, 3.17, 3.18, 3.19, 3.20, 3.21) and will not be repeated here.

At times throughout this dissertation, the polarizability $\alpha_{FM}(\omega)$ will be used:

$$\alpha_{FM}(\omega) = \alpha_F^S(\omega) + (\mathcal{A}\cos\theta_k)\frac{M}{2F}\alpha_F^a(\omega) + \left(\frac{3\cos^2\theta_p - 1}{2}\right)\frac{3M^2 - F(F+1)}{F(2F-1)}\alpha_F^T(\omega).$$

Note that $\alpha_{FM}(\omega)$ implicitly depends on the polarization parameters \mathcal{A} , θ_k , and θ_p .

The energy shift may then be written

$$\delta E_{FM}(\omega) = -\left(\frac{\mathcal{E}}{2}\right)^2 \alpha_{FM}(\omega).$$

The clock shift due to the presence of the electromagnetic wave is given by

$$\delta\nu(\omega) = \frac{1}{2\pi} [\delta E_{F'M'}(\omega) - \delta E_{FM}(\omega)] = -\frac{1}{2\pi} \left(\frac{\mathcal{E}}{2}\right)^2 [\alpha_{F'M'}(\omega) - \alpha_{FM}(\omega)], \quad (3.24)$$

where FM ($F'M'$) labels the lower (upper) hyperfine clock level.

3.6 The 1D Optical Lattice Trap

In this section, the expressions derived above for the ac Stark effect are used to show how atoms may be trapped in the intermediary region of two counter-propagating lasers. These so-called optical lattice traps are reviewed in Ref. [12].

From Eq. (3.1), it follows that the superposition of electric fields for two plane electromagnetic waves is

$$\mathcal{E}(\mathbf{r}, t) = \frac{1}{2} [\mathcal{E}_1 \hat{\boldsymbol{\epsilon}}_1 e^{-i(\omega_1 t - \mathbf{k}_1 \cdot \mathbf{r})} + \mathcal{E}_2 \hat{\boldsymbol{\epsilon}}_2 e^{-i(\omega_2 t - \mathbf{k}_2 \cdot \mathbf{r})}] + \text{c.c.}$$

In particular, for⁵

$$\mathbf{k}_1 = -\mathbf{k}_2 \equiv \mathbf{k} \quad (\omega_1 = \omega_2 \equiv \omega), \quad \hat{\boldsymbol{\epsilon}}_1 = \hat{\boldsymbol{\epsilon}}_2 \equiv \hat{\boldsymbol{\epsilon}}, \quad \mathcal{E}_1 = \mathcal{E}_2 \equiv \frac{\mathcal{E}}{2}, \quad (3.25)$$

⁵Note that $-i(\hat{\boldsymbol{\epsilon}}_1^* \times \hat{\boldsymbol{\epsilon}}_1) \cdot \hat{\mathbf{k}}_1 = i(\hat{\boldsymbol{\epsilon}}_2^* \times \hat{\boldsymbol{\epsilon}}_2) \cdot \hat{\mathbf{k}}_2$, which is to say $\mathcal{A}_1 = -\mathcal{A}_2$. With the association $\mathcal{A} = -i(\hat{\boldsymbol{\epsilon}}^* \times \hat{\boldsymbol{\epsilon}}) \cdot \hat{\mathbf{k}}$, then one further obtains $\mathcal{A}_1 = -\mathcal{A}_2 \equiv \mathcal{A}$. Furthermore, one should note that the intensities for the individual lasers are $|\mathbf{S}_1| = |\mathbf{S}_2| = \frac{c}{8\pi} \left(\frac{\mathcal{E}}{2}\right)^2 = \frac{1}{4} \frac{c}{8\pi} \mathcal{E}^2$.

this is

$$\begin{aligned}
\mathcal{E}(\mathbf{r}, t) &= \frac{1}{2} \left[\frac{\mathcal{E}}{2} \hat{\mathbf{e}} e^{-i(\omega t - \mathbf{k} \cdot \mathbf{r})} + \frac{\mathcal{E}}{2} \hat{\mathbf{e}} e^{-i(\omega t + \mathbf{k} \cdot \mathbf{r})} \right] + \text{c.c.} \\
&= \frac{1}{2} \mathcal{E} \hat{\mathbf{e}} e^{-i\omega t} \left[\frac{e^{i\mathbf{k} \cdot \mathbf{r}} + e^{-i\mathbf{k} \cdot \mathbf{r}}}{2} \right] + \text{c.c.} \\
&= \cos(\mathbf{k} \cdot \mathbf{r}) \left[\frac{1}{2} \mathcal{E} \hat{\mathbf{e}} e^{-i\omega t} + \text{c.c.} \right] \\
&= \cos(\mathbf{k} \cdot \mathbf{r}) \bar{\mathcal{E}}(t),
\end{aligned}$$

where $\bar{\mathcal{E}}(t)$ is equivalent to the uniform oscillating electric field of Eq. (3.2). The spatial-dependent factor $\cos(\mathbf{k} \cdot \mathbf{r})$ here describes a *standing wave*. This standing wave is also referred to as a 1D optical lattice.

Within the long-wavelength regime, an atom again effectively “sees” a uniform oscillating field. For the previously considered case of a single plane electromagnetic wave, the *local* field seen by the atom did not depend on the particular position of the atom in space (moving the atom in the $\pm \hat{\mathbf{k}}$ -direction would again amount only to a time-delay). However, for the current case of a standing wave, the *local* field seen by the atom now depends on the position of the atom in space by the factor $\cos(\mathbf{k} \cdot \mathbf{r})$. The expressions derived in the previous sections for the energy shift of an atom in the presence of a plane electromagnetic wave are applicable to this standing wave case as well. One needs only to generalize now to the local field of the standing wave; mathematically this is implemented by taking $\mathcal{E} \rightarrow \mathcal{E} \cos(\mathbf{k} \cdot \mathbf{r})$. In particular, the energy shift for an atom at position \mathbf{r} is given by

$$\delta E_{FM}(\mathbf{r}, \omega) = -\cos^2(\mathbf{k} \cdot \mathbf{r}) \left(\frac{\mathcal{E}}{2} \right)^2 \alpha_{FM}(\omega). \quad (3.26)$$

This spatial-dependence of the energy can be associated with a potential $U(\mathbf{r}) = \delta E_{FM}(\mathbf{r}, \omega)$, which then governs the center-of-mass motion of the atom. For $\alpha_{FM}(\omega) >$

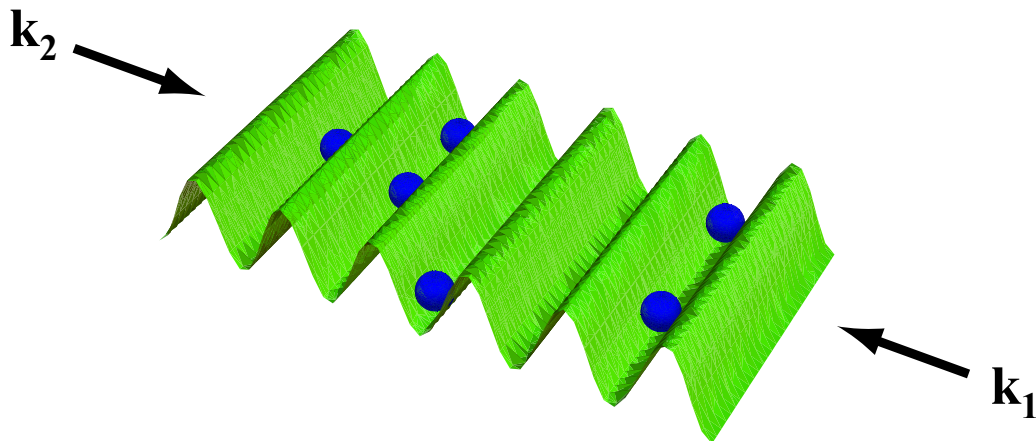


Figure 3.5: (Color online) Illustration of a 1D optical lattice trap. The counter-propagating plane waves give rise to potential wells (green) which are capable of constraining atoms (blue) in the axial direction. In practice, a varying beam waist of the lasers confines the atoms in the radial direction as well.

0, this potential has minima at positions $\mathbf{k} \cdot \mathbf{r} = n\pi$ (n being an integer), corresponding to regions of maximum intensity in the optical lattice (i.e., the anti-nodes of the standing wave). For $\alpha_{FM}(\omega) < 0$, the potential has minima at positions $\mathbf{k} \cdot \mathbf{r} = (n + 1/2)\pi$, corresponding to regions of zero intensity in the optical lattice (i.e., the nodes of the standing wave). In either scenario, the planes in space corresponding to the potential minima are separated by $\lambda/2$, where $\lambda = 2\pi c/\omega$ is the wavelength of the counter-propagating plane waves. Furthermore, the depth of the potential wells is given by $(\mathcal{E}/2)^2 |\alpha_{FM}(\omega)|$ in both cases. For a large enough trap depth (i.e., intensity), atoms may be trapped in the potential minima with negligible tunneling between wells. This is referred to as a 1D optical lattice trap. A 1D optical lattice trap is depicted in Figure 3.5.

The potential $U(\mathbf{r})$ determines the translational (vibrational) modes of the optical lattice trap. In general, the confining potential $U(\mathbf{r})$ associated with a given atomic

level $|FM\rangle$ does not precisely match the confining potential $U'(\mathbf{r})$ associated with a different atomic level $|F'M'\rangle$. As a result, the energy associated with a given transition between states must account for energy differences in the vibrational levels in addition to the energy associated with the Stark-perturbed atomic transition. It is a convenient consequence, however, that if the magic condition is satisfied for the atomic transition (the magic condition being $\alpha_{F'M'}(\omega) = \alpha_{FM}(\omega)$ and thus no relative Stark shift), then the trapping potentials are subsequently identical—i.e., $U'(\mathbf{r}) = U(\mathbf{r})$ —and there is no difference in vibrational levels.⁶

This concludes the general discussion of the ac Stark effect. In the following chapters, the formulae derived above are utilized for in for applications to microwave atomic clocks. Namely, this includes a high-accuracy calculation of the blackbody radiation shift in the ^{133}Cs primary frequency standard (Chapter 4) and a proposal for microwave atomic clocks based on ^{27}Al or $^{69,71}\text{Ga}$ atoms in an engineered optical lattice (Chapter 5).

⁶Taichenachev *et al.* [78] have, however, recently pointed out that magnetic dipole ($M1$) and electric quadrupole ($E2$) interactions cause shifts in the trap levels which may in fact be significant at the level of precision of current optical lattice clocks.

Chapter 4

High-Accuracy Calculation of the Blackbody Radiation Shift in the ^{133}Cs Primary Frequency Standard

4.1 Introduction

In principle, an ideal atomic clock measures a transition frequency for an atom which is completely decoupled from its environment. In practice, however, the atomic sample is subject to thermal radiation from its surroundings (among other things). The electric field associated with this blackbody radiation (BBR) perturbs the atomic sample in accordance with the theory of the ac Stark effect presented in the previous Chapter.

As was mentioned in Chapter 1, the definition of the SI second makes specific reference to a ^{133}Cs atom at a temperature of 0 K—that is, a ^{133}Cs atom in the absence of BBR. For ^{133}Cs frequency standards operating at room temperature, the presence of the BBR necessitates a substantial systematic correction as the fractional

clock shift is of the order 10^{-14} . Moreover, recently there has been some controversy over the precise size of this shift. At a temperature of 300 K, the values from various groups [74, 27, 41, 54, 82] differ at the 10^{-15} level, while modern Cs clocks aim at accuracies better than 10^{-16} .

The persistent discrepancies in the BBR shift have prompted the efforts at the US National Institute for Standards and Technology (NIST) on removing the sensitivity to BBR by operating the primary standard at cryogenic temperatures [31, 44]. However, because of the weight limitations, this direct approach would hardly be feasible if a next-generation atomic clock were to be operated at the International Space Station [38]. This ongoing controversy and implications for atomic time-keeping serve as motivations for this work. Here, results are presented for a calculation of the ^{133}Cs BBR shift based on high-accuracy relativistic many-body techniques of atomic structure. The evaluated uncertainty for this calculation implies a 6×10^{-17} fractional uncertainty in the clock frequency with the value of the BBR shift consistent with the most accurate (0.2%-accurate) measurement [74]. However, the obtained 0.35%-accurate value is in a substantial (10%) disagreement with recent semi-empirical calculations [54, 82]. It is shown that this discrepancy is due to contributions of the intermediate continuum states omitted in those calculations.

4.2 Problem Set-Up

The blackbody radiation is assumed to be isotropic; qualitatively this implies that the atomic system can have no preferential direction in space. From this it further follows that the BBR clock shift may be described completely by the scalar polarizability (contributions from the axial and tensor polarizabilities are “washed out” due to their directional-dependencies). As such, the problem begins with consideration of

the second order scalar polarizability. Taking $K = 0$ in Eq. (3.11) yields the simplified expression

$$\alpha_F^{S,(2)}(\omega) = \frac{1}{3(2J+1)} \sum_{\gamma'J'} (-1)^{J-J'+1} \langle \gamma J || \mathbf{D} || \gamma' J' \rangle \langle \gamma' J' || \mathbf{D} || \gamma J \rangle \times \left[\frac{1}{E_{\gamma J} - E_{\gamma' J'} + \omega} + \frac{1}{E_{\gamma J} - E_{\gamma' J'} - \omega} \right]. \quad (4.1)$$

Note that $\alpha_F^{S,(2)}(\omega)$ does not depend on F . As a result, the following conclusion applies to a general atomic system: there is no *relative* energy shift associated with the second order scalar polarizability between the levels of a given hyperfine manifold.¹ This realization will be useful in Chapter 5 as well. Thus, the leading effect is from the third order scalar polarizability. Taking $K = 0$ in Eqs. (3.17—3.20) it is found that the third order scalar polarizability may be parameterized as

$$\alpha_F^{S,(3)}(\omega) = \frac{2}{3} \sqrt{I(I+1)(2I+1)} g_I \mu_N (-1)^{I+J+F} \begin{Bmatrix} I & J & F \\ J & I & 1 \end{Bmatrix} \times [T(\omega) + C(\omega) + B(\omega) + N(\omega)], \quad (4.2)$$

where the terms $T(\omega)$, $C(\omega)$, $B(\omega)$, and $N(\omega)$ are independent of F (and I , for that matter). The term $T(\omega)$, which corresponds to the contribution of the top term, is given by

$$T(\omega) = \frac{1}{2} \frac{1}{(2J+1)} \sum_{\gamma''J''\gamma'J'} (-1)^{J-J'+1} \frac{\langle \gamma J || \mathbf{T} || \gamma'' J'' \rangle \langle \gamma'' J'' || \mathbf{D} || \gamma' J' \rangle \langle \gamma' J' || \mathbf{D} || \gamma J \rangle}{(E_{\gamma J} - E_{\gamma'' J''})} \times \left[\frac{1}{(E_{\gamma J} - E_{\gamma' J'} + \omega)} + \frac{1}{(E_{\gamma J} - E_{\gamma' J'} - \omega)} \right] \delta_{J''J}.$$

¹It should be emphasized that this statement applies to the perturbation formalism of this dissertation, in which the zeroth order atomic states are unperturbed by the hyperfine interaction.

The contribution from the center term is given by

$$C(\omega) = \frac{1}{2} \sum_{\gamma'' J'' \gamma' J'} (-1)^{J''+J'+1} \begin{Bmatrix} J'' & 1 & J' \\ J & 1 & J \end{Bmatrix} \langle \gamma J \| \mathbf{D} \| \gamma'' J'' \rangle \langle \gamma'' J'' \| \mathcal{T} \| \gamma' J' \rangle \langle \gamma' J' \| \mathbf{D} \| \gamma J \rangle \times \left[\frac{1}{(E_{\gamma J} - E_{\gamma'' J''} + \omega)(E_{\gamma J} - E_{\gamma' J'} + \omega)} + \frac{1}{(E_{\gamma J} - E_{\gamma'' J''} - \omega)(E_{\gamma J} - E_{\gamma' J'} - \omega)} \right].$$

The contribution from the bottom term is given by

$$B(\omega) = [T(\omega)]^*.$$

And the contribution from the normalization term is given by

$$N(\omega) = \frac{1}{2} \frac{\langle \gamma J \| \mathcal{T} \| \gamma J \rangle}{(2J+1)} \sum_{\gamma' J'} (-1)^{J-J'} \langle \gamma J \| \mathbf{D} \| \gamma' J' \rangle \langle \gamma' J' \| \mathbf{D} \| \gamma J \rangle \times \left[\frac{1}{(E_{\gamma J} - E_{\gamma' J'} + \omega)^2} + \frac{1}{(E_{\gamma J} - E_{\gamma' J'} - \omega)^2} \right].$$

For the ^{133}Cs ground state, the nuclear and electronic angular momenta are given by $I = 7/2$ and $J = 1/2$, respectively. The state with $F = I - J = 3$ ($F = I + J = 4$) is known to be the lower (upper) level of the hyperfine doublet. These values may be used to reduce the prefactor of Eq. (4.2), giving

$$\begin{aligned} \alpha_{F=3}^{\text{S},(3)}(\omega) &= -\frac{3}{\sqrt{6}} g_I \mu_N [T(\omega) + C(\omega) + B(\omega) + N(\omega)], \\ \alpha_{F=4}^{\text{S},(3)}(\omega) &= \frac{7}{3\sqrt{6}} g_I \mu_N [T(\omega) + C(\omega) + B(\omega) + N(\omega)]. \end{aligned} \quad (4.3)$$

The nuclear gyromagnetic ratio g_I for ^{133}Cs is found from Table 2.1 to be $g_I = 0.7380$.

At room temperature, the characteristic photon frequency of the blackbody spec-

trum is much lower than the allowed electric dipole transition frequencies of the ^{133}Cs atom; as a consequence, the overall BBR shift may be accurately described in terms of the *static* scalar polarizability. The static scalar polarizability is obtained from the taking $\omega = 0$ in the above expressions. With this in mind, the following association will be made for the remainder of this chapter: $T = T(\omega)|_{\omega=0}$ and similar for C and N . Furthermore T will be assumed real from this point (i.e., $B = T$).²

For an independent-particle model (i.e., the wavefunctions are represented by Slater determinants; see Appendix E), T , C , and N may be cast in terms of single

²If this assumption seems to brash, one may simply make the association $T = \text{Re}[T(\omega)]|_{\omega=0}$. For the numerical evaluation T will be real.

particle matrix elements and energies as³

$$\begin{aligned}
T &= \frac{1}{(2j_v + 1)} \sum_{kl \neq v} (-1)^{j_v - j_l + 1} \frac{\langle v || \mathbf{t} || k \rangle \langle k || \mathbf{r} || l \rangle \langle l || \mathbf{r} || v \rangle}{(\varepsilon_v - \varepsilon_k)(\varepsilon_v - \varepsilon_l)} \delta_{\kappa_k \kappa_v}, \\
C &= \sum_{kl \neq v} (-1)^{j_k + j_l + 1} \begin{Bmatrix} j_k & 1 & j_l \\ j_v & 1 & j_v \end{Bmatrix} \frac{\langle v || \mathbf{r} || k \rangle \langle k || \mathbf{t} || l \rangle \langle l || \mathbf{r} || v \rangle}{(\varepsilon_v - \varepsilon_k)(\varepsilon_v - \varepsilon_l)}, \\
N &= \frac{\langle v || \mathbf{t} || v \rangle}{(2j_v + 1)} \left(\sum_{k \in \text{core}} - \sum_{k \in \text{virt}} \right) (-1)^{j_v - j_k} \frac{\langle v || \mathbf{r} || k \rangle \langle k || \mathbf{r} || v \rangle}{(\varepsilon_v - \varepsilon_k)^2}, \quad (4.4)
\end{aligned}$$

where v , k , and l label single-particle orbitals with v in particular denoting the valence orbital. The summations over k and l include all orbitals (core and virtual) with the exception of v . With each orbital taken to be a Dirac spinor in the form of Eq. (E.16), the labels then specify the quantum numbers (n, κ) of the spinor. Specifically, the valence electron for the Cs ground state is $|v\rangle = |6s_{1/2}\rangle$. The reduced matrix elements $\langle i || \mathbf{r} || j \rangle$ and $\langle i || \mathbf{t} || j \rangle$ appearing in these equations are the single-particle reduced matrix elements for the electric dipole and (electronic) hyperfine interaction operators. Expressions for these reduced matrix elements between Dirac spinors are given in Section E.10 of the Appendix. Selection rules impose the following limitations on

³The independent-particle model T , C , and N here actually redistribute the contributions from core-excited intermediate states. For example, the following two summations represent core-excited terms contributing to the center term and bottom term, respectively:

$$\sum_{as} \frac{\langle a || \mathbf{r} || s \rangle \langle v || \mathbf{t} || a \rangle \langle s || \mathbf{r} || v \rangle}{(\varepsilon_s - \varepsilon_a)(\varepsilon_v - \varepsilon_s)}, \quad \sum_{as} \frac{\langle a || \mathbf{r} || s \rangle \langle s || \mathbf{r} || v \rangle \langle v || \mathbf{t} || a \rangle}{(\varepsilon_s - \varepsilon_a)(\varepsilon_a - \varepsilon_v)},$$

where the summation over a is limited to core orbitals and the summation over s is limited to virtual orbitals. With some basic algebraic tricks, these two terms taken together may be written

$$\sum_{as} \frac{\langle v || \mathbf{t} || a \rangle \langle a || \mathbf{r} || s \rangle \langle s || \mathbf{r} || v \rangle}{(\varepsilon_v - \varepsilon_a)(\varepsilon_v - \varepsilon_s)}.$$

This term is then associated with the top term in the independent-particle expressions. Although these core-excited effects are redistributed, the sum $(2T + C + N)$ still contains all such contributions. Furthermore, as contributions from core-excited intermediate states are highly suppressed, the T , C , and N should not be altered significantly by this redistribution.

the angular symmetries of the intermediate states: $s_{1/2}$ for $|k\rangle$, $p_{1/2,3/2}$ for $|l\rangle$ in the top term, $p_{1/2,3/2}$ for both $|k\rangle$ and $|l\rangle$ in the center term, and $p_{1/2,3/2}$ for $|k\rangle$ in the normalization term.

The third order polarizabilities $\alpha_{F=3,4}^{S,(3)}(0)$ provide the underlying description of the atomic response to the blackbody radiation. In the context of the BBR clock shift, however, results are conventionally presented in terms of the BBR coefficient β and/or the scalar Stark coefficient k_s to be discussed below.

The electromagnetic energy density inside a box with perfectly conductive walls is given by $u = \alpha^3 \pi^2 T_{\text{env}}^4 / 15$, where α is the fine structure constant and T_{env} is the temperature. This may be related to the (time-averaged) energy density of a plane electromagnetic wave, $u = \mathcal{E}^2 / 8\pi$, to obtain a characteristic electric field amplitude for the blackbody radiation of $\mathcal{E}^2 = 8\alpha^3 \pi^3 T_{\text{env}}^4 / 15$.⁴ Employing Eq. (3.24), the relative BBR clock shift is then seen to be

$$\frac{\delta\nu^{\text{BBR}}}{\nu} = -\frac{\alpha^3 \pi^2 T_{\text{env}}^4}{15\nu} \left[\alpha_{F=4}^{S,(3)}(0) - \alpha_{F=3}^{S,(3)}(0) \right].$$

This relative shift may be parameterized in terms of the dimensionless BBR coefficient β ,

$$\frac{\delta\nu^{\text{BBR}}}{\nu} = \beta \left(\frac{T_{\text{env}}}{T_0} \right)^4, \quad (4.5)$$

with the reference temperature of $T_0 = 300 \text{ K} = 9.500 \times 10^{-4} \text{ a.u.}$ ⁵ By comparison of

⁴Itano *et al.* [29] choose to work with the (root)-mean-squared field, $\mathcal{E}_{\text{rms}}^2 = 4\alpha^3 \pi^3 T_{\text{env}}^4 / 15$. The factor of two difference is accounted for by their choice to use the static Stark equation $\delta E_{FM} = (\mathcal{E}^2/2)\alpha_F^S(0)$ (here \mathcal{E} being the magnitude of the static electric field) as opposed to the ac Stark equation $\delta E_{FM} = (\mathcal{E}/2)^2 \alpha_F^S(0)$ (here \mathcal{E} being the amplitude of the ac electric field with $\omega \rightarrow 0$).

⁵In their seminal paper on the BBR clock shift, Itano *et al.* also gave consideration to the effects of the frequency distribution of the BBR spectrum. It was determined therein that the frequency-dependence of the polarizability could be accounted for by including the small corrective factor ϵ in

the two previous expressions, one may easily deduce the relation for β ,

$$\beta = \frac{4}{15} \frac{(\alpha\pi)^3 T_0^4}{\nu} k_s, \quad k_s = -\frac{1}{4\pi} \left[\alpha_{F=4}^{S,(3)}(0) - \alpha_{F=3}^{S,(3)}(0) \right], \quad (4.6)$$

where k_s introduced here is the scalar Stark coefficient (k_s is dimensionally the same as $\alpha_F^S(\omega)$ —namely, energy divided by electric field squared). Results below will be given both in terms of β and k_s ; it should be noted that these two quantities are related by a simple constant factor. For ^{133}Cs , with $\nu = 9.193 \times 10^9 \text{ Hz} = 2.224 \times 10^{-7} \text{ a.u.}$, the conversion factor is $k_s/\beta = 8.495 \times 10^{10} \text{ a.u.} = 1.327 \times 10^4 \text{ Hz}/(\text{V/m})^2$. From Eqs. (4.3, 4.6) it is found that the scalar Stark coefficient for ^{133}Cs may be written

$$k_s = -\frac{4}{\pi 3\sqrt{6}} g_I \mu_N (2T + C + N).$$

4.3 Results and Discussion

To obtain an initial approximation of k_s , Eqs. (4.4) were solved within the V^{N-1} DHF approximation (Appendix E) using a finite basis set built from B-spline functions (Appendix F). The B-spline set consisted of 70 B-splines of order 7 having a maximum extent of $R_{\text{cav}} = 220 \text{ a.u.}$ As discussed in Appendix F, the finite extent of the B-splines may be associated with an infinite potential wall at $r = R_{\text{cav}}$ (in common terminology, the atom is constrained to a cavity of radius R_{cav}). The large choice of R_{cav} here ensures that the lowest energy states of the atom are unperturbed by the presence of the cavity wall. In particular, the lowest 12 eigenstates for each

Eq. (4.5),

$$\frac{\delta\nu^{\text{BBR}}}{\nu} = \beta \left(\frac{T_{\text{env}}}{T_0} \right)^4 \left[1 + \epsilon \left(\frac{T_{\text{env}}}{T_0} \right)^2 \right],$$

For ^{133}Cs , ϵ was determined to be 1.4×10^{-2} .

κ are found to produce energies and matrix elements which are in close numerical agreement with data from a finite-difference DHF code (i.e., DHF solutions for no cavity). As a consequence, the low-energy DHF states obtained from the finite basis set method may be given a one-to-one correspondence with true physical states of the unconstrained atom. The higher-energy states of the finite basis spectrum may then successfully account for the remaining innumerable (bound and continuous) spectrum in the summations of Eqs. (4.4), as described in Appendix F.

Numerical evaluation of k_s —that is, Eqs. (4.4)—in the DHF approximation produces the result

$$k_s^{\text{DHF}} = -2.799 \times 10^{-10} \text{ Hz}/(\text{V/m})^2.$$

The fractional contributions of the individual terms are $\left(\frac{2T}{2T+C+R}\right)^{\text{DHF}} = 0.418$, $\left(\frac{C}{2T+C+R}\right)^{\text{DHF}} = 0.003$, and $\left(\frac{R}{2T+C+R}\right)^{\text{DHF}} = 0.580$. It is clear that the top (bottom) and normalization terms dominate over the center term. The bulk (99.8%) of the normalization term is accumulated due to the principal $6s_{1/2} - 6p_{1/2,3/2}$ transitions in the summation. For the top term, the saturation of the summation is not as rapid, but still the dominant contributions come from the lowest-energy excitations. Limiting the summations to the first four excited states for each κ recovers only 68% of the total value for the top term. Additionally, core-excited states contribute only 0.1% to the final value.

The above observations determine the strategy for more accurate calculations. The entire set of atomic states are grouped into “main” low-lying-energy states (principal quantum numbers $n \leq 12$) and remaining “tail” states. The contributions from the “main” states are accounted for by using high-accuracy experimental and *ab initio* values. The contributions from the “tail” states are obtained by using either the DHF values or a mixed approach.

First, the high-accuracy data used in the calculations will be described. Namely,

dipole and hyperfine matrix elements and energies are needed. Experimental values for the dipole matrix elements for the following six transitions were taken from the literature (see compilations in Refs. [68, 54]): $6s_{1/2} - 6p_{1/2,3/2}$, $7s_{1/2} - 6p_{1/2,3/2}$, $7s_{1/2} - 7p_{1/2,3/2}$. Crucial to the accuracy of the present analysis were the matrix elements for the principal $6s_{1/2} - 6p_{1/2,3/2}$ transitions. For $\langle 6s_{1/2} || \mathbf{D} || 6p_{3/2} \rangle$, a 0.005%-accurate value from Ref. [1] was used.⁶ The value for $\langle 6s_{1/2} || \mathbf{D} || 6p_{1/2} \rangle$ was obtained by combining the above $6s_{1/2} - 6p_{3/2}$ matrix element and a 0.03%-accurate measured ratio [61] of these matrix elements. These six experimental matrix elements were supplemented by 92 values ($n s_{1/2} - n' p_{1/2,3/2}$ values for $n, n' = 6 - 12$) from high-accuracy *ab initio* calculations based on the relativistic linearized coupled-cluster singles-doubles (LCCSD) method. The underlying formalism, implementation, and results for alkali atoms are described in Ref. [68]. For dipole matrix elements the accuracy of the *ab initio* LCCSD method is a few 0.1%.

As to the high-accuracy values of the matrix elements of the hyperfine coupling, the diagonal matrix elements of the \mathcal{T} tensor are directly related to the conventional hyperfine constants: $A_{\text{hfs}} = g_I \mu_N / j_v [(2j_v)/(2j_v + 1)/(2j_v + 2)]^{1/2} \langle v || \mathcal{T} || v \rangle$. For the “main” $n = 6 - 12$ states, hyperfine constants were borrowed from the compilation of Ref. [3]. Off-diagonal matrix elements between the s -states were evaluated using the geometric-mean formula

$$\left| \langle n s_{1/2} || \mathcal{T} || n' s_{1/2} \rangle \right| = \left| \langle n s_{1/2} || \mathcal{T} || n s_{1/2} \rangle \langle n' s_{1/2} || \mathcal{T} || n' s_{1/2} \rangle \right|^{1/2}.$$

This expression has been shown to hold to about 10^{-3} in Ref. [22] (radiative cor-

⁶In the form $\langle 6s_{1/2} || \mathbf{D} || 6p_{3/2} \rangle$, the states $|6s_{1/2}\rangle$ and $|6p_{3/2}\rangle$ represent the true many-body states in which there is no core-excitation. The corresponding single-particle matrix elements are simply $\langle 6s_{1/2} || -\mathbf{r} || 6p_{3/2} \rangle$.

rections would start to play a role at a few 0.1% as well). If the principal quantum number $6 \leq n \leq 12$ in the above expression, then the experimental value is used for its corresponding diagonal element on the right-hand side of the equality. If also $6 \leq n' \leq 12$, then the appropriate experimental value is also used for the corresponding diagonal element on the right-hand side, otherwise the DHF value is taken. (n and n' can be obviously interchanged in this prescription.) This mixed approach has allowed a uniform improvement in the accuracy of the calculations. Indeed, in the numerically important top term, the hyperfine matrix elements come in the combination $\langle n s_{1/2} \| \mathcal{T} \| 6 s_{1/2} \rangle$. As n grows, the correlations become less important, so the dominant correlation correction comes from the $6 s_{1/2}$ state. Using the described mixed approach accounts for these dominant correlations. The geometric-mean formula holds only for the s states. For the off-diagonal matrix elements between various combinations of $6 p_{1/2,3/2}$ and $n p_{1/2,3/2}$ ($n = 6 - 9$) states, an augmented LCCSD method was employed which incorporates a perturbative treatment of the valence triple excitations (LCCSDpvT method) [68]. The accuracy of these matrix elements is a few percent. As these matrix elements enter the relatively small center term, the effect on the overall theoretical error is negligible.

Finally, experimental energy values from the NIST tabulation [55] were used for states with principal quantum number $n = 6 - 12$; DHF values were used otherwise.

With this described set, the scalar Stark coefficient and BBR coefficient were evaluated to be

$$\begin{aligned} k_s &= -(2.271 \pm 0.008) \times 10^{-10} \text{ Hz}/(\text{V/m})^2, \\ \beta &= -(1.710 \pm 0.006) \times 10^{-14}. \end{aligned} \tag{4.7}$$

The fractional contributions of the individual terms are $\frac{2T}{2T+C+R} = 0.442$, $\frac{C}{2T+C+R} =$

-0.002 , and $\frac{R}{2T+C+R} = 0.560$. When comparing with the DHF values, the most substantial modification due to correlations is in the center term, which changes the sign. Fortunately, this term is relatively small, and this extreme change does not substantially affect the final result.

The overall uncertainty of the results was determined from the uncertainties of the individual matrix elements and energy values used in the computation. Standard uncertainty analysis was done throughout all mathematical operations. For energy values taken from NIST, the uncertainty is assumed negligible. For all other experimental values, the reported uncertainty is used. The *ab initio* matrix elements (DHF, LCCSD, or LCCSDpvT) were assigned an assumed uncertainty. These assumed uncertainties were based on comparison between calculated and high-accuracy experimental values. This resulted in a relative uncertainty for both the scalar Stark coefficient and the BBR shift of 0.35%. Several consistency checks were also performed—e.g., replacing experimental matrix elements and energies by *ab initio* LCCSD values or replacing the DHF values for states with $n = 13 - 27$ with the LCCSD values. The final result was stable to such modifications within the stated uncertainty in Eq. (4.7). These tests provide additional confidence with respect to the method of uncertainty analysis. It is also worth noting that the present calculation does not include radiative corrections which may contribute at the level of a few 0.1% (some radiative corrections—e.g., vacuum polarization—are absorbed into the final value here already as *experimental* hyperfine constants were used).

A comparison with recent theoretical and experimental work is presented in Table 4.3 and Figure 4.1. While agreeing with the most accurate measurement by Simon *et al.* [74], the present results are in substantial disagreement with the calculations of Refs. [54, 82]. The principal differences between the present work and those calculations are: (i) more sophisticated treatment of correlations, and (ii) rigorous

Table 4.1: Values of the scalar Stark coefficient k_s for ^{133}Cs reported by various groups in units of $10^{-10} \text{ Hz}/(\text{V}/\text{m})^2$. Letters (a)—(e) correspond to the values in Figure 4.1.

Approach	k_s [$10^{-10} \text{ Hz}/(\text{V}/\text{m})^2$]	References
theory	-1.97 ± 0.09	Ref. [54], (c)
theory	-2.06 ± 0.01	Ref. [82], (e)
theory	-2.28	Ref. [58], (b)
expt.	-2.05 ± 0.04	Ref. [27], (d)
expt.	-2.271 ± 0.004	Ref. [74], (a)
theory	-2.271 ± 0.008	present

summation over the *complete* set of intermediate states in perturbative expressions. As discussed above, the method here employed the numerically complete basis-set approach which approximates Rydberg states and the continuum with a quasi-spectrum. To illuminate the importance of these contributions, the summations were truncated at $n = 12$. The resulting value deviates from the final k_s result by 7%. The fact that continuum needs to be included is hardly surprising, as, for example, about 20% of the textbook polarizability of the ground state of the hydrogen atom comes from the continuum states. Calculations of Ref. [58] include the continuum via a Green’s function technique and the result given therein is in agreement with the value obtained here.

To conclude, reported here are the results of a relativistic many-body calculation of the BBR shift, one of the leading systematic corrections in the ^{133}Cs frequency standard and a subject of recent controversy. The 0.35%-accurate result presented here re-validates high-precision Stark shift measurements of Ref. [74]. This work also clarifies the origin of the reported discrepancy between that measurement and recent calculations of Refs. [54, 82].

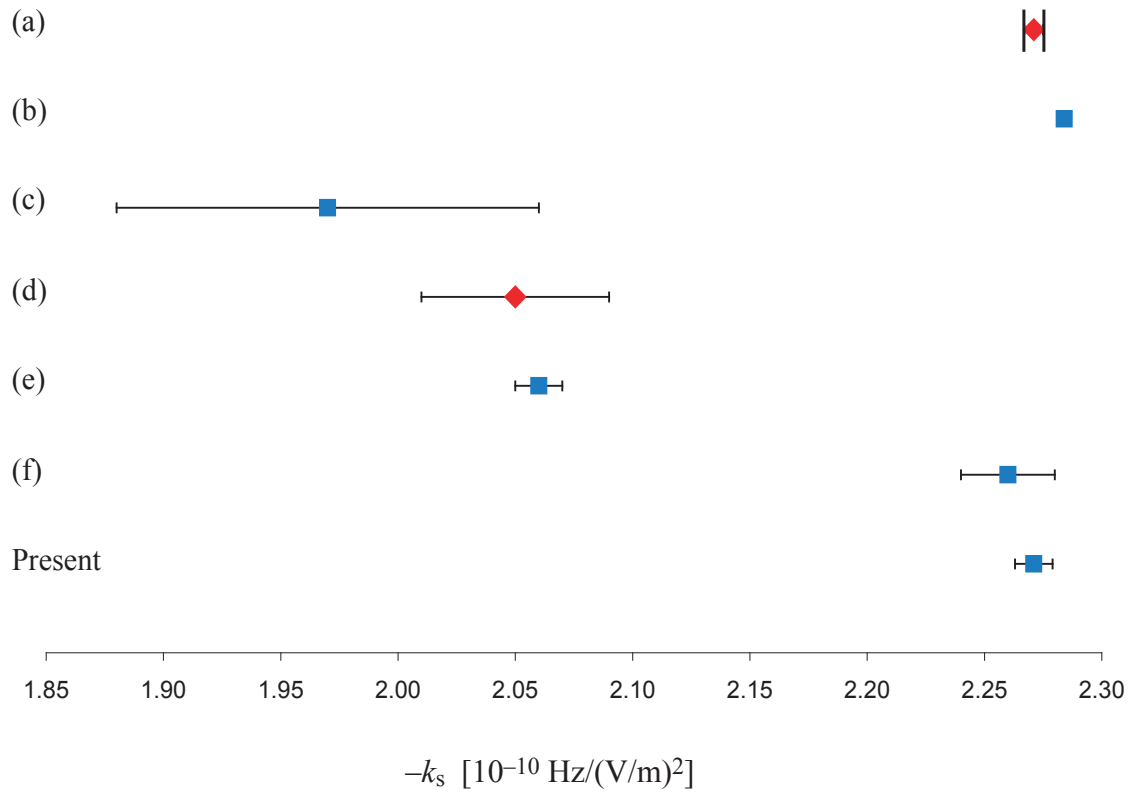


Figure 4.1: (Color online) Values of the scalar Stark coefficient k_s for ^{133}Cs reported by various groups. Red diamonds mark experimental values and blue squares mark theoretical values. References for (a)—(e) are given in Table 4.3. Value (f) is from Ref. [2]; this value was published at the same time as the present value in consecutive Physical Review Letters. The values are given from top-down in chronological order (1998—present).

Chapter 5

Micromagic Clock: Microwave Clock Based on Atoms in an Engineered Optical Lattice

5.1 Introduction

Recently, it has been realized that the accuracy and stability of atomic clocks can be substantially improved by trapping atoms in a standing wave of laser light (optical lattices) operated at a certain “magic” wavelength [37, 84]. The laser wavelength is tuned so that the differential light perturbations of the two clock levels vanishes exactly. In other words, while remaining confined (this eliminates the Doppler and recoil shifts), the atoms behave spectroscopically as if they were in a vacuum. Millions of atoms can be trapped and interrogated simultaneously, vastly improving stability of the clock. Such setup was experimentally realized [79, 40, 45] for optical frequency clock transitions in divalent atoms yielding accuracies competitive to the fountain clocks [45]. However, because these lattice clocks operate at an optical frequency, to

relate to the definition of the second, they require state of the art frequency combs to bridge the optical frequency to the microwave counters.

Here the fruitful ideas of the optical lattice clocks are extended to microwave frequencies. A new class of atomic microwave clocks based on hyperfine transitions in the ground state of Al or Ga atoms trapped in optical lattices is proposed. This work includes the determination of magic wavelengths as well as an analysis of various systematic effects. Compared to a large chamber of the fountain clock, the atoms are confined to a tiny volume offering improved control over systematic errors. A relative compactness of the clockwork could benefit spacecraft applications such as navigation systems and precision tests of fundamental theories.

5.2 Problem Set-Up

The following experimental set-up is envisioned: a sample of atoms with $J = 1/2$ are trapped in a 1D optical lattice formed by counter-propagating laser beams of linear polarization and angular frequency ω . With the choice of linear polarization ($\mathcal{A} = 0$), it is seen from Eq. (3.22) that the energy shift associated with the axial polarizability vanishes to all orders. With Eq. (3.24), the clock shift is then given by

$$\delta\nu(\omega) = -\frac{1}{2\pi} \left(\frac{\mathcal{E}}{2}\right)^2 \left\{ [\alpha_{F'}^S(\omega) - \alpha_F^S(\omega)] + \left(\frac{3\cos^2\theta_p - 1}{2}\right) \left[\frac{3M'^2 - F'(F' + 1)}{F'(2F' - 1)} \alpha_{F'}^T(\omega) - \frac{3M^2 - F(F + 1)}{F(2F - 1)} \alpha_F^T(\omega) \right] \right\}, \quad (5.1)$$

where FM ($F'M'$) again labels the lower (upper) hyperfine clock level and, for linear polarization, the parameter θ_p represents the angle between the (real) polarization vector $\hat{\boldsymbol{\epsilon}}$ and the quantization axis $\hat{\mathbf{e}}_z$ (note that for the experimental set-up the quantizing magnetic field \mathbf{B} defines the z -axis). To minimize the effects of residual

circular polarization, the further choice $M' = M = 0$ is advantageous. The “magic” frequencies ω^* (or magic wavelengths $\lambda^* = c/2\pi\omega^*$) satisfy the condition $\delta\nu(\omega^*) = 0$, indicating a vanishing shift to the clock frequency.

Again, the problem begins with a consideration of the second order polarizabilities. As determined in the previous chapter, the second order scalar polarizability does not depend on the F quantum number (see Eq. (4.1)), and so it cannot contribute to any relative shift between the hyperfine levels. Furthermore, as mentioned in the previous paragraph, with the assumption of linear polarization the axial polarizability does not contribute in any order. This leaves just the second order tensor polarizability to consider. However, as the underlying operator describing the second order tensor polarizability has the character of a rank-2 tensor operator acting only within the electronic subspace, it must subsequently have a null effect when operating within the $J = 1/2$ model space. This result is evident from the selection rule $K \leq 2J$ associated with the second six- j symbol of Eq. (3.11). Thus for linear polarization, it is concluded that in the second order there is no relative shift between the two levels of a $J = 1/2$ hyperfine manifold.¹

And so it is once again necessary to proceed to evaluation of the third order effects. For a better qualitative understanding of this problem, it will be useful to consider the relationship between the respective third order scalar and tensor polarizabilities for each of the two hyperfine levels. In the previous chapter it was found that the F -dependence of the scalar polarizability can be factored out of the perturbation expressions; this is exemplified in Eq. (4.2), in which the entire F -dependence is

¹The specification of linear polarization can be relaxed in this statement, for if $\cos\theta_k = \hat{\mathbf{k}} \cdot \hat{\mathbf{e}}_z = 0$ or $M' = M = 0$, then the contribution from the axial polarizability is also seen to vanish in all orders.

subsumed by the product of a phase factor and a six- j symbol,

$$(-1)^{I+J+F} \left\{ \begin{array}{ccc} I & J & F \\ J & I & 1 \end{array} \right\}.$$

For the axial and tensor polarizabilities, a general factorization such as this is not possible. However, the current application is limited to $J = 1/2$ atomic states and linear polarization, and so it pays to consider these specifications.

Returning to the expression for the reduced polarizability of the top term, Eq. (3.17), the F -dependence is noted to be

$$\sum_{J''J'} (-1)^{J+J''} \left\{ \begin{array}{ccc} I & I & 1 \\ J & J'' & F \end{array} \right\} \left\{ \begin{array}{ccc} K & J'' & J \\ I & F & F \end{array} \right\} \left\{ \begin{array}{ccc} K & J'' & J \\ J' & 1 & 1 \end{array} \right\} \sum_{\gamma''\gamma'} (\dots),$$

where (\dots) indicates the remainder of the expression which depends on J , J'' , and J' but not F (note that there is also a factor $(2F + 1)$ preceding the summation; this is common to all terms and may be neglected for the current purposes). For the specific case of $J = 1/2$ and $K = 2$, the triangular selection rules for the six- j symbols only allow $J'' = 3/2$, and so the above expression may be written

$$\left\{ \begin{array}{ccc} I & I & 1 \\ \frac{1}{2} & \frac{3}{2} & F \end{array} \right\} \left\{ \begin{array}{ccc} 2 & \frac{3}{2} & \frac{1}{2} \\ I & F & F \end{array} \right\} \sum_{J''J'} \delta_{J''\frac{3}{2}} \left\{ \begin{array}{ccc} 2 & \frac{3}{2} & \frac{1}{2} \\ J' & 1 & 1 \end{array} \right\} \sum_{\gamma''\gamma'} (\dots).$$

Note that the F -dependence has been factored outside of the summations here. Similarly, the F -dependence of the center term, Eq. (3.18), can be factored out for the

special case of $J = 1/2$ and $K = 2$,²

$$\begin{aligned}
& (-1)^{I-\frac{1}{2}-F+1} \sum_{J''J'} \left\{ \begin{array}{cccc} - & I & F & \frac{1}{2} \\ 1 & - & 2 & 1 \\ J' & 1 & - & J'' \\ \frac{1}{2} & I & F & - \end{array} \right\} \sum_{\gamma''\gamma'} (\dots) = \\
& 4 \left\{ \begin{array}{ccc} I & I & 1 \\ \frac{1}{2} & \frac{3}{2} & F \end{array} \right\} \left\{ \begin{array}{ccc} 2 & \frac{3}{2} & \frac{1}{2} \\ I & F & F \end{array} \right\} \sum_{J''J'} (-1)^{J''-\frac{1}{2}} \left\{ \begin{array}{ccc} 1 & 1 & 2 \\ \frac{1}{2} & \frac{3}{2} & J' \end{array} \right\} \left\{ \begin{array}{ccc} J' & J'' & 1 \\ \frac{1}{2} & \frac{3}{2} & 1 \end{array} \right\} \\
& \times \sum_{\gamma''\gamma'} (\dots).
\end{aligned}$$

The F -dependence here is identical to the F -dependence of the top term. Furthermore, for $J = 1/2$ and $K = 2$ the normalization term, Eq. (3.20), vanishes due to the triangular selection rule $K \leq 2J$ associated with one of the six- j symbols. Thus it is concluded that for $J = 1/2$ the F -dependence may be factored out of the third order tensor polarizability just as it may for the third order scalar polarizability.

Another way of stating the conclusion of the preceding paragraph is that, for $J = 1/2$, the third order tensor polarizabilities for the two ($F = I - 1/2$ and $F = I + 1/2$) hyperfine states are proportional. With the reduction of the six- j symbols, the

²This result is by no means obvious. It follows from Eq. (10.13.35) and Eq. (10.9.9) of Ref. [83].

following ratios may be obtained for the third order scalar and tensor polarizabilities³

$$\frac{\alpha_{F=I-\frac{1}{2}}^{\text{S},(3)}(\omega)}{\alpha_{F=I+\frac{1}{2}}^{\text{S},(3)}(\omega)} = -\frac{(I+1)}{I}, \quad \frac{\alpha_{F=I-\frac{1}{2}}^{\text{T},(3)}(\omega)}{\alpha_{F=I+\frac{1}{2}}^{\text{T},(3)}(\omega)} = -\frac{(I-1)(2I-1)}{I(2I+1)}. \quad (5.2)$$

The realization that the respective third order scalar and tensor polarizabilities are proportional for the two hyperfine levels has important implications for the likelihood of finding magic wavelengths in particular atomic systems. Due to this proportionality property, $\delta\nu(\omega)$ may be written in terms of the third order polarizabilities for the $F = I + 1/2$ state alone.⁴ For example, consider the expression for $\delta\nu(\omega)$, Eq. (5.1), for the specific case of $\mathbf{B} \parallel \hat{\boldsymbol{\varepsilon}}$ and $M' = M = 0$; with this particular choice of parameters $\delta\nu(\omega)$ is found to be

$$\delta\nu(\omega) = -\frac{1}{2\pi} \left(\frac{\mathcal{E}}{2}\right)^2 (\pm 1) \frac{(2I+1)}{I} \left\{ \alpha_{F=I+\frac{1}{2}}^{\text{S},(3)}(\omega) - \frac{1}{2} \alpha_{F=I+\frac{1}{2}}^{\text{T},(3)}(\omega) \right\},$$

where the top (bottom) sign applies if the $F + 1/2$ state is the upper (lower) level of the hyperfine manifold. Clearly the scalar and tensor contributions must be of same order of magnitude in order to satisfy the magic condition $\delta\nu(\omega^*) = 0$. This is a general qualitative statement that applies to other geometries as well. Below, certain atomic systems will be shown to have a favorable ground state structure which allows

³It can also be shown that for $J = 1/2$ the F -dependence may be factored out of third order axial polarizability and the following ratio holds as well:

$$\frac{\alpha_{F=I-\frac{1}{2}}^{\text{a},(3)}(\omega)}{\alpha_{F=I+\frac{1}{2}}^{\text{a},(3)}(\omega)} = \frac{(I+1)(2I-1)}{I(2I+1)}.$$

⁴One might choose to alternatively express $\delta\nu(\omega)$ in terms of the third order polarizabilities for the $F = I - 1/2$ state alone; however, from Eqs. (5.2) it is evident that for $I < 3/2$ the tensor polarizability for the $F = I - 1/2$ state is necessarily zero and the alternative expression would not be possible.

Table 5.1: Comparison of the theoretical and experimental [67] ac frequency shifts for the clock transition in Cs. I_L is the laser intensity.

λ [nm]	ω [a.u.]	$\delta\nu_L/I_L$ [Hz/(mW/cm ²)]	
		Theor.	Expt.
780	0.0584	-1.95×10^{-2}	$-2.27(40) \times 10^{-2}$
532	0.0856	-3.73×10^{-4}	$-3.51(70) \times 10^{-4}$

for the necessary cancellation between scalar and tensor contributions.

5.3 Results and Discussion

In a similar fashion to the determination of the BBR shift in ¹³³Cs (Chapter 4), the numerical evaluation of the third-order polarizabilities began with the V^{N-1} DHF approximation solved from a B-spline basis set. From there, correlation effects were treated by means of the correlation potential method [23] which provides the set of Brueckner orbitals. Furthermore, the evaluation of matrix elements included additional corrections by means of the random phase approximation (RPA). The theoretical procedure used to obtain numerical values of the third order polarizabilities is discussed more extensively in Ref. [67].

First, results for the metrologically important ¹³³Cs atom are discussed. The calculated differential polarizability for the cesium clock transition is presented in Fig. 5.1 as a function of laser frequency. The two peaks correspond to the $6s - 6p$ and $6s - 7p$ resonances. The graph never crosses zero, which implies an absence of magic wavelengths. Experimental results for two laser wavelengths are also shown. Calculated and experimental relative frequency shifts are compared in Table 5.1 and found to be in agreement with each other, providing additional confidence in the theoretical analysis.

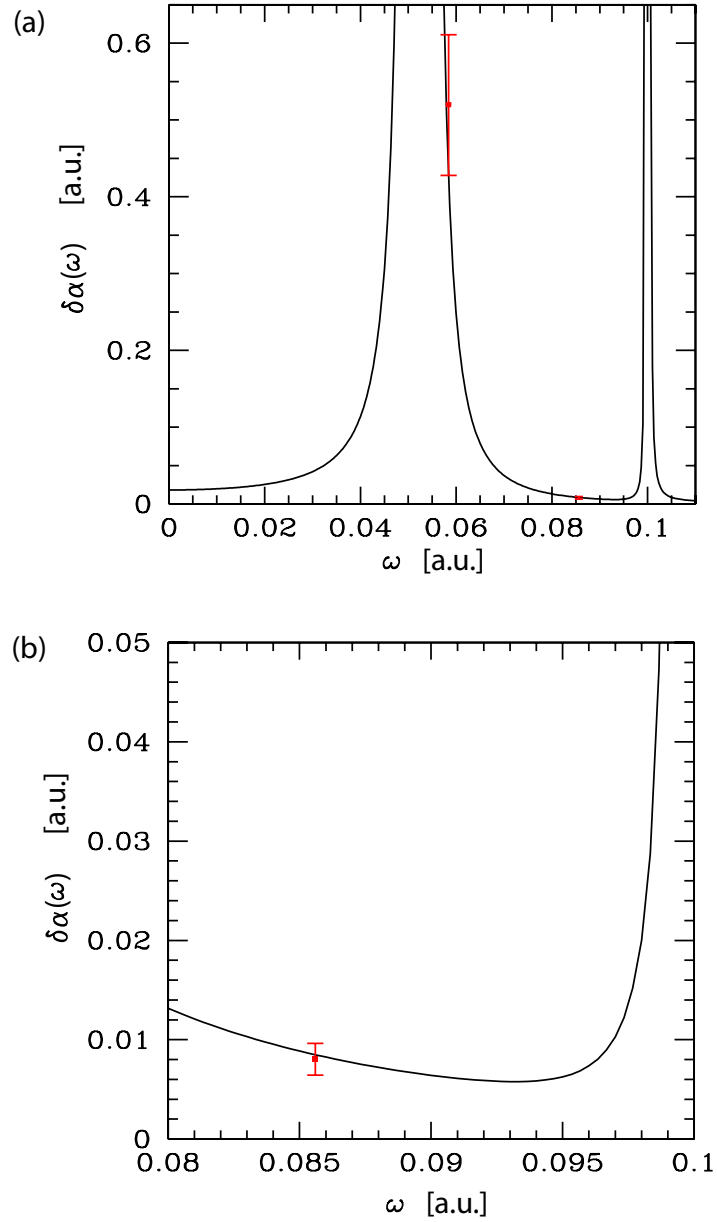


Figure 5.1: (Color online) Differential polarizability $\delta\alpha(\omega) \equiv \alpha_{F=4,M=0}(\omega) - \alpha_{F=3,M=0}(\omega)$ of the Cs clock transition in the $\mathbf{B} \parallel \hat{\mathbf{k}}$ configuration as a function of the laser frequency. Two experimental measurements at 780 nm ($\omega = 0.0584$ a.u.) and 532 nm ($\omega = 0.0856$ a.u.) are compared with theoretical predictions (solid curve). Part (a) provides an expansive view, whereas part (b) provides better graphical resolution in the neighborhood of the 532 nm experimental point.

The above result is in contrast to the findings of Ref. [85], in which a multitude of magic wavelengths were identified for ^{133}Cs . The findings of that work, however, are erroneous as the analysis was limited to only the second order (in limiting the analysis to the second order, one should actually conclude that *all* wavelengths are magic). A more critical discussion of these results may be found in Ref. [67].

Qualitatively speaking, the tensor contribution for Cs is much smaller than the scalar contribution and this leads to unfavorable conditions for the necessary cancellation.⁵ The situation is expected to be similar for other atomic systems with an $s_{1/2}$ valence electron (e.g., alkali-metal atoms). On the other hand, atomic systems with a $p_{1/2}$ valence electron may have “enhanced” tensor contributions and consequently have better potential to realize the magic condition. The advantage of the $p_{1/2}$ state comes from the fact it is part of a fine-structure manifold: there is a nearby $p_{3/2}$ state separated by a relatively small energy interval determined by the relativistic corrections to the atomic structure. The hyperfine interaction between the states of the same fine-structure manifold is amplified due to small energy denominators entering top and bottom terms of the third order polarizabilities. This amplification occurs only for the tensor contribution: for the scalar contribution the intermediate state must be of the of $p_{1/2}$ symmetry, whereas for the tensor contribution the intermediate state must be of the (strongly coupled) $p_{3/2}$ symmetry.

This qualitative discussion is illustrated with numerical examples for the group III atoms, starting with aluminum ($Z = 13$). The clock transition is between the hyperfine structure levels $F = 3$ and $F = 2$ in the ground $3p_{1/2}$ state of ^{27}Al isotope ($I = 5/2$). The clock frequency has been measured to be 1.50614(5) GHz [42], placing

⁵An alternative approach, as outlined in Ref. [25], is to allow $\mathcal{A}\cos\theta_k \neq 0$ and use non-zero M -states. With this approach, the axial polarizability contributes in the second order and may be used to cancel the dominant third order scalar contribution.

it in the microwave region. The clock frequency is six times smaller than that for Cs; this leads to a decreased stability of the Al clock. At the same time, the interrogation times in lattices may be substantially longer than in a fountain, improving the stability. Moreover, realizing a clock in an optical lattice is an important step towards harnessing a vast improvement in sensitivity offered by massive entanglement [14] (as in quantum information processing). Should such a massive entanglement be attained, the stability of the μ Magic clock would greatly improve.

The μ Magic clock requires ultracold atoms. Cooling Al has already been demonstrated [51] with the goal of atomic nanofabrication. The laser cooling was carried out on the closed $3p_{3/2} - 3d_{5/2}$ transition with the recoil limit of $7.5 \mu\text{K}$. Once trapped, the atoms can be readily transferred from the metastable $3p_{3/2}$ cooling state to the ground (clock) state. Lattice-trapped Al was also considered for quantum information processing [63].

The polarizabilities were computed for two experimental geometries, $\mathbf{B} \parallel \hat{\mathbf{k}}$ (or more generally, $\mathbf{B} \perp \hat{\boldsymbol{\varepsilon}}$) and $\mathbf{B} \parallel \hat{\boldsymbol{\varepsilon}}$, and three magic frequencies were identified,

$$\begin{aligned} \mathbf{B} \parallel \hat{\mathbf{k}} : \quad & \lambda^* = 390 \text{ nm}, \quad \alpha^{\text{S},(2)}(\omega^*) = -211 \text{ a.u.}, \\ & \lambda^* = 338 \text{ nm}, \quad \alpha^{\text{S},(2)}(\omega^*) = +142 \text{ a.u.}, \\ \mathbf{B} \parallel \hat{\boldsymbol{\varepsilon}} : \quad & \lambda^* = 400 \text{ nm}, \quad \alpha^{\text{S},(2)}(\omega^*) = +401 \text{ a.u.} \end{aligned}$$

The first and third magic wavelengths presented here are blue- and red-detuned from the $3p_{1/2} - 4s_{1/2}$ transition at 394.5 nm, respectively, whereas the second one may be regarded as red-detuned from the $3p_{1/2} - 3d_{3/2}$ transition at 308.3 nm. Existence of the magic wavelengths could be verified by measuring the clock shifts in an atomic beam illuminated by lasers tuned somewhat below/above ω^* (i.e., by “bracketing”), as in Ref. [67]; clock shifts would have opposite signs for the two frequencies of the

lasers.

The third-order Stark shifts of the clock levels as a function of ω are shown in Fig. 5.2(a). At the magic wavelength the Stark shifts are identical and the clock transition is unperturbed. The cancellation between scalar and tensor contributions to the clock shift is illustrated in Fig. 5.2(b).

The values of polarizability $\alpha^{S,(2)}(\omega^*)$ determine the depths of the optical potentials. In general, a laser of intensity 10 kW/cm^2 would be able to hold atoms of temperature $10 \mu\text{K}$. The atoms are trapped in the intensity minima of the standing wave for $\alpha^{S,(2)}(\omega^*) < 0$ and in the maxima otherwise. Both cases are realized depending on the geometry. For the blue-detuned case, one could use hollow beams to confine atoms in the radial direction.

As discussed in Chapters 1 and 4, the factor currently limiting the accuracy of the neutral-atom clocks is the blackbody radiation. The BBR coefficient for ^{27}Al was found to be $\beta(^{27}\text{Al}) = -8.7 \times 10^{-16}$, which is about 20 times smaller than the coefficient for the Cs standard. Moreover, a typical inhomogeneity of 0.1 K results in an estimate of the fractional accuracy at 10^{-18} . The entire experimental chamber could be cooled down cryogenically, reducing the uncertainty even further; here the small volume of the chamber offers an advantage over the fountains [45].

While the choice of the $M = 0$ substates eliminates the first-order Zeeman shift, sensitivity to the magnetic field comes through in the second-order Zeeman shift due to mixing of different hyperfine components by \mathbf{B} . The relative shift may be approximated with the formulae of Appendix G, in which the following general expression

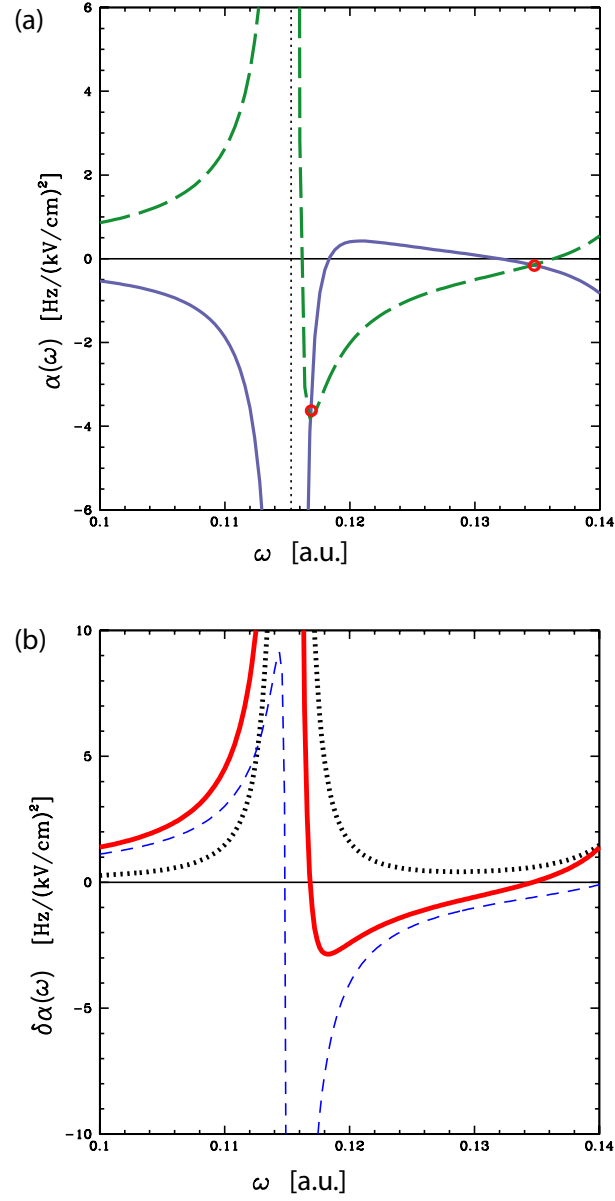


Figure 5.2: (Color online) (a) Third-order polarizabilities $\alpha_{F=3,M=0}^{(3)}(\omega)$ (dashed line) and $\alpha_{F=2,M=0}^{(3)}(\omega)$ (solid line) for the Al μ Magic clock levels in the $\mathbf{B} \parallel \hat{\mathbf{k}}$ geometry as a function of the lattice laser frequency. The polarizabilities are identical at the magic frequencies (red circles) above the $3p_{1/2} - 4s_{1/2}$ resonance (vertical dotted line). (b) Differential polarizability $\delta\alpha(\omega) \equiv \alpha_{F=3,M=0}^{(3)}(\omega) - \alpha_{F=2,M=0}^{(3)}(\omega)$ for the Al clock in the $\mathbf{B} \parallel \hat{\mathbf{k}}$ geometry as a function of the lattice laser frequency. Dotted line: scalar contribution; dashed line: tensor contribution; solid line: total differential polarizability. The differential polarizability vanishes at the magic frequencies.

may be obtained⁶

$$\frac{\delta\nu^{\text{Zee},(2)}}{\nu} \simeq \frac{2}{(2\pi\nu)^2} \left| \langle F=I+\frac{1}{2}, M=0 | V_{\text{Zee}} | F=I-\frac{1}{2}, M=0 \rangle \right|^2 \simeq \frac{1}{2} g_J^2 \left(\frac{\mu_B B}{2\pi\nu} \right)^2.$$

For ${}^2P_{1/2}$ states in non-relativistic limit $g_J = 2/3$ and one may find $\delta\nu^{\text{Zee}}/\nu \simeq 1.9 \times 10^{-7} B^2$, where B is taken in Gauss. This issue of the second order Zeeman shift is similar to that in the fountain clocks (Cs, Rb,...), where specific efforts to map the magnetic field over the flight zone are made. However, since in the lattice the atoms are confined to a tiny volume, one could control/shield the magnetic fields to a better degree than in the fountain clocks.

So far it has been assumed that the light is linearly polarized. In practice there is always a small degree of circular polarization \mathcal{A} present. The residual circular component leads to an undesired clock shift through the axial polarizability $\alpha_F^{\text{a}}(\omega)$. This effect is equivalent to a “pseudo-magnetic” field along $\hat{\mathbf{k}}$. For the $p_{1/2}$ clock levels $\alpha_F^{\text{a}}(\omega)$ arises already in the second order; it is found to be in the order of 100 a.u. For the $M = 0$ levels the relevant clock shift is zero in the first order in $\alpha_F^{\text{a}}(\omega)$. However, the shift could appear in the second order in $\mathcal{A}\alpha_F^{\text{a}}(\omega)$ since the vector term mixes different hyperfine components. For a typical residual circular polarization $\mathcal{A} \sim 10^{-5}$ and a misalignment angle of 10^{-2} , the fractional frequency shift is just 10^{-21} .

Atoms of Al are bosons and the collisional clock shifts may become of issue, as in the fountain clocks [60, 76]. The advantage of the lattice clocks over the fountain clocks is that one could fill the lattice with no more than one atom per site, strongly suppressing the interatomic interactions and the associated shifts.

⁶This is general to within the assumptions that $M' = M = 0$ and $J = 1/2$, which further implies that I necessarily has a half-integer value.

Scattering of the lattice laser photons leads to heating and reduces the interrogation time. At 10 kW/cm^2 the heating rate is in the order of 10^{-2} sec^{-1} . Heating can be suppressed by using the blue-detuned magic wavelength for which the atoms are trapped at the intensity minima. This also reduces effects of hyperpolarizability on the clock shift and multi-photon ionization rates.

A similar analysis was also carried out for the isotopes $^{69,71}\text{Ga}$ ($I = 3/2$), also part of the same group III of the periodic table as Al. Cooling of this atom is pursued in atomic nanofabrication [64, 16]. The clock transition is between the hyperfine structure components $F = 1$ and $F = 2$ of the $4p_{1/2}$ ground state and has been measured to be $2.6779875(10) \text{ GHz}$ and $3.4026946(13) \text{ GHz}$ for ^{69}Ga and ^{71}Ga , respectively [46]. In contrast to Al, only a single magic wavelength was identified at 450 nm in the $\mathbf{B} \parallel \hat{\boldsymbol{\epsilon}}$ geometry. This is red-detuned from the $4p_{1/2} - 5s_{1/2}$ transition frequency of 403.4 nm . For this magic wavelength $\alpha^{S,(2)}(\omega^*) = 94 \text{ a.u.}$; furthermore the very small BBR coefficient $\beta(^{69,71}\text{Ga}) = -6.63 \times 10^{-17}$ was also obtained. Magic wavelengths were not found for other group III atoms.

To summarize, a class of microwave lattice clocks (μMagic clocks) based on Al and Ga atoms has been proposed. Calculations reveal magic wavelengths for these clocks in which the laser-induced differential Stark shift vanishes. This is a result of canceling scalar and tensor contributions to the relative ac Stark shift. The tensor polarizability in the $p_{1/2}$ electron state is enhanced due to the mixing of $p_{1/2}$ and $p_{3/2}$ states by the hyperfine interaction. A similar mechanism for the magic wavelengths may work in microwave hyperfine transitions in other atoms which have fine-structure multiplets in the ground state. In atoms with the valence electron in the $s_{1/2}$ state (Cs, Rb, ...) magic wavelengths are absent (for $M = 0$ clock states or linear polarization). The present proposal reveals a potential for developing a new compact atomic clock operating in the microwave domain.

Chapter 6

Conclusion

This dissertation included presentations of a high-accuracy calculation of the black-body radiation shift in the ^{133}Cs primary frequency standard as well as a proposal for a new class of microwave atomic clocks based on atoms in an engineered optical lattice (μMagic clocks), with particular focus on ^{27}Al and $^{69,71}\text{Ga}$ atoms.

From a theoretical standpoint, both of these problems are rooted in the theory of the ac Stark effect on the hyperfine structure of atomic systems. To describe this effect, a consistent and general formalism based on Floquet perturbation theory for a temporally-periodic perturbation was developed. This formalism treats the hyperfine and ac electric field interactions perturbatively on equal footing. Explicit expressions were given for the energy shifts (i) zeroth order in the hyperfine interaction and second order in the electric field interaction and (ii) first order in the hyperfine interaction and second order in the electric field interaction. These are the leading two orders describing *relative* shifts between hyperfine energy levels due to the presence of the ac electric field, and likewise, the shifts to the (microwave) atomic clock frequency. These effects were parameterized by the second and third order polarizabilities, respectively, these being strictly properties of the particular atom (or, more specifically,

the particular atomic isotope).

Relativistic atomic many-body theory was implemented into this theory of the ac Stark effect to, firstly, perform a high-accuracy calculation of the BBR shift in the ^{133}Cs primary frequency standard. This BBR shift is one of the leading systematic corrections in the ^{133}Cs frequency standard and a subject of recent controversy. The resulting 0.35%-accurate value re-validates high-precision Stark shift measurements of Ref. [74]. Moreover, the origin of the discrepancy between that measurement and recent calculations of Refs. [54, 82] was identified.

Additionally, a class of microwave lattice clocks (μMagic clocks) based on Al and Ga atoms was also proposed. Relativistic atomic many-body calculations revealed magic wavelengths for these clocks in which the laser-induced differential ac Stark shift vanishes. This is a result of canceling scalar and tensor contributions to the relative ac Stark shift. The tensor polarizability in the $p_{1/2}$ electron state is enhanced due to the mixing of $p_{1/2}$ and $p_{3/2}$ states by the hyperfine interaction. A similar mechanism for the magic wavelengths may work in microwave hyperfine transitions in other atoms which have fine-structure multiplets in the ground state. On the other hand, atoms with the valence electron in the $s_{1/2}$ state (e.g., Cs) lack magic wavelengths (for $M = 0$ clock states or linear polarization). This proposal reveals a potential for developing a new compact atomic clock operating in the microwave domain.

Bibliography

- [1] C. Amiot, O. Dulieu, R. F. Gutterres, and F. Masnou-Seeuws. Determination of the Cs_2 $0_g^-(P_{3/2})$ potential curve of Cs $6P_{1/2,3/2}$ atomic radiative lifetimes from photoassociation spectroscopy. *Phys. Rev. A*, 66:052506, 2002.
- [2] E. J. Angstmann, V. A. Dzuba, and V. V. Flambaum. Frequency shift of the cesium clock transition due to blackbody radiation. *Phys. Rev. Lett.*, 97(4):040802, 2006.
- [3] E. Arimondo, M. Inguscio, and P. Violino. Experimental determinations of the hyperfine structure in the alkali atoms. *Rev. Mod. Phys.*, 49:31, 1977.
- [4] C. Audoin, B. Guinot, and S. Lyle. *The measurement of time: time, frequency, and the atomic clock*. Cambridge University Press, Cambridge, UK, 2001.
- [5] H. Bachau, E. Cormier, P. Decleva, J. E. Hansen, and F. Martin. Applications of B-splines in atomic and molecular physics. *Rep. Prog. Phys.*, 64:1815–1943, 2001.
- [6] Z. W. Barber, C. W. Hoyt, C. W. Oates, L. Hollberg, A. V. Taichenachev, and V. I. Yudin. Direct excitation of the forbidden clock transition in neutral ^{174}Yb atoms confined to an optical lattice. *Phys. Rev. Lett.*, 96(8):083002, 2006.
- [7] R. E. Beehler. A historical review of atomic frequency standards. *Proceedings of the IEEE*, 55(6):792–805, June 1967.
- [8] K. Beloy and A. Derevianko. Application of the dual-kinetic-balance sets in the relativistic many-body problem of atomic structure. *Comp. Phys. Comm.*, 179:310–319, 2008.
- [9] K. Beloy, A. Derevianko, V. A. Dzuba, and V. V. Flambaum. Micromagic clock: Microwave clock based on atoms in an engineered optical lattice. *Phys. Rev. Lett.*, 102(12):120801, 2009.
- [10] K. Beloy, U. I. Safronova, and A. Derevianko. High-accuracy calculation of the blackbody radiation shift in the ^{133}Cs primary frequency standard. *Phys. Rev. Lett.*, 97(4):040801, 2006.

- [11] J. C. Bergquist, S. R. Jefferts, and D. J. Wineland. Time measurement at the millenium. *Phys. Today*, 54:37–42, 2001.
- [12] I. Bloch. Ultracold quantum gases in optical lattices. *Nature Physics*, 1:23–30, 2007.
- [13] R. Bluhm. Lorentz and CPT tests in matter and antimatter. *Nucl. Instr. and Meth. in Phys. Res. B*, 221:6–11, 2004.
- [14] J. J. Bollinger, W. M. Itano, D. J. Wineland, and D. J. Heinzen. Optimal frequency measurements with maximally correlated states. *Phys. Rev. A*, 54(6):4649(R), Dec 1996.
- [15] A. Bruschi, R. Le Targat, X. Baillard, M. Fouché, and P. Lemonde. Hyperpolarizability effects in a Sr optical lattice clock. *Phys. Rev. Lett.*, 96(10):103003, 2006.
- [16] A. Camposio, O.M. Marago, B. Fazio, B. Kloter, D. Meschede, U. Rasbach, C. Weber, and E. Arimondo. Resist-assisted atom lithography with group III elements. *Appl. Phys. B*, 85:487–491, 2006.
- [17] M. Chwalla, J. Benhelm, K. Kim, G. Kirchmair, T. Monz, M. Riebe, P. Schindler, A. S. Villar, W. Hänsel, C. F. Roos, R. Blatt, M. Abgrall, G. Santarelli, G. D. Rovera, and Ph. Laurent. Absolute frequency measurement of the $^{40}\text{Ca}^+$ $4s\ ^2S_{1/2} - 3d\ ^2D_{5/2}$ clock transition. *Phys. Rev. Lett.*, 102(2):023002, 2009.
- [18] C. de Boor. *A practical guide to splines*. Springer-Verlag, New York, revised edition, 2001.
- [19] S. A. Diddams, J. C. Bergquist, S. R. Jefferts, and C. W. Oates. Standards of time and frequency at the outset of the 21st century. *Science*, 306(5700):1318–1324, 2004.
- [20] S. A. Diddams, T. Udem, J. C. Bergquist, E. A. Curtis, R. E. Drullinger, L. Hollberg, W. M. Itano, W. D. Lee, C. W. Oates, K. R. Vogel, and D. J. Wineland. An optical clock based on a single trapped $^{199}\text{Hg}^+$ ion. *Science*, 293(5531):825–8, 2001.
- [21] P. Dubé, A. A. Madej, J. E. Bernard, L. Marmet, J.-S. Boulanger, and S. Cundy. Electric quadrupole shift cancellation in single-ion optical frequency standards. *Phys. Rev. Lett.*, 95(3):033001, Jul 2005.
- [22] V. A. Dzuba and V. V. Flambaum. Off-diagonal hyperfine interaction and parity non-conservation in cesium. *Phys. Rev. A*, 62:052101, 2000.

- [23] V. A. Dzuba, V. V. Flambaum, P. G. Silvestrov, and O. P. Sushkov. Correlation potential method for the calculation of energy levels, hyperfine structure and E1 transition amplitudes in atoms with one unpaired electron. *J. Phys. B*, 20:1399–1412, 1987.
- [24] V. V. Flambaum. Variation of fundamental constants: theory and observations. 2007. e-print atom-ph/0705.3704v2.
- [25] V. V. Flambaum, V. A. Dzuba, and A. Derevianko. Magic frequencies for cesium primary-frequency standard. *Phys. Rev. Lett.*, 101(22):220801, 2008.
- [26] T. M. Fortier, N. Ashby, J. C. Bergquist, M. J. Delaney, S. A. Diddams, T. P. Heavner, L. Hollberg, W. M. Itano, S. R. Jefferts, K. Kim, F. Levi, L. Lorini, W. H. Oskay, T. E. Parker, J. Shirley, and J. E. Stalnaker. Precision atomic spectroscopy for improved limits on variation of the fine structure constant and local position invariance. *Phys. Rev. Lett.*, 98(7):070801, 2007.
- [27] A. Godone, D. Calonico, F. Levi, S. Micalizio, and C. Calosso. Stark-shift measurement of the $^2S_{1/2}$, $F = 3 - F = 4$ hyperfine transition of ^{133}Cs . *Phys. Rev. A*, 71:063401, 2005.
- [28] T. P. Heavner, S. R. Jefferts, E. A. Donley, J. H. Shirley, and T. E. Parker. NIST-F1: recent improvements and accuracy evaluations. *Metrologia*, 42:411–422, 2005.
- [29] W. M. Itano, L. L. Lewis, and D. J. Wineland. Shift of $^2S_{1/2}$ hyperfine splittings due to blackbody radiation. *Phys. Rev. A*, 25:1233–1235, 1982.
- [30] J. D. Jackson. *Classical Electrodynamics*. John Willey & Sons, New York, 3rd edition, 1999.
- [31] S. R. Jefferts, T. P. Heavner, E. A. Donley, J. Shirley, and T. E. Parker. Second generation cesium fountain primary frequency standards at NIST. In *Proc. 2003 Joint Mtg. IEEE Intl. Freq. Cont. Symp. and EFTF Conf.*, pages 1084–1088, Piscataway, NJ, USA: IEEE, 2003.
- [32] S. R. Jefferts, T. P. Heavner, T. E. Parker, and J. H. Shirley. NIST cesium fountains—current status and future prospects. *Proc. SPIE*, 6673:667309, 2007.
- [33] S. R. Jefferts, J. H. Shirley, T. E. Parker, T. P. Heavner, D. M. Meekhof, C. W. Nelson, F. Levi, G. Costanzo, A. DeMarchi, R. E. Drullinger, L. Hollberg, W. D. Lee, and F. L. Walls. Accuracy evaluation of NIST-F1. *Metrologia*, 39:321–336, 2002.
- [34] W. R. Johnson. *Atomic Structure Theory: Lectures on Atomic Physics*. Springer, New York, NY, 2007.

- [35] W. R. Johnson, S. A. Blundell, and J. Sapirstein. Finite basis sets for the Dirac equation constructed from B-splines. *Phys. Rev. A*, 37(2):307–15, 1988.
- [36] H. Katori, M. Takamoto, and T. Akatsuka. Optical lattice clocks with non-interacting bosons and fermions. *The Review of Laser Engineering*, 36(APLS):1004–1007, 2008.
- [37] H. Katori, M. Takamoto, V. G. Pal’chikov, and V. D. Ovsiannikov. Ultrastable optical clock with neutral atoms in an engineered light shift trap. *Phys. Rev. Lett.*, 91:173005, 2003.
- [38] C. Lammerzahl, G. Ahlers, N. Ashby, M. Barmatz, P. L. Biermann, H. Dittus, V. Dohm, R. Duncan, K. Gibble, J. Lipa, N. Lockerbie, N. Mulders, and C. Salomon. Experiments in fundamental physics scheduled and in development for the ISS. *General Relativity and Gravitation*, 36:615–649, 2004.
- [39] P. W. Langhoff, S. T. Epstein, and M. Karplus. Aspects of time-dependent perturbation theory. *Rev. Mod. Phys.*, 44(3):602–644, Jul 1972.
- [40] R. Le Targat, X. Baillard, M. Fouché, A. Bruschi, O. Tcherbakoff, G. D. Rovera, and P. Lemonde. Accurate optical lattice clock with ^{87}Sr atoms. *Phys. Rev. Lett.*, 97:130801, 2006.
- [41] F. Levi, D. Calonico, L. Lorini, S. Micalizio, and A. Godone. Measurement of the blackbody radiation shift of the ^{133}Cs hyperfine transition in an atomic fountain. *Phys. Rev. A*, 70(3):033412, 2004.
- [42] H. Lew and G. Wessel. The hyperfine structure of the $3p^2P_{1/2}$ state of Al^{27} . *Phys. Rev.*, 90(1):1–3, 1953.
- [43] I. Lindgren and J. Morrison. *Atomic Many-Body Theory*. Springer-Verlag, Berlin, second edition, 1986.
- [44] M. A. Lombardi, T. P. Heavner, and S. R. Jefferts. NIST primary frequency standards and the realization of the SI second. *Measure*, 2:74–89, 2007.
- [45] A. D. Ludlow, T. Zelevinsky, G. K. Campbell, S. Blatt, M. M. Boyd, M. H. G. de Miranda, M. J. Martin, J. W. Thomsen, S. M. Foreman, Jun Ye, T. M. Fortier, J. E. Stalnaker, S. A. Diddams, Y. Le Coq, Z. W. Barber, N. Poli, N. D. Lemke, K. M. Beck, and C. W. Oates. Sr lattice clock at 1×10^{-16} fractional uncertainty by remote optical evaluation with a Ca clock. *Science*, 319(5871):1805–1808, 2008.
- [46] A. Lurio and A. G. Prodell. Hfs separations and hfs anomalies in the $^2P_{1/2}$ state of Ga^{69} , Ga^{71} , Tl^{203} , and Tl^{205} . *Phys. Rev.*, 101(1):79–83, 1956.
- [47] L. Maleki. Space tests of relativistic gravity with precision clocks and atom interferometers. *Gen. Relativ. Gravit.*, 40:895–905, 2008.

- [48] N. L. Manakov, V. D. Ovsianikov, and L. P. Rapoport. Atoms in a laser field. *Phys. Rep.*, 141(6):319–433, 1986.
- [49] H. S. Margolis, G. P. Barwood, G. Huang, H. A. Klein, S. N. Lea, K. Szymaniec, and P. Gill. Hertz-level measurement of the optical clock frequency in a single $^{88}\text{Sr}^+$ ion. *Science*, 306(5700):1355–1358, 2004.
- [50] W. Markowitz, R. Glenn Hall, L. Essen, and J. V. L. Parry. Frequency of cesium in terms of ephemeris time. *Phys. Rev. Lett.*, 1(3):105–107, Aug 1958.
- [51] R. W. McGowan, D. M. Giltner, and S. A. Lee. Light force cooling, focusing, and nanometer-scale deposition of aluminium atoms. *Opt. Lett.*, 20(24):2535, 1995.
- [52] J. G. McNeff. The global positioning system. *IEEE Transactions on Microwave Theory and Techniques*, 50(3):645–652, 2002.
- [53] E. Merzbacher. *Quantum Mechanics*. Wiley, John & Sons, 3 edition, 1998.
- [54] S. Micalizio, A. Godone, D. Calonico, F. Levi, and L. Lorini. Blackbody radiation shift of the ^{133}Cs hyperfine transition frequency. *Phys. Rev. A*, 69(5):053401, 2004.
- [55] C. E. Moore. *Atomic energy levels*, volume III. National Bureau of Standards, Washington, D.C., 1958.
- [56] C. T. Munger. Ideal basis sets for the Dirac Coulomb problem: Eigenvalue bounds and convergence proofs. *J. Math. Phys.*, 48(2):022301, 2007.
- [57] W. H. Oskay, S. A. Diddams, E. A. Donley, T. M. Fortier, T. P. Heavner, L. Hollberg, W. M. Itano, S. R. Jefferts, M. J. Delaney, K. Kim, F. Levi, T. E. Parker, and J. C. Bergquist. Single-atom optical clock with high accuracy. *Phys. Rev. Lett.*, 97(2):020801, 2006.
- [58] V. G. Pal’chikov, Yu. S. Domnin, and A. V. Novoselov. Black-body radiation effects and light shifts in atomic frequency standards. *J. Opt. B*, 5(2):S131–5, 2003.
- [59] T. E. Parker, S. R. Jefferts, T. P. Heavner, and E. A. Donley. Operation of the NIST-F1 caesium fountain primary frequency standard with a maser ensemble, including the impact of frequency transfer noise. *Metrologia*, 42:423–430, 2005.
- [60] F. Pereira Dos Santos, H. Marion, S. Bize, Y. Sortais, A. Clairon, and C. Salomon. Controlling the cold collision shift in high precision atomic interferometry. *Phys. Rev. Lett.*, 89(23):233004, Nov 2002.
- [61] R. J. Rafac and C. E. Tanner. Measurement of the ratio of the cesium D -line transition strengths. *Phys. Rev. A*, 58(2):1087–97, 1998.

- [62] N. F. Ramsey. A molecular beam resonance method with separated oscillating fields. *Phys. Rev.*, 78(6):695–699, Jun 1950.
- [63] B. Ravaine, A. Derevianko, and P. R. Berman. Quantum computing with magnetic atoms in optical lattices of reduced periodicity. *Phys. Rev. A*, 74(2):022330, 2006.
- [64] S. J. Rehse, K. M. Bockel, and S. A. Lee. Laser collimation of an atomic gallium beam. *Phys. Rev. A*, 69(6):063404, Jun 2004.
- [65] T. Rosenband, D. B. Hume, P. O. Schmidt, C. W. Chou, A. Brusch, L. Lorini, W. H. Oskay, R. E. Drullinger, T. M. Fortier, J. E. Stalnaker, S. A. Diddams, W. C. Swann, N. R. Newbury, W. M. Itano, D. J. Wineland, and J. C. Bergquist. Frequency ratio of Al^+ and Hg^+ single-ion optical clocks; metrology at the 17th decimal place. *Science*, 319(5871):1808–1812, 2008.
- [66] T. Rosenband, P. O. Schmidt, D. B. Hume, W. M. Itano, T. M. Fortier, J. E. Stalnaker, K. Kim, S. A. Diddams, J. C. J. Koelemeij, J. C. Bergquist, and D. J. Wineland. Observation of the $^1S_0 \rightarrow ^3P_0$ clock transition in $^{27}\text{Al}^+$. *Phys. Rev. Lett.*, 98(22):220801, 2007.
- [67] P. Rosenbusch, S. Ghezali, V. A. Dzuba, V. V. Flambaum, K. Beloy, and A. Derevianko. ac Stark shift of the Cs microwave atomic clock transitions. *Phys. Rev. A*, 79(1):013404, 2009.
- [68] M. S. Safronova, W. R. Johnson, and A. Derevianko. Relativistic many-body calculations of energy levels, hyperfine constants, electric-dipole matrix elements, and static polarizabilities for alkali-metal atoms. *Phys. Rev. A*, 60(6):4476–87, 1999.
- [69] H. Sambe. Steady states and quasienergies of a quantum-mechanical system in an oscillating field. *Phys. Rev. A*, 7(6):2203–2213, Jun 1973.
- [70] T. Schneider, E. Peik, and Chr. Tamm. Sub-hertz optical frequency comparisons between two trapped $^{171}\text{Yb}^+$ ions. *Phys. Rev. Lett.*, 94(23):230801, Jun 2005.
- [71] C. Schwartz. Theory of hyperfine structure. *Phys. Rev.*, 97:380–95, 1955.
- [72] V. M. Shabaev, I. I. Tupitsyn, V. A. Yerokhin, G. Plunien, and G. Soff. Dual kinetic balance approach to basis-set expansions for the Dirac equation. *Phys. Rev. Lett.*, 93(13):130405, 2004.
- [73] J. M. Shaull. Adjustment of high-precision frequency and time standards. *Proceedings of the IRE*, 38(1):6–15, 1950.
- [74] E. Simon, P. Laurent, and A. Clairon. Measurement of the Stark shift of the Cs hyperfine splitting in an atomic fountain. *Phys. Rev. A*, 57:436–39, 1998.

- [75] N. J. Stone. Table of nuclear magnetic dipole and electric quadrupole moments. *At. Data and Nucl. Data Tables*, 90(1):75 – 176, 2005.
- [76] K. Szymaniec, W. Chalupczak, E. Tiesinga, C. J. Williams, S. Weyers, and R. Wynands. Cancellation of the collisional frequency shift in caesium fountain clocks. *Phys. Rev. Lett.*, 98(15):153002, 2007.
- [77] A. V. Taichenachev, V. I. Yudin, C. W. Oates, C. W. Hoyt, Z. W. Barber, and L. Hollberg. Magnetic field-induced spectroscopy of forbidden optical transitions with application to lattice-based optical atomic clocks. *Phys. Rev. Lett.*, 96:083001, 2006.
- [78] A. V. Taichenachev, V. I. Yudin, V. D. Ovsianikov, V. G. Pal’chikov, and C. W. Oates. Frequency shifts in an optical lattice clock due to magnetic-dipole and electric-quadrupole transitions. *Phys. Rev. Lett.*, 101(19):193601, 2008.
- [79] M. Takamoto, F. L. Hong, R. Higashi, and H. Katori. An optical lattice clock. *Nature (London)*, 435:321–324, 2005.
- [80] M. Takamoto, H. Katori, S. I. Marmo, V. D. Ovsianikov, and V. G. Pal’chikov. Prospects for optical clocks with a blue-detuned lattice. *Phys. Rev. Lett.*, 102(6):063002, 2009.
- [81] B. N. Taylor and A. Thompson, editors. *The International System of Units (SI)*. U.S. Government Printing Office, Gaithersburg, Maryland, USA, 2008 edition, 2008.
- [82] S. Ulzega, A. Hofer, P. Moroshkin, and A. Weis. Reconciliation of experimental and theoretical electric tensor polarizabilities of the cesium ground state. *Europhys. Lett.*, 76(6):1074–1080, 2006.
- [83] D. A. Varshalovich, A. N. Moskalev, and V. K. Khersonskii. *Quantum Theory of Angular Momentum*. World Scientific, Singapore, 1988.
- [84] J. Ye, H. J. Kimble, and H. Katori. Quantum State Engineering and Precision Metrology Using State-Insensitive Light Traps. *Science*, 320(5884):1734–1738, 2008.
- [85] X. Zhou, X. Chen, and J. Chen. High-accuracy microwave atomic clock via magic optical lattice. 2005. arXiv:0512244.

Appendix A

Atomic Units

A.1 Definitions

The relationships of atomic physics have an abundance of such factors as the reduced Planck's constant (\hbar), the mass and charge of the electron (m_e , $-e$), and the Bohr radius (a_B). Less cumbersome expressions may be obtained by employing the natural system of units for atomic problems, simply referred to as atomic units. This system of units may be defined by giving the three dimensionally independent constants \hbar , m_e , and a_B a value of 1 atomic unit (1 a.u.).

The above defined atomic units correspond to the physical quantities of angular momentum, mass, and length, respectively. Atomic units for other physical quantities may be derived from dimensional considerations. For example, the atomic unit for frequency may be derived as

$$1 \text{ a.u. [frequency]} = \frac{1 \text{ a.u. [angular momentum]}}{1 \text{ a.u. [mass]} \times (1 \text{ a.u. [length]})^2} = \frac{\hbar}{m_e a_B^2} .$$

Another example follows from the expression for the Bohr radius, $a_B = \hbar/\alpha m_e c$,

where $\alpha \simeq 1/137$ is the dimensionless fine structure constant. This expression may be rearranged as

$$\alpha c = \frac{\hbar}{m_e a_B},$$

from which it is evident that αc ($=\hbar/m_e a_B$) is representative of the atomic unit for velocity. Furthermore, the atomic unit for charge is e ($-e$ being the electron charge), as can be verified by the expression for the fine structure constant $\alpha = e^2/\hbar c$.¹

As an example of the practicality of atomic units, consider the eigenvalue equation

$$-\frac{\hbar^2}{2m_e} \frac{d^2 P(r)}{dr^2} + \left[-\frac{e^2}{r} + \frac{\hbar^2}{2m_e} \frac{l(l+1)}{r^2} \right] P(r) = EP(r).$$

This eigenvalue equation gives the energies and radial wavefunctions of the non-relativistic hydrogen atom. Expressing all quantities in atomic units yields the streamlined expression

$$-\frac{1}{2} \frac{d^2 P(r)}{dr^2} + \left[-\frac{1}{r} + \frac{1}{2} \frac{l(l+1)}{r^2} \right] P(r) = EP(r).$$

¹The convention of this dissertation is to use Gaussian electromagnetic expressions in favor of SI electromagnetic expressions. When working with SI electromagnetic expressions, definitions $\hbar = 1$ a.u., $m_e = 1$ a.u., and $a_B = 1$ a.u. do not uniquely define the atomic unit for charge. Charge $e = 1$ a.u. only follows after an additional definition for permittivity $4\pi\epsilon_0 = 1$ a.u. (or vice-versa). This is related to the fact that—in contrast to the Gaussian system—the unit of charge in the SI system cannot be expressed directly in terms of the units of length, mass, and time. The difference in reference system is not a trivial one, as is exemplified by the value of the Bohr magneton in either case:

$$\text{Gaussian : } \mu_B = \frac{e\hbar}{2m_e c} = \frac{\alpha}{2} \text{ a.u.}, \quad \text{SI : } \mu_B = \frac{e\hbar}{2m_e} = \frac{1}{2} \text{ a.u.}$$

A.2 Atomic Unit Conversion Table

Table A.1 provides a reference for conversions to and from atomic units for some basic physical quantities. An expression for each atomic unit is given along with an equivalent value in appropriate units. The conversion for temperature follows from an additional definition, $k_B = 1$ a.u., where k_B is the Boltzmann constant.

Table A.1: Atomic unit conversion table.

Physical Quantity		1 a.u.
Mass	m_e	$= 9.10939 \times 10^{-31}$ kg
Length	a_B	$= 5.29177 \times 10^{-11}$ m
Velocity	αc	$= 2.18769 \times 10^6$ m/s
Angular Momentum	\hbar	$= 1.05457 \times 10^{-34}$ J s
Electric Charge	e	$= 1.60218 \times 10^{-19}$ C (SI) 4.80320×10^{-10} statC (Gaussian)
Frequency	$\alpha c/a_B$	$= 4.13414 \times 10^{16}$ Hz
Energy	$m_e (\alpha c)^2$	$= 4.35975 \times 10^{-18}$ J = 27.2114 eV
Intensity	$m_e (\alpha c/a_B)^3$	$= 6.43642 \times 10^{15}$ mW/cm ²
Temperature	$m_e (\alpha c)^2 / k_B$	$= 3.15775 \times 10^5$ K

Appendix B

Angular Momentum and Spinor Spherical Harmonics

B.1 Brief Review of Angular Momentum Theory

This appendix provides a review of quantum angular momentum theory. Orbital and spin-1/2 angular momentum are considered in particular, leading to the introduction of the spinor spherical harmonics. The review here is kept brief; a more complete coverage can be found in one of several books on the theory of quantum angular momentum (e.g., Ref. [83]).

As the generator of infinitesimal rotations, the Hermitian operator \mathbf{J} represents the physical observable of angular momentum. Its components satisfy the commutation relations

$$[J_x, J_y] = iJ_z, \quad [J_y, J_z] = iJ_x, \quad [J_z, J_x] = iJ_y. \quad (\text{B.1})$$

As a consequence of these commutation relations, each component commutes with

the squared angular momentum operator

$$[\mathbf{J}, J^2] = 0,$$

where $J^2 = \mathbf{J} \cdot \mathbf{J} = J_x^2 + J_y^2 + J_z^2$. The ket $|jm\rangle$ representing an eigenstate of J^2 and J_z satisfies the eigenvalue equations

$$J^2|jm\rangle = j(j+1)|jm\rangle,$$

$$J_z|jm\rangle = m|jm\rangle.$$

The states $|jm\rangle$ will be referred to as angular momentum eigenstates of \mathbf{J} . The j are necessarily non-negative integers or half-integers (with a definite integer/half-integer character for a given system). For a given j , there exists all states with $m = -j, -j+1, \dots, j-1, j$. The angular momentum eigenstates are orthogonal and conventionally normalized such that

$$\langle j'm'|jm\rangle = \delta_{j'j}\delta_{m'm}.$$

A system may be composed of two subsystems which have angular momentum operators \mathbf{J}_1 and \mathbf{J}_2 . As each of these operators acts only on the coordinates of the respective subsystem, the operators \mathbf{J}_1 and \mathbf{J}_2 commute (that is, their components commute). The total angular momentum operator satisfying the commutation relations for the combined space, Eq. (B.1), is given by $\mathbf{J} = \mathbf{J}_1 + \mathbf{J}_2$. The operators J_1^2 and J_2^2 commute with J^2 and J_z , whereas $J_{1,z}$ and $J_{2,z}$ do not. The eigenstates of J_1^2 , J_2^2 , J^2 , and J_z can be taken as a linear combination of the eigenstates of J_1^2 , $J_{1,z}$, J_2^2 , and $J_{2,z}$:

$$|(\gamma_1 j_1 \gamma_2 j_2)jm\rangle = \sum_{m_1, m_2} C_{j_1 m_1 j_2 m_2}^{jm} |\gamma_1 j_1 m_1, \gamma_2 j_2 m_2\rangle, \quad (\text{B.2})$$

where $C_{j_1 m_1 j_2 m_2}^{jm}$ represents the conventional Clebsch-Gordon coefficients and γ_1 and γ_2 encapsulate additional quantum numbers needed to uniquely specify the state. The Clebsch-Gordon coefficient $C_{j_1 m_1 j_2 m_2}^{jm}$ vanishes unless $|j_1 - j_2| \leq j \leq j_1 + j_2$ (the *triangular condition*), $m_1 + m_2 = m$, and $j_1 + j_2 + j = n$, where n is an integer. The inverse relationship is

$$|\gamma_1 j_1 m_1, \gamma_2 j_2 m_2\rangle = \sum_j C_{j_1 m_1 j_2 m_2}^{jm} |(\gamma_1 j_1 \gamma_2 j_2) j m\rangle.$$

The notation $|\gamma_1 j_1 m_1, \gamma_2 j_2 m_2\rangle$ appearing above is used to represent the product state $|\gamma_1 j_1 m_1\rangle |\gamma_2 j_2 m_2\rangle$. The matrix element of an operator T which, say, operates only on coordinates of the first subsystem may be written in terms of the matrix elements of the isolated subsystem:

$$\langle \gamma'_1 j'_1 m'_1, \gamma'_2 j'_2 m'_2 | T | \gamma_1 j_1 m_1, \gamma_2 j_2 m_2 \rangle = \langle \gamma'_1 j'_1 m'_1 | T | \gamma_1 j_1 m_1 \rangle \delta_{\gamma'_2 \gamma_2} \delta_{j'_2 j_2} \delta_{m'_2 m_2}.$$

Often the more symmetrical 3- j symbols are used in favor of the Clebsch-Gordon coefficients; the 3- j symbol is related to the Clebsch-Gordon coefficient by

$$\begin{pmatrix} j_1 & j_2 & j_3 \\ m_1 & m_2 & m_3 \end{pmatrix} = \frac{(-1)^{j_1 - j_2 - m_3}}{\sqrt{2j_3 + 1}} C_{j_1 m_1 j_2 m_2}^{j_3, -m_3}.$$

Selection rules for the 3- j symbol follow directly from the selection rules of the Clebsch-Gordon coefficients—namely, $|j_1 - j_2| \leq j_3 \leq j_1 + j_2$ and $m_1 + m_2 + m_3 = 0$. Here it is also worth presenting the 6- j , 9- j , and 12- j (II) symbols which also appear throughout this dissertation. The 6- j symbol may be written as a summation over

3- j symbols as

$$\begin{aligned} \left\{ \begin{array}{ccc} j_1 & j_2 & j_3 \\ j_4 & j_5 & j_6 \end{array} \right\} &= \sum_{\text{all } m} (-1)^{j_1 - m_1 + j_2 - m_2 + j_3 - m_3 + j_4 - m_4 + j_5 - m_5 + j_6 - m_6} \\ &\times \begin{pmatrix} j_1 & j_2 & j_3 \\ -m_1 & -m_2 & -m_3 \end{pmatrix} \begin{pmatrix} j_1 & j_5 & j_6 \\ m_1 & -m_5 & m_6 \end{pmatrix} \\ &\times \begin{pmatrix} j_2 & j_6 & j_4 \\ m_2 & -m_6 & m_4 \end{pmatrix} \begin{pmatrix} j_3 & j_4 & j_5 \\ m_3 & -m_4 & m_5 \end{pmatrix}, \end{aligned}$$

where the summation runs over all allowed m -values. The 9- j symbol may be written

$$\begin{aligned} \left\{ \begin{array}{ccc} j_1 & j_2 & j_3 \\ j_4 & j_5 & j_6 \\ j_7 & j_8 & j_9 \end{array} \right\} &= \sum_J (-1)^{2J} (2J + 1) \\ &\times \left\{ \begin{array}{ccc} j_1 & j_2 & j_3 \\ j_6 & j_9 & J \end{array} \right\} \left\{ \begin{array}{ccc} j_4 & j_5 & j_6 \\ j_2 & J & j_8 \end{array} \right\} \left\{ \begin{array}{ccc} j_7 & j_8 & j_9 \\ J & j_1 & j_4 \end{array} \right\}. \end{aligned}$$

And the 12- j symbol of the second kind may be written

$$\begin{aligned} \left\{ \begin{array}{cccc} - & j_1 & j_2 & j_3 \\ j_4 & - & j_5 & j_6 \\ j_7 & j_8 & - & j_9 \\ j_{10} & j_{11} & j_{12} & - \end{array} \right\} &= (-1)^{j - 5 - j_3 - j_{10} + j_8} \sum_J (2J + 1) \\ &\times \left\{ \begin{array}{ccc} j_2 & j_5 & j_{12} \\ j_3 & j_6 & j_9 \\ j_1 & j_4 & J \end{array} \right\} \left\{ \begin{array}{ccc} j_{11} & j_{10} & j_{12} \\ j_8 & j_7 & j_9 \\ j_1 & j_4 & J \end{array} \right\}. \end{aligned}$$

Symmetry relations and selection rules of the 3-, 6-, 9-, and 12- j (II) symbols—as well

as several useful relationships among them—can be found in Ref. [83].

B.2 Orbital and Spin-1/2 Angular Momentum

The orbital angular momentum operator is given by

$$\mathbf{L} = -i\mathbf{r} \times \nabla.$$

The angular momentum eigenstates of \mathbf{L} are the spherical harmonics $Y_{lm}(\theta, \phi)$, satisfying the eigenvalue equations

$$L^2 Y_{lm}(\theta, \phi) = l(l+1) Y_{lm}(\theta, \phi),$$

$$L_z Y_{lm}(\theta, \phi) = m Y_{lm}(\theta, \phi).$$

The spherical harmonics are orthonormal

$$\int_0^{2\pi} \int_0^\pi Y_{l'm'}^*(\theta, \phi) Y_{lm}(\theta, \phi) \sin\theta d\theta d\phi = \delta_{l'l} \delta_{m'm}.$$

The angular momentum operator for a spin-1/2 particle is taken as

$$\mathbf{S} = \frac{1}{2} \boldsymbol{\sigma}.$$

where σ_x , σ_y , and σ_z are the 2×2 Pauli matrices

$$\sigma_x = \begin{pmatrix} 0 & 1 \\ 1 & 0 \end{pmatrix}, \quad \sigma_y = \begin{pmatrix} 0 & -i \\ i & 0 \end{pmatrix}, \quad \sigma_z = \begin{pmatrix} 1 & 0 \\ 0 & -1 \end{pmatrix}. \quad (\text{B.3})$$

The angular momentum eigenstates of \mathbf{S} are the two-component column matrices (or

spinors) χ_{\pm} , given explicitly by

$$\chi_+ = \begin{pmatrix} 1 \\ 0 \end{pmatrix}, \quad \chi_- = \begin{pmatrix} 0 \\ 1 \end{pmatrix}.$$

These satisfy the eigenvalue equations¹

$$\begin{aligned} S^2 \chi_{\pm} &= \frac{3}{4} \chi_{\pm}, \\ S_z \chi_{\pm} &= \pm \frac{1}{2} \chi_{\pm}. \end{aligned}$$

The spinors χ_{\pm} are orthonormal

$$\chi_+^\dagger \chi_+ = \chi_-^\dagger \chi_- = 1, \quad \chi_+^\dagger \chi_- = \chi_-^\dagger \chi_+ = 0.$$

B.3 Spinor Spherical Harmonics and C -Tensor Matrix Elements

Following from Eq. (B.2), the angular momentum eigenstates of the total angular momentum $\mathbf{J} = \mathbf{L} + \mathbf{S}$ for a spin-1/2 system are represented by the *spinor spherical harmonics*

$$\Omega_{jlm}(\theta, \phi) = \sum_{m_l m_s} C_{lm_l \frac{1}{2} m_s}^{jm} Y_{lm_l}(\theta, \phi) \chi_{m_s},$$

where $\chi_{\pm 1/2} = \chi_{\pm}$. From here on, the spinor spherical harmonics will be expressed in terms of the angular quantum number κ , $\Omega_{\kappa m}(\theta, \phi) \equiv \Omega_{j_{\kappa} l_{\kappa} m}(\theta, \phi)$, where κ uniquely

¹It is quite easy to see that $\sigma_{x,y,z}^2 = I$, where I is the 2×2 identity matrix, and consequently that $S^2 = (1/4)(\sigma_y^2 + \sigma_x^2 + \sigma_z^2) = (3/4)I$. Therefore any spinor (that is, any linear combination $a\chi_+ + b\chi_-$) is also an eigenspinor of S^2 with eigenvalue $3/4$; this not unexpected, as the current theory is formalized specifically for a spin-1/2 system.

Table B.1: Conventional spectroscopic notation for the angular quantum number κ for each $|\kappa| \leq 5$. The letters s, p, d, f, g, h correspond to $l_\kappa = 0, 1, 2, 3, 4, 5$, respectively, and the subscripts attached to each letter indicate j_κ .

κ	-1	+1	-2	+2	-3	+3	-4	+4	-5	+5
spec. not.	$s_{1/2}$	$p_{1/2}$	$p_{3/2}$	$d_{3/2}$	$d_{5/2}$	$f_{5/2}$	$f_{7/2}$	$g_{7/2}$	$g_{9/2}$	$h_{9/2}$

specifies the quantum numbers j and l according to

$$j_\kappa = |\kappa| - \frac{1}{2}, \quad l_\kappa = j_\kappa + \frac{1}{2} \text{sign}(\kappa), \quad (\text{B.4})$$

where $\text{sign}(\kappa) = \kappa/|\kappa|$. The allowed values of κ range according to $\kappa = \pm 1, \pm 2, \dots$. It is worth noting that $l_\kappa(l_\kappa + 1) = \kappa(\kappa + 1)$ and $j_\kappa(j_\kappa + 1) = \kappa^2 - 1/4$. The conventional spectroscopic notation associated with each $|\kappa| \leq 5$ is given in Table B.1. (The seemingly arbitrary quantum number κ has its usefulness in the Dirac relativistic electron theory where it provides a clean formulation of the radial wave equations for a spherically symmetric potential; see Appendix E.)

The spinor spherical harmonics satisfy the eigenvalue equations

$$\begin{aligned} L^2 \Omega_{\kappa m}(\theta, \phi) &= l_\kappa(l_\kappa + 1) \Omega_{\kappa m}(\theta, \phi), \\ S^2 \Omega_{\kappa m}(\theta, \phi) &= \frac{3}{4} \Omega_{\kappa m}(\theta, \phi), \\ J^2 \Omega_{\kappa m}(\theta, \phi) &= j_\kappa(j_\kappa + 1) \Omega_{\kappa m}(\theta, \phi), \\ J_z \Omega_{\kappa m}(\theta, \phi) &= m \Omega_{\kappa m}(\theta, \phi), \\ \mathcal{P} \Omega_{\kappa m}(\theta, \phi) &= (-1)^{l_\kappa} \Omega_{\kappa m}(\theta, \phi), \end{aligned}$$

where $\mathcal{P} = \mathcal{I}$ is the parity (coordinate inversion) operator having the effect $\mathcal{I}f(\mathbf{r}) =$

$f(-\mathbf{r})$. Furthermore, they are orthonormal

$$\int_0^{2\pi} \int_0^\pi \Omega_{\kappa'm'}^\dagger(\theta, \phi) \Omega_{\kappa m}(\theta, \phi) \sin\theta d\theta d\phi = \delta_{\kappa'\kappa} \delta_{m'm}. \quad (\text{B.5})$$

From the eigenvalue relations above it can further be shown that the spinor spherical harmonics are eigenspinors of the operator $\boldsymbol{\sigma} \cdot \mathbf{L}$. To see this, first consider the relation

$$J^2 = \mathbf{J} \cdot \mathbf{J} = (\mathbf{L} + \mathbf{S}) \cdot (\mathbf{L} + \mathbf{S}) = L^2 + S^2 + 2\mathbf{S} \cdot \mathbf{L},$$

which is to say

$$\boldsymbol{\sigma} \cdot \mathbf{L} = J^2 - L^2 - S^2.$$

From the above eigenvalue relations it follows that²

$$\begin{aligned} \boldsymbol{\sigma} \cdot \mathbf{L} \Omega_{\kappa m}(\theta, \phi) &= \left[j_\kappa (j_\kappa + 1) - l_\kappa (l_\kappa + 1) - \frac{3}{4} \right] \Omega_{\kappa m}(\theta, \phi) \\ &= \left[\kappa^2 - \frac{1}{4} - \kappa (\kappa + 1) - \frac{3}{4} \right] \Omega_{\kappa m}(\theta, \phi) \\ &= -(\kappa + 1) \Omega_{\kappa m}(\theta, \phi). \end{aligned} \quad (\text{B.6})$$

Matrix elements of “ C -tensors” between the spinor spherical harmonics are prevalent in applications of atomic physics and will be considered here. The components of a C -tensor are simply spherical harmonics with a different normalization

$$C_{kq}(\theta, \phi) = \sqrt{\frac{4\pi}{2k+1}} Y_{kq}(\theta, \phi).$$

²Of course, this implies that the spinor spherical harmonics are also eigenspinors of the operator $\mathbf{S} \cdot \mathbf{L}$. However, in Dirac’s relativistic electron theory (Section E.5) the spin angular momentum operator \mathbf{S} takes on the form of a 4×4 matrix; for this reason it is preferable to consider $\boldsymbol{\sigma} \cdot \mathbf{L}$ as $\boldsymbol{\sigma}$ (and \mathbf{L} as well) does not change form in that theory.

The matrix elements to be considered are given by

$$\langle \kappa' m' | C_{kq} | \kappa m \rangle \equiv \int_0^{2\pi} \int_0^\pi \Omega_{\kappa' m'}^\dagger(\theta, \phi) C_{kq}(\theta, \phi) \Omega_{\kappa m}(\theta, \phi) \sin\theta d\theta d\phi.$$

$C_{kq}(\theta, \phi)$ is a rank- k spherical tensor operator (see Appendix C), and so from the Wigner-Eckart theorem, Eq. (C.4), these matrix elements may be written in terms of a 3- j symbol and a reduced matrix element

$$\langle \kappa' m' | C_{kq} | \kappa m \rangle = (-1)^{j_{\kappa'} - m'} \begin{pmatrix} j_{\kappa'} & k & j_{\kappa} \\ -m' & q & m \end{pmatrix} \langle \kappa' || C_k || \kappa \rangle.$$

Explicit evaluation of the reduced matrix element yields

$$\langle \kappa' || C_k || \kappa \rangle = (-1)^{j_{\kappa} + k + 1/2} \sqrt{(2j_{\kappa'} + 1)(2j_{\kappa} + 1)} \begin{pmatrix} j_{\kappa'} & k & j_{\kappa} \\ -1/2 & 0 & 1/2 \end{pmatrix} \Pi(l_{\kappa'} + k + l_{\kappa}), \quad (\text{B.7})$$

where

$$\Pi(l) = \begin{cases} 1 & \text{if } l \text{ is even} \\ 0 & \text{if } l \text{ is odd} \end{cases}.$$

The appearance of the conditional factor $\Pi(l_{\kappa'} + k + l_{\kappa})$ can be attributed to the fact that the C -tensors transform under coordinate inversion according to $PC_{kq}(\theta, \phi)P^\dagger = (-1)^k C_{kq}(\theta, \phi)$; consequently

$$\langle \kappa' m' | C_{kq} | \kappa m \rangle = \langle \kappa' m' | P^\dagger PC_{kq} P^\dagger P | \kappa m \rangle = (-1)^{l_{\kappa'} + k + l_{\kappa}} \langle \kappa' m' | C_{kq} | \kappa m \rangle,$$

from which the conditional factor may be deduced. From Eqs. (B.4) one may find

the relations $j_{-\kappa} = j_{\kappa}$ and $l_{-\kappa} = l_{\kappa} - \text{sign}(\kappa)$; with these relations it then follows

$$\langle -\kappa' || C_k || -\kappa \rangle = \langle \kappa' || C_k || \kappa \rangle.$$

Appendix C

Irreducible Spherical Tensor Operators

C.1 Definitions

The purpose of this appendix is to provide a brief overview of irreducible spherical tensor operators (or, for brevity, spherical tensors) and to introduce the notations used throughout this dissertation. The expressions provided within this appendix are, for the most part, given without proof. For a more detailed description of spherical tensors, including several useful relationships, the reader is again referred to one of several books on the theory of quantum angular momentum (e.g., Ref. [83]).

A rank- k spherical tensor T_k is a set of $2k + 1$ operators. The components (i.e., operators) are expressed as T_{kq} with $q = -k, -k + 1, \dots, k - 1, k$. Spherical tensors satisfy the following commutation relations with the angular momentum operator \mathbf{J}

$$\begin{aligned} [J_z, T_{kq}] &= qT_{kq}, \\ [J_{\pm}, T_{kq}] &= \sqrt{k(k+1) - q(q \pm 1)}T_{kq \pm 1}, \end{aligned} \tag{C.1}$$

where $J_{\pm} = J_x \pm iJ_y$ represents the conventional raising and lowering operators. These commutation relations ensure that the components of the tensor T_k transform under rotations in a similar manner as do the m -substates of the angular momentum eigenstates. In particular, a spherical tensor of rank 0 is a *scalar* operator and a spherical tensor of rank 1 is a *vector* operator.

C.2 Coupling Spherical Tensors

Suppose there exists two spherical tensors, P_{k_1} and Q_{k_2} . These two spherical tensors may be coupled to form a spherical tensor of rank k with components given by the formula

$$\{P_{k_1} \otimes Q_{k_2}\}_{kq} = \sum_{q_1 q_2} C_{k_1 q_1 k_2 q_2}^{kq} P_{k_1 q_1} Q_{k_2 q_2},$$

where $C_{k_1 q_1 k_2 q_2}^{kq}$ again represents the conventional Clebsch-Gordon coefficients. This composite spherical tensor necessarily satisfies the commutation relations, Eq. (C.1). From the triangular selection rule of the Clebsch-Gordon coefficients, it is apparent that (to be non-trivial) the rank of the composite tensor is limited by $|k_1 - k_2| \leq k \leq k_1 + k_2$. The scalar product for two tensors of equal rank is taken as

$$P_k \cdot Q_k \equiv (-1)^{-k} \sqrt{2k+1} \{P_k \otimes Q_k\}_{00} = \sum_q (-1)^q P_{kq} Q_{k-q}. \quad (\text{C.2})$$

If the two spherical tensors Q_{k_1} and R_{k_2} commute (that is, all components of the respective tensors commute), the following useful recoupling relation may be shown to hold:

$$(P_{k_1} \cdot Q_{k_1}) (R_{k_2} \cdot S_{k_2}) = \sum_k (-1)^{k-k_1-k_2} \{P_{k_1} \otimes R_{k_2}\}_k \cdot \{Q_{k_1} \otimes S_{k_2}\}_k. \quad (\text{C.3})$$

Furthermore, following directly from symmetry relations of the Clebsch-Gordon coefficients one may easily find the relation $\{Q_{k_1} \otimes R_{k_2}\}_k = (-1)^{k_1+k_2-k} \{R_{k_2} \otimes Q_{k_1}\}_k$.

C.3 Wigner-Eckart Theorem

The angular momentum eigenstates may be represented by the ket $|\gamma jm\rangle$, where γ encapsulates all quantum numbers beyond the angular quantum numbers j and m required to specify the state. The matrix elements of a generic spherical tensor T_k between these angular momentum states—i.e., the matrix elements $\langle \gamma' j' m' | T_{kq} | \gamma jm \rangle$ —are to be considered. From the transformation properties of spherical tensors under rotations, it may be shown that the matrix element $\langle \gamma' j' m' | T_{kq} | \gamma jm \rangle$ may be written in terms of the Clebsch-Gordon coefficient $C_{jmkq}^{j'm'}$ and a factor which is completely independent of m , m' , and q . This implies that all dependence of the matrix element on the particular orientation of the system is contained within the Clebsch-Gordon coefficient. This is the Wigner-Eckart theorem, and it is conventionally expressed as

$$\begin{aligned} \langle \gamma' j' m' | T_{kq} | \gamma jm \rangle &= \frac{(-1)^{2k}}{\sqrt{2j'+1}} C_{jmkq}^{j'm'} \langle \gamma' j' || T_k || \gamma j \rangle \\ &= (-1)^{j'-m'} \begin{pmatrix} j' & k & j \\ -m' & q & m \end{pmatrix} \langle \gamma' j' || T_k || \gamma j \rangle, \end{aligned} \quad (\text{C.4})$$

where the factor $\langle \gamma' j' || T_k || \gamma j \rangle$ introduced here is referred to as the reduced matrix element. The last expression here employs the more symmetric 3- j symbol in favor of the Clebsch-Gordon coefficient (see Appendix B).

A reduced matrix element of the spherical tensor $\{P_{k_1} \otimes Q_{k_2}\}_k$ may be expressed

in terms of reduced matrix elements of the uncoupled spherical tensors P_{k_1} and Q_{k_2} :

$$\begin{aligned} \langle \gamma' j' || \{P_{k_1} \otimes Q_{k_2}\}_k || \gamma j \rangle &= \sqrt{2k+1} \sum_{j''} (-1)^{j'+j+k} \begin{Bmatrix} j' & k & j \\ k_2 & j'' & k_1 \end{Bmatrix} \\ &\times \sum_{\gamma''} \langle \gamma' j' || P_{k_1} || \gamma'' j'' \rangle \langle \gamma'' j'' || Q_{k_2} || \gamma j \rangle. \end{aligned}$$

Now consider a system composed of two separate subsystems, having a total angular momentum operator $\mathbf{J} = \mathbf{J}_1 + \mathbf{J}_2$, where \mathbf{J}_1 and \mathbf{J}_2 are the angular momentum operators associated with the two subsystems (e.g., orbital angular momentum and spin angular momentum). Following Eq. (B.2) the angular momentum eigenstates of \mathbf{J} are written $|(\gamma_1 j_1 \gamma_2 j_2) j m\rangle$. If the spherical tensor P_{k_1} only operates on the first subsystem and spherical tensor Q_{k_2} only operates on the second subsystem, one may find the relation

$$\begin{aligned} \langle (\gamma'_1 j'_1 \gamma'_2 j'_2) j' || \{P_{k_1} \otimes Q_{k_2}\}_k || (\gamma_1 j_1 \gamma_2 j_2) j \rangle &= \sqrt{(2j'+1)(2k+1)(2j+1)} \\ &\times \begin{Bmatrix} j'_1 & j_1 & k_1 \\ j'_2 & j_2 & k_2 \\ j' & j & k \end{Bmatrix} \\ &\times \langle \gamma'_1 j'_1 || P_{k_1} || \gamma_1 j_1 \rangle \langle \gamma'_2 j'_2 || Q_{k_2} || \gamma_2 j_2 \rangle. \end{aligned}$$

Following directly from this result are the two useful relations

$$\begin{aligned}
\langle (\gamma'_1 j'_1 \gamma'_2 j'_2) j' || P_k || (\gamma_1 j_1 \gamma_2 j_2) j \rangle &= \delta_{\gamma'_2 \gamma_2} \delta_{j'_2 j_2} (-1)^{j'_1 + j_2 + j + k} \sqrt{(2j' + 1)(2j + 1)} \\
&\quad \times \begin{Bmatrix} j' & k & j \\ j_1 & j_2 & j'_1 \end{Bmatrix} \langle \gamma'_1 j'_1 || P_k || \gamma_1 j_1 \rangle, \\
\langle (\gamma'_1 j'_1 \gamma'_2 j'_2) j' || Q_k || (\gamma_1 j_1 \gamma_2 j_2) j \rangle &= \delta_{\gamma'_1 \gamma_1} \delta_{j'_1 j_1} (-1)^{j_1 + j_2 + j' + k} \sqrt{(2j' + 1)(2j + 1)} \\
&\quad \times \begin{Bmatrix} j' & k & j \\ j_2 & j_1 & j'_2 \end{Bmatrix} \langle \gamma'_2 j'_2 || Q_k || \gamma_2 j_2 \rangle.
\end{aligned}$$

With the use of the Wigner-Eckart theorem and the expression for the scalar product, one may further obtain the relation for the matrix element of the scalar product of P_k and Q_k

$$\begin{aligned}
\langle (\gamma'_1 j'_1 \gamma'_2 j'_2) j' m' | P_k \cdot Q_k | (\gamma_1 j_1 \gamma_2 j_2) j m \rangle &= \delta_{j' j} \delta_{m' m} (-1)^{j_1 + j'_2 + j} \begin{Bmatrix} j'_1 & j_1 & k \\ j_2 & j'_2 & j \end{Bmatrix} \\
&\quad \times \langle \gamma'_1 j'_1 || P_k || \gamma_1 j_1 \rangle \langle \gamma'_2 j'_2 || Q_k || \gamma_2 j_2 \rangle.
\end{aligned}$$

C.4 Additional Notational Conventions and Additional Expressions Specific to Vectors

The primary notational conventions for spherical tensors may be inferred from the preceding sections of this appendix. In this section, a few additional notational conventions used throughout this dissertation will be presented. Furthermore, some useful expressions specific to vectors will also be given.

If two spherical tensors—one of which being a scalar—are coupled, the components

of the resulting spherical tensor are simply

$$\begin{aligned}\{S_0 \otimes P_k\}_{kq} &= S_{00}P_{kq} , \\ \{P_k \otimes S_0\}_{kq} &= P_{kq}S_{00} .\end{aligned}$$

When S_0 is understood to be a scalar, the subscript 0 can be dropped and the composite tensors here are then sufficiently represented by SP_k and P_kS , respectively. With this notation, it is further found that

$$\{P_{k_1} \otimes SQ_{k_2}\}_k = \{P_{k_1}S \otimes Q_{k_2}\}_k .$$

A vector may be written unitalicized, in bold, and without the subscript 1. Specific examples are the position vector \mathbf{r} and angular momentum operators \mathbf{L} , \mathbf{S} , and \mathbf{J} . Following from Eq. (C.2), the scalar product of two vectors is

$$\mathbf{A} \cdot \mathbf{B} = -\sqrt{3} \{\mathbf{A} \otimes \mathbf{B}\}_{00}$$

Furthermore, the vector cross product has the relation

$$\mathbf{A} \times \mathbf{B} = -i\sqrt{2} \{\mathbf{A} \otimes \mathbf{B}\}_1 .$$

The spherical components of a vector operator \mathbf{A} are given by the scalar product with the spherical basis vectors

$$A_\mu = \hat{\mathbf{e}}_\mu \cdot \mathbf{A} \quad (\mu = 0, \pm 1) ,$$

where the spherical basis vectors are

$$\hat{\mathbf{e}}_0 = \hat{\mathbf{e}}_z, \quad \hat{\mathbf{e}}_{\pm 1} = \mp \frac{1}{\sqrt{2}} (\hat{\mathbf{e}}_x \pm \hat{\mathbf{e}}_y).$$

For example, the z -component of the angular momentum operator \mathbf{J} is

$$J_z = J_0 = \hat{\mathbf{e}}_0 \cdot \mathbf{J} = \hat{\mathbf{e}}_z \cdot \mathbf{J}.$$

The following specific relations are useful in the derivations of Chapter 3 (see Ref. [83])

$$\begin{aligned} \{\mathbf{A} \otimes \mathbf{B}\}_{00} &= -\frac{1}{\sqrt{3}} (\mathbf{A} \cdot \mathbf{B}), \\ \{\mathbf{A} \otimes \mathbf{B}\}_{10} &= \frac{i}{\sqrt{2}} (\mathbf{A} \times \mathbf{B}) \cdot \hat{\mathbf{e}}_z, \\ \{\mathbf{A} \otimes \mathbf{B}\}_{20} &= \frac{1}{\sqrt{6}} [3(\mathbf{A} \cdot \hat{\mathbf{e}}_z)(\mathbf{B} \cdot \hat{\mathbf{e}}_z) - (\mathbf{A} \cdot \mathbf{B})]. \end{aligned} \quad (\text{C.5})$$

Appendix D

Floquet Perturbation Theory

D.1 Foundations and the Floquet Perturbation Expansion

The purpose of this appendix is to present the aspects of time-dependent perturbation theory pertinent to the derivation of the ac Stark effect in Chapter 3. Specifically, this regards a perturbation which varies harmonically in time; however, this discussion begins with the somewhat more general case of a periodic perturbation. Non-degeneracy and non-resonance will be assumed, though the cases of degeneracy and resonance will be briefly discussed in Section D.3. The formalism presented here largely follows that of Sambe [69].

The exact wavefunction satisfies the Schrödinger equation

$$\left[H(\xi, t) - i \frac{\partial}{\partial t} \right] \Psi(\xi, t) = 0,$$

where ξ encapsulates all space and spin coordinates. The Hamiltonian is periodic in

time with period τ , having the implication

$$H(\xi, t + \tau) = H(\xi, t).$$

As a consequence of the Floquet theorem of differential equations, solutions of this Schrödinger equation may be written in the form

$$\Psi(\xi, t) = \phi(\xi, t)e^{-i\mathcal{E}t}, \quad (\text{D.1})$$

where \mathcal{E} is a real constant and $\phi(\xi, t)$ has periodicity τ ,

$$\phi(\xi, t + \tau) = \phi(\xi, t). \quad (\text{D.2})$$

Defining the operator

$$\mathcal{H}(\xi, t) \equiv H(\xi, t) - i\frac{\partial}{\partial t},$$

it follows from Eq. (D.1) that the Schrödinger equation can then be represented by the eigenvalue equation

$$\mathcal{H}(\xi, t)\phi(\xi, t) = \mathcal{E}\phi(\xi, t). \quad (\text{D.3})$$

Despite its explicit time dependence, this expression is reminiscent of the time-*independent* Schrödinger eigenvalue equation. Following Ref. [69], the operator $\mathcal{H}(\xi, t)$ will be referred to as the steady state Hamiltonian and the resulting eigenfunctions as steady states. For this particular work, it is the eigenvalue \mathcal{E} which will be of interest. The physical significance of \mathcal{E} is discussed in Section D.2.

To begin the perturbation formalism, the Hamiltonian is partitioned into two

Hermitian operators: an unperturbed Hamiltonian $H_0(\xi)$ and a perturbation $V(\xi, t)$,

$$H(\xi, t) = H_0(\xi) + V(\xi, t),$$

where it is assumed that the entire time dependence of $H(\xi, t)$ may be associated with the perturbation. Further it is assumed that the eigenvalues and eigenfunctions of the unperturbed Hamiltonian are known, satisfying

$$H_0(\xi)f_n(\xi) = E_n f_n(\xi),$$

with $n = 0, 1, 2, \dots$. The functions $f_n(\xi)$ constitute a complete orthogonal basis set for a Hilbert space (e.g., all functions which are square integrable in the coordinate space \mathbf{r}). The inner product for two functions $g(\xi)$ and $h(\xi)$ within this Hilbert space is given by

$$\langle g|h \rangle = \int g^*(\xi)h(\xi)d\xi,$$

where the integration is over the entire configuration space.

The unperturbed steady state Hamiltonian is defined in a similar fashion:

$$\mathcal{H}_0(\xi, t) = \mathcal{H}(\xi, t) - V(\xi, t) = H_0(\xi) - i\frac{\partial}{\partial t}.$$

The zeroth-order eigenvalue equation is taken as

$$\mathcal{H}_0(\xi, t)\phi_{nq}^{(0)}(\xi, t) = \mathcal{E}_{nq}^{(0)}\phi_{nq}^{(0)}(\xi, t),$$

where the zeroth order eigenvalues and eigenfunctions given explicitly in terms of E_n

and $f_n(\xi)$ are

$$\begin{aligned}\mathcal{E}_{nq}^{(0)} &= E_n + q\omega, \\ \phi_{nq}^{(0)}(\xi, t) &= f_n(\xi)e^{iq\omega t},\end{aligned}$$

where $\omega = 2\pi/\tau$ and $q = 0, \pm 1, \pm 2 \dots$ to satisfy the periodicity requirement, Eq. (D.2). The set of all functions $\phi_{nq}^{(0)}(\xi, t)$ (with $n = 0, 1, 2, \dots$; $q = 0, \pm 1, \pm 2 \dots$) constitute a complete orthogonal basis set in an extended Hilbert space which additionally includes functions with periodicity τ . The inner product of two functions $u(\xi, t)$ and $v(\xi, t)$ residing in this extended Hilbert space is defined by

$$\langle\langle u|v\rangle\rangle = \frac{1}{\tau} \int_{-\tau/2}^{\tau/2} \int u^*(\xi, t)v(\xi, t)d\xi dt.$$

The foundations have now been laid to consider the Floquet perturbation expansion. The Floquet perturbation equations may be formalized in direct analogy with the formalism of time-independent perturbation theory (see, for example, [53, 43]). This begins with an expansion of the eigenvalue and eigenfunction of interest for the steady state eigenvalue equation, Eq. (D.3), in orders of the perturbation (e.g., $\mathcal{E}_{nq} = \mathcal{E}_{nq}^{(0)} + \mathcal{E}_{nq}^{(1)} + \mathcal{E}_{nq}^{(2)} + \dots$). Equating terms of like orders results in the hierarchy of equations (given explicitly here through the third order)

$$\begin{aligned}[\mathcal{H}_0(\xi, t) - \mathcal{E}_{nq}^{(0)}] \phi_{nq}^{(0)}(\xi, t) &= 0, \\ [\mathcal{H}_0(\xi, t) - \mathcal{E}_{nq}^{(0)}] \phi_{nq}^{(1)}(\xi, t) &= [\mathcal{E}_{nq}^{(1)} - V(\xi, t)] \phi_{nq}^{(0)}(\xi, t), \\ [\mathcal{H}_0(\xi, t) - \mathcal{E}_{nq}^{(0)}] \phi_{nq}^{(2)}(\xi, t) &= [\mathcal{E}_{nq}^{(1)} - V(\xi, t)] \phi_{nq}^{(1)}(\xi, t) + \mathcal{E}_{nq}^{(2)} \phi_{nq}^{(0)}(\xi, t), \\ [\mathcal{H}_0(\xi, t) - \mathcal{E}_{nq}^{(0)}] \phi_{nq}^{(3)}(\xi, t) &= [\mathcal{E}_{nq}^{(1)} - V(\xi, t)] \phi_{nq}^{(2)}(\xi, t) + \mathcal{E}_{nq}^{(2)} \phi_{nq}^{(1)}(\xi, t) + \mathcal{E}_{nq}^{(3)} \phi_{nq}^{(0)}(\xi, t), \\ &\vdots\end{aligned}$$

where the first of these is the zeroth order equation which has already been introduced. Employing the completeness of the unperturbed eigenfunctions $\phi_{n'q'}^{(0)}(\xi, t)$ in the extended Hilbert space, one may form the appropriate inner products to solve for the higher orders of \mathcal{E}_{nq} . Using bra-ket notation for matrix elements of the extended Hilbert space, these are

$$\begin{aligned}
\mathcal{E}_{nq}^{(1)} &= \langle\langle nq|V|nq\rangle\rangle, \\
\mathcal{E}_{nq}^{(2)} &= \sum_{n'q'} \frac{\langle\langle nq|V|n'q'\rangle\rangle\langle\langle n'q'|V|nq\rangle\rangle}{\mathcal{E}_{nq}^{(0)} - \mathcal{E}_{n'q'}^{(0)}}, \\
\mathcal{E}_{nq}^{(3)} &= \sum_{n'q'n''q''} \frac{\langle\langle nq|V|n''q''\rangle\rangle\langle\langle n''q''|V|n'q'\rangle\rangle\langle\langle n'q'|V|nq\rangle\rangle}{\left(\mathcal{E}_{nq}^{(0)} - \mathcal{E}_{n''q''}^{(0)}\right)\left(\mathcal{E}_{nq}^{(0)} - \mathcal{E}_{n'q'}^{(0)}\right)} \\
&\quad - \langle\langle nq|V|nq\rangle\rangle \sum_{n'q'} \frac{\langle\langle nq|V|n'q'\rangle\rangle\langle\langle n'q'|V|nq\rangle\rangle}{\left(\mathcal{E}_{nq}^{(0)} - \mathcal{E}_{n'q'}^{(0)}\right)^2}, \\
&\quad \vdots
\end{aligned} \tag{D.4}$$

where the bra and ket states here represent the unperturbed steady states. The summations here are understood to exclude the cases $(n'q') = (nq)$ and $(n''q'') = (nq)$, which would lead to vanishing denominators. In arriving at these expressions, intermediate normalization was enforced (i.e., $\langle\langle\phi_{nq}^{(0)}|\phi_{nq}\rangle\rangle = 1$). Expressed in this form, the resemblance of the Floquet eigenvalue perturbation expressions to the time-independent perturbation expressions is immediately recognizable.

D.2 A Perturbation with Static and Harmonic Time-Dependent Parts

In this section, the specific case of a perturbation consisting of a static part as well as a harmonically oscillating part is considered. Such a periodic perturbation may be

written

$$V(\xi, t) = V_s(\xi) + V_-(\xi)e^{-i\omega t} + V_+(\xi)e^{+i\omega t}, \quad (\text{D.5})$$

where $V_s^\dagger(\xi) = V_s(\xi)$ and $V_-^\dagger(\xi) = V_+(\xi)$ to ensure the Hermitian character of the perturbation. It is useful to first analyze the matrix elements of this perturbation between the unperturbed steady states—that is, the matrix elements $\langle\langle n'q'|V|nq\rangle\rangle$.

The individual contribution for the static part gives

$$\begin{aligned} \langle\langle n'q'|V_s|nq\rangle\rangle &= \frac{1}{\tau} \int_{-\tau/2}^{\tau/2} \int [f_{n'}(\xi)e^{iq'\omega t}]^* V_s(\xi) [f_n(\xi)e^{iq\omega t}] d\xi dt \\ &= \frac{1}{\tau} \int_{-\tau/2}^{\tau/2} e^{i(q-q')\omega t} dt \int f_{n'}^*(\xi)V_s(\xi)f_n(\xi)d\xi \\ &= \delta_{q',q}\langle n'|V_s|n\rangle, \end{aligned}$$

and the contributions for the harmonic part give

$$\begin{aligned} \langle\langle n'q'|V_\pm e^{\pm i\omega t}|nq\rangle\rangle &= \frac{1}{\tau} \int_{-\tau/2}^{\tau/2} \int [f_{n'}(\xi)e^{iq'\omega t}]^* V_\pm(\xi)e^{\pm i\omega t} [f_n(\xi)e^{iq\omega t}] d\xi dt \\ &= \frac{1}{\tau} \int_{-\tau/2}^{\tau/2} e^{i(q-q'\pm 1)\omega t} dt \int f_{n'}^*(\xi)V_\pm(\xi)f_n(\xi)d\xi \\ &= \delta_{q',q\pm 1}\langle n'|V_\pm|n\rangle. \end{aligned}$$

Thus, since the time integral may be performed explicitly, these results may be used to reduce the eigenvalue perturbation expressions, Eqs. (D.4), in terms of “ordinary” matrix elements (i.e., matrix elements of the non-extended Hilbert space). Further using the explicit form $\mathcal{E}_{nq}^{(0)} = E_n + q\omega$ in the denominators, Eqs. (D.4) can easily be

reduced to ($\mathcal{E}_{nq}^{(0)}$ is also included here for completeness)

$$\begin{aligned}
\mathcal{E}_{nq}^{(0)} &= E_n + q\omega, \\
\mathcal{E}_{nq}^{(1)} &= \langle n|V_s|n\rangle, \\
\mathcal{E}_{nq}^{(2)} &= \sum_{n'} \frac{\langle n|V_s|n'\rangle\langle n'|V_s|n\rangle}{E_n - E_{n'}} + \sum_{n'} \frac{\langle n|V_+|n'\rangle\langle n'|V_-|n\rangle}{E_n - E_{n'} + \omega} + \sum_{n'} \frac{\langle n|V_-|n'\rangle\langle n'|V_+|n\rangle}{E_n - E_{n'} - \omega}, \\
\mathcal{E}_{nq}^{(3)} &= \sum_{n'n''} \frac{\langle n|V_s|n''\rangle\langle n''|V_s|n'\rangle\langle n'|V_s|n\rangle}{(E_n - E_{n''})(E_n - E_{n'})} - \langle n|V_s|n\rangle \sum_{n'} \frac{\langle n|V_s|n'\rangle\langle n'|V_s|n\rangle}{(E_n - E_{n'})^2} \\
&\quad + \sum_{n'n''} \frac{\langle n|V_s|n''\rangle\langle n''|V_+|n'\rangle\langle n'|V_-|n\rangle}{(E_n - E_{n''})(E_n - E_{n'} + \omega)} + \sum_{n'n''} \frac{\langle n|V_s|n''\rangle\langle n''|V_-|n'\rangle\langle n'|V_+|n\rangle}{(E_n - E_{n''})(E_n - E_{n'} - \omega)} \\
&\quad + \sum_{n'n''} \frac{\langle n|V_+|n''\rangle\langle n''|V_s|n'\rangle\langle n'|V_-|n\rangle}{(E_n - E_{n''} + \omega)(E_n - E_{n'} + \omega)} + \sum_{n'n''} \frac{\langle n|V_-|n''\rangle\langle n''|V_s|n'\rangle\langle n'|V_+|n\rangle}{(E_n - E_{n''} - \omega)(E_n - E_{n'} - \omega)} \\
&\quad + \sum_{n'n''} \frac{\langle n|V_+|n''\rangle\langle n''|V_-|n'\rangle\langle n'|V_s|n\rangle}{(E_n - E_{n''} + \omega)(E_n - E_{n'})} + \sum_{n'n''} \frac{\langle n|V_-|n''\rangle\langle n''|V_+|n'\rangle\langle n'|V_s|n\rangle}{(E_n - E_{n''} - \omega)(E_n - E_{n'})} \\
&\quad - \langle n|V_s|n\rangle \sum_{n'} \frac{\langle n|V_+|n'\rangle\langle n'|V_-|n\rangle}{(E_n - E_{n'} + \omega)^2} - \langle n|V_s|n\rangle \sum_{n'} \frac{\langle n|V_-|n'\rangle\langle n'|V_+|n\rangle}{(E_n - E_{n'} - \omega)^2}, \\
&\quad \vdots
\end{aligned} \tag{D.6}$$

where appropriate values of n' and n'' are again excluded from the summations.

It may be shown for all $k > 0$ (as is plainly shown above for $k = 1, 2, 3$), that the terms $\mathcal{E}_{nq}^{(k)}$ are in fact independent of the quantum number q . Thus, the eigenvalues \mathcal{E}_{nq} and $\mathcal{E}_{nq'}$ only differ by an integer multiple of ω associated with the zeroth order term—specifically, $\mathcal{E}_{nq'} = \mathcal{E}_{nq} + (q' - q)\omega$. From the eigenvalue equation, Eq. (D.3), it can be seen that the corresponding eigenfunctions must be related by $\phi_{nq'}(\xi, t) = e^{i(q'-q)\omega t} \phi_{nq}(\xi, t)$. However, it is found the total wavefunctions $\Psi_{nq'}(\xi, t)$ and $\Psi_{nq}(\xi, t)$ (as given by Eq. (D.1)) are identical:

$$\Psi_{nq'}(\xi, t) = \phi_{nq'}(\xi, t)e^{-i\mathcal{E}_{nq'}t} = \phi_{nq}(\xi, t)e^{-i\mathcal{E}_{nq}t} = \Psi_{nq}(\xi, t).$$

Consequently, the “quantum number” q does not specify unique physical states.

In principle then, the eigenvalue \mathcal{E}_{nq} and its zeroth-order value $\mathcal{E}_{nq}^{(0)}$ alone do not have any physical significance; the appropriate physical observable is given by the q -independent term

$$\delta E_n \equiv \mathcal{E}_{nq} - \mathcal{E}_{nq}^{(0)}.$$

Using the approximation $\phi_{nq}(\xi, t) \simeq \phi_{nq}^{(0)}(\xi, t)$ in the expression for the total wavefunction, the following approximate expression is obtained,

$$\Psi_n(\xi, t) \simeq \phi_{nq}^{(0)}(\xi, t)e^{-i\mathcal{E}_{nq}t} = f_n(\xi)e^{-i(E_n + \delta E_n)t}.$$

From this, it is apparent that δE_n may be associated with the mean energy shift of n -th level of the system. Expanding δE_n in orders of the perturbation, $\delta E_n = \delta E_n^{(1)} + \delta E_n^{(2)} + \dots$, it is apparent that $\delta E_n^{(k)} = \mathcal{E}_{nq}^{(k)}$ (for $k > 0$, as $\delta E_n^{(0)} = 0$).

Though providing a clear physical association for δE_n , the argument in the preceding paragraph is somewhat unsatisfactory. For instance, there is no justification given for truncating $\phi_{nq}(\xi, t)$ at the zeroth order term while simultaneously keeping all orders of \mathcal{E}_{nq} appearing in the phase factor. A more rigorous analysis of the physical significance of δE_n has been performed by Langhoff *et al.* [39] by employing the time-dependent Hellmann-Feynman theorem; these authors conclude that δE_n indeed “corresponds to the energy of induction associated with the application of an oscillatory perturbation to the system and provides the physically significant level shift.” The derivation provided therein will not be repeated here.

More physical insight can be gained from considering the specific system of an atom interacting with monochromatic electromagnetic radiation (i.e., a laser). In a rigorous treatment, the radiation is properly described within a quantum mechanical framework (quantum electrodynamics). However, for most cases of interest a classical description of the radiation is satisfactory. The perturbation describing the interac-

tion of the (quantum mechanical) atom with the classical electromagnetic field takes the form of the general perturbation presented at the beginning of this section; thus the expressions given in this section are assumed to be applicable to this scenario. For this case, the unperturbed eigenfunction $\phi_{nq}^{(0)}(\xi, t)$ may be interpreted as a “dressed” atomic state—that is, an atomic state (given by quantum number n) supplemented by a particular number of photons present in the field (given by the quantum number q). The energy of the composite system is further represented by $\mathcal{E}_{nq}^{(0)} = E_n + q\omega$. The intermediate states in the perturbation expressions, Eq. (D.4), represent dressed states in which the atomic state (n) and/or the total number of photons in the field (q) is changed. It should be noted, however, that this interpretation of the perturbed system presupposes some knowledge of the quantum nature of the electromagnetic field, as the photon itself—and its corresponding energy ω —are strictly products of quantum electrodynamics. Thus, some of the quantum nature of light is evident in this semi-classical treatment. It is also worth noting that, as the response of the atom itself does not depend on q , this dressed state interpretation assumes that there must be a sufficient “supply” of photons in the field.

D.3 Additional Comments: Degeneracy, Resonance, and Applicability

From Eqs. (D.4), it is seen that $\mathcal{E}_{nq}^{(k)}$ ($k > 0$) may diverge if there are any steady states with zeroth order eigenvalues satisfying $\mathcal{E}_{n'q'}^{(0)} \simeq \mathcal{E}_{nq}^{(0)}$ —or more descriptively $E_{n'} + q'\omega \simeq E_n + q\omega$. There are two modes by which this may occur: $E_{n'} \simeq E_n$ (degeneracy) and $E_{n'} - E_n \simeq p\omega$, for $p = \pm 1, \pm 2, \dots$ (resonance). Either scenario may be handled analogously to degenerate time-independent perturbation theory (e.g., incorporate the offending steady states into a model space and diagonalize the effective

Hamiltonian of this space [43]). In regard to resonances in particular, one may then obtain information about *transitions* between the unperturbed stationary states [69]. Both degenerate and resonant levels will be generically referred to as degenerate below.

The possibility of divergences immediately raises questions about the applicability of the Floquet perturbation expressions, Eqs. (D.4). For many practical situations, there will inevitably be multiple levels in the unperturbed spectrum satisfying $E_{n'} \simeq E_n + p\omega$ for some (possibly large) integers p . Calculations would become very cumbersome if all such levels needed to be treated as degenerate. Sambe [69], however, shows that the (non-degenerate) first-order expressions remain valid so long as there are no levels with $E_{n'} \simeq E_n \pm \omega$, second-order expressions remain valid so long as there are no levels with $E_{n'} \simeq E_n \pm 2\omega$, etcetera. Therefore, when retaining only low order expressions, levels with $E_{n'} \simeq E_n + p\omega$ for high- $|p|$ pose no general threat for divergences.

For the particular case of the harmonic oscillating perturbation, one may see directly from Eq. (D.6) that only levels with $E_{n'} \simeq E_n \pm \omega$ threaten to cause divergences even through the third-order. Returning to the atom-laser scenario of the previous section as a specific example, an atomic level with $E_{n'} \simeq E_n + 2\omega$ would only need to be treated degenerately in the fourth-order. Such a fourth-order treatment includes effects of two-photon atomic transitions.

Appendix E

Atomic Structure Theory

E.1 Slater Determinant Wavefunctions

Suppose a system of N identical fermions is described by a Hamiltonian of the form

$$H(\xi_1, \xi_2, \dots, \xi_N) = \sum_{q=1}^N h(\xi_q), \quad (\text{E.1})$$

where $h(\xi_q)$ is a Hermitian operator acting only on the coordinates of the q -th particle, collectively represented by ξ_q (for the remainder of Appendix E the indices p and q will be reserved for coordinate indices and subsequently will be understood to range $1, 2, \dots, N$). The operator $h(\xi)$ represents a single-particle Hamiltonian, and therefore has a complete set of eigenfunctions $\phi_\gamma(\xi)$ and corresponding eigenvalues ε_γ given by

$$h(\xi)\phi_\gamma(\xi) = \varepsilon_\gamma\phi_\gamma(\xi),$$

where the label γ here encapsulates all quantum numbers necessary to describe the single-particle state. The set of eigenfunctions $\phi_\gamma(\xi)$ will be taken to be orthonormal.

It is easy to see that the product wave function

$$\Phi_{ab\dots n}(\xi_1, \xi_2, \dots, \xi_N) = \phi_a(\xi_1)\phi_b(\xi_2) \dots \phi_n(\xi_N), \quad (\text{E.2})$$

satisfies the time-independent Schrödinger equation

$$H(\xi_1, \xi_2, \dots, \xi_N)\Phi_{ab\dots n}(\xi_1, \xi_2, \dots, \xi_N) = E_{ab\dots n}\Phi_{ab\dots n}(\xi_1, \xi_2, \dots, \xi_N), \quad (\text{E.3})$$

with eigenvalues $E_{ab\dots n} \equiv \varepsilon_a + \varepsilon_b + \dots + \varepsilon_n$. However, the product wavefunction, Eq. (E.2), is not a properly antisymmetrized wavefunction, i.e., it does not acquire an overall π phase change with the permutation of any two coordinate indices. The properly antisymmetrized wavefunction is given by the determinant

$$\Phi_{ab\dots n}(\xi_1, \xi_2, \dots, \xi_N) = \frac{1}{\sqrt{N!}} \begin{vmatrix} \phi_a(\xi_1) & \phi_a(\xi_2) & \dots & \phi_a(\xi_N) \\ \phi_b(\xi_1) & \phi_b(\xi_2) & \dots & \phi_b(\xi_N) \\ \vdots & \vdots & \ddots & \vdots \\ \phi_n(\xi_1) & \phi_n(\xi_2) & \dots & \phi_n(\xi_N) \end{vmatrix}. \quad (\text{E.4})$$

A wavefunction of this form is referred to as a Slater determinant. The Slater determinant also satisfies the time-independent Schrödinger equation, Eq. (E.3), with the same eigenvalues as the corresponding product wavefunction. Note here that if any two quantum numbers are equivalent (e.g., $a = b$), then the corresponding rows of the underlying matrix are identical and the determinant (i.e., the wavefunction) vanishes; this is a realization of the Pauli exclusion principle (which itself is merely a consequence of the antisymmetrization requirement). The factor of $1/\sqrt{N!}$ is included here such that the Slater determinant wavefunction is normalized.

E.2 Variations of the Slater Determinant

At this point it will be useful to consider the variation of the Slater determinant $\Phi_{ab\dots n}(\xi_1, \xi_2, \dots, \xi_N)$, given by Eq. (E.4), with respect to small variations in the single-particle wavefunctions (orbitals) $\delta\phi_a(\xi)$, $\delta\phi_b(\xi)$, \dots . First, the simplified case of the variation of a two-particle Slater determinant will be considered; this is given by

$$\delta\Phi_{ab}(\xi_1, \xi_2) = \frac{1}{\sqrt{2!}} \begin{vmatrix} \delta\phi_a(\xi_1) & \delta\phi_a(\xi_2) \\ \phi_b(\xi_1) & \phi_b(\xi_2) \end{vmatrix} + \frac{1}{\sqrt{2!}} \begin{vmatrix} \phi_a(\xi_1) & \phi_a(\xi_2) \\ \delta\phi_b(\xi_1) & \delta\phi_b(\xi_2) \end{vmatrix}.$$

The variation of the orbital $\phi_a(\xi)$ can be written in terms of the complete set of orbitals

$$\delta\phi_a(\xi) = \sum_{\gamma} x_a^{\gamma} \phi_{\gamma}(\xi),$$

with x_a^{γ} being small coefficients (a similar expression exists for $a \rightarrow b$). In terms of these coefficients

$$\begin{aligned} \delta\Phi_{ab}(\xi_1, \xi_2) &= \sum_{\gamma} x_a^{\gamma} \frac{1}{\sqrt{2!}} \begin{vmatrix} \phi_{\gamma}(\xi_1) & \phi_{\gamma}(\xi_2) \\ \phi_b(\xi_1) & \phi_b(\xi_2) \end{vmatrix} + \sum_{\gamma} x_b^{\gamma} \frac{1}{\sqrt{2!}} \begin{vmatrix} \phi_a(\xi_1) & \phi_a(\xi_2) \\ \phi_{\gamma}(\xi_1) & \phi_{\gamma}(\xi_2) \end{vmatrix} \\ &= \sum_{\gamma} x_a^{\gamma} \Phi_{\gamma b}(\xi_1, \xi_2) + \sum_{\gamma} x_b^{\gamma} \Phi_{a\gamma}(\xi_1, \xi_2). \end{aligned}$$

It is easy to see that the coefficients x_a^a and x_b^b multiply the original determinant, whereas the coefficient x_a^b and x_b^a multiply vanishing determinants. Thus, the variation may be written

$$\delta\Phi_{ab}(\xi_1, \xi_2) = (x_a^a + x_b^b) \Phi_{ab}(\xi_1, \xi_2) + \sum_{\gamma \notin \{ab\}} x_a^{\gamma} \Phi_{\gamma b}(\xi_1, \xi_2) + \sum_{\gamma \notin \{ab\}} x_b^{\gamma} \Phi_{a\gamma}(\xi_1, \xi_2).$$

This result is readily generalized to an N -particle Slater determinant

$$\begin{aligned}
\delta\Phi_{ab\dots n}(\xi_1, \xi_2, \dots, \xi_N) &= x\Phi_{ab\dots n}(\xi_1, \xi_2, \dots, \xi_N) \\
&+ \sum_{\gamma \notin \{ab\dots n\}} x_a^\gamma \Phi_{\gamma b\dots n}(\xi_1, \xi_2, \dots, \xi_N) \\
&+ \sum_{\gamma \notin \{ab\dots n\}} x_b^\gamma \Phi_{a\gamma\dots n}(\xi_1, \xi_2, \dots, \xi_N) \\
&+ \dots \\
&+ \sum_{\gamma \notin \{ab\dots n\}} x_n^\gamma \Phi_{ab\dots\gamma}(\xi_1, \xi_2, \dots, \xi_N), \quad (\text{E.5})
\end{aligned}$$

where $x \equiv (x_a^a + x_b^b + \dots + x_n^n)$. Imposing normalization as a variational constraint may be done directly by setting $x = 0$. Eq. (E.5) will be useful in deriving the Hartree-Fock equations in Section E.4.

E.3 Matrix Elements Between Slater Determinant Wavefunctions

Following Ref. [43], a given reference Slater determinant will now be written in Dirac bra-ket notation as $|\alpha\rangle$. In this section and the remainder of Appendix E, the labels a, b, c, \dots will now be used to denote any single-particle state which is included in the reference Slater determinant $|\alpha\rangle$; these will be referred to collectively as “occupied” orbitals. Remaining orbitals not included in $|\alpha\rangle$ will be labeled by r, s, t, \dots and referred to as “virtual” orbitals. Labels i, j, k, \dots will represent all (i.e., occupied and virtual) orbitals. A new wavefunction, orthogonal to $|\alpha\rangle$, may be formed by replacing any given occupied orbital a by any given virtual orbital r in the Slater determinant; this new Slater determinant is then represented by $|\alpha_a^r\rangle$. Likewise, a Slater determinant formed by replacing two occupied orbitals with two virtual orbitals

is represented by $|\alpha_{ab}^{rs}\rangle$. This notation can clearly be extended through all N possible excitations of the occupied orbitals.¹

A general one-particle operator F and two-particle operator G have the form²

$$\begin{aligned} F(\xi_1, \xi_2, \dots, \xi_N) &= \sum_p f(\xi_p), \\ G(\xi_1, \xi_2, \dots, \xi_N) &= \sum_{p < q} g(\xi_p, \xi_q), \end{aligned} \tag{E.6}$$

where $g(\xi, \xi')$ is invariant with respect to a swap of coordinates ($\xi \leftrightarrow \xi'$). Matrix elements of $f(\xi)$ and $g(\xi, \xi')$ connecting single particle orbitals are given the shorthand notation

$$\begin{aligned} f_{ij} &\equiv \int \phi_i^*(\xi) f(\xi) \phi_j(\xi) d\xi, \\ g_{ijkl} &\equiv \iint \phi_i^*(\xi) \phi_j^*(\xi') g(\xi, \xi') \phi_k(\xi) \phi_l(\xi') d\xi d\xi'. \end{aligned}$$

From the symmetry of $g(\xi, \xi')$, it follows that $g_{ijkl} = g_{jilk}$; furthermore, if $f(\xi)$ and $g(\xi, \xi')$ are Hermitian, then $f_{ji} = f_{ij}^*$ and $g_{klij} = g_{ijkl}^*$.

Matrix elements of the one- and two-particle operators, Eqs. (E.6), between Slater determinants take a particularly simple form; the expressions are given here without

¹Note that a , for example, does not label a *specific* occupied state. To clarify this, suppose that the set of all orbitals $\phi_i(\xi)$ are enumerated such that $i = 1, 2, \dots, N$ correspond to the occupied orbitals; in this case, a is allowed to take on any value 1 to N . A summation over a would then imply a summation from 1 to N . The same logic can be extended to virtual orbitals as well.

²Some terminology used throughout this dissertation is clarified here. ‘‘One-particle’’ operator will be used to describe the operator $F(\xi_1, \xi_2, \dots, \xi_N)$ whereas ‘‘single-particle’’ operator will be used to describe the operator $f(\xi)$. This distinction is not standard.

proof. For diagonal matrix elements between Slater determinants,

$$\begin{aligned}\langle\alpha|F|\alpha\rangle &= \sum_a f_{aa}, \\ \langle\alpha|G|\alpha\rangle &= \frac{1}{2} \sum_{ab} (g_{abab} - g_{abba}).\end{aligned}\tag{E.7}$$

In regard to $\langle\alpha|G|\alpha\rangle$, g_{abab} here is referred to as the direct term whereas g_{abba} is referred to as the exchange term. For matrix elements between Slater determinants differing by a single orbital

$$\begin{aligned}\langle\alpha_a^r|F|\alpha\rangle &= f_{ra}, \\ \langle\alpha_a^r|G|\alpha\rangle &= \sum_b (g_{rbab} - g_{rbba}).\end{aligned}\tag{E.8}$$

For matrix elements between Slater determinants differing by two orbitals,

$$\begin{aligned}\langle\alpha_{ab}^{rs}|F|\alpha\rangle &= 0, \\ \langle\alpha_{ab}^{rs}|G|\alpha\rangle &= (g_{rsab} - g_{rsba}).\end{aligned}\tag{E.9}$$

Finally, matrix elements of one- and two-particle operators between Slater determinants differing by more than two orbitals vanish.³

³In the following section, the “occupied” orbitals are given a special distinction in the context of the Hartree-Fock method. The expressions provided here, however, are not specific to that particular distinction of “occupied” and “virtual” orbitals. As an example, consider a Slater determinant $|\beta\rangle = |\alpha_b^r\rangle$. This Slater determinant has the diagonal matrix element $\langle\beta|F|\beta\rangle = \langle\alpha_b^r|F|\alpha_b^r\rangle = \sum_a f_{aa} - f_{bb} + f_{rr}$, which is to say that the occupied orbital “ b ” is removed from the summation and replaced with the virtual orbital “ r ”. Further still, consider the Slater determinant $|\beta\rangle$ that consists of all occupied orbitals and *additionally* the virtual orbital r . In this case the diagonal matrix element is $\langle\beta|F|\beta\rangle = \sum_a f_{aa} + f_{rr}$. An effective general formalism is afforded by creation and absorption (annihilation) operators (see, e.g., Ref. [43]). A presentation of this general formalism, however, would come at the cost of a proper introduction of the creation and absorption operators.

E.4 The Hartree-Fock Method

Suppose the N -identical fermion system is described by a Hamiltonian composed of a one-particle operator (F) and two-particle operator (G),

$$H(\xi_1, \xi_2, \dots, \xi_N) = F(\xi_1, \xi_2, \dots, \xi_N) + G(\xi_1, \xi_2, \dots, \xi_N),$$

with both operators being Hermitian. Approximate solutions to the Hamiltonian may be found by invoking the variational principle, that is, by minimizing the expectation value of the Hamiltonian for a given set of constraints. The Hartree-Fock method begins by constraining the wavefunction to the form of a Slater determinant. If the Slater determinant of interest is labeled $|\alpha\rangle$, then the variation of this Slater determinant (see Eq. (E.5)) may be represented as

$$|\delta\alpha\rangle = \sum_{ar} x_a^r |\alpha_a^r\rangle,$$

where normalization is automatically constrained (i.e., $\delta\langle\alpha|\alpha\rangle = 0$). Minimizing the expectation value of the Hamiltonian gives the expression

$$\delta\langle\alpha|H|\alpha\rangle = \langle\delta\alpha|H|\alpha\rangle + \langle\alpha|H|\delta\alpha\rangle = 2\text{Re} \left[\sum_{ar} x_a^r \langle\alpha_a^r|H|\alpha\rangle^* \right] = 0,$$

Since this equality must hold for arbitrary variations (i.e., arbitrary x_a^r), the variational (stationary) solution must then satisfy

$$\langle\alpha_a^r|H|\alpha\rangle = 0,$$

for all possible occupied orbitals a and virtual orbitals r . In terms of the matrix elements, this condition may be written

$$f_{ra} + \sum_b (g_{rbab} - g_{rbba}) = 0. \quad (\text{E.10})$$

At this point it is convenient to introduce the (single-particle) Hartree-Fock operator, $h^{\text{HF}}(\xi)$, defined by its single-particle matrix elements

$$h_{ij}^{\text{HF}} = f_{ij} + \sum_b (g_{ibjb} - g_{ibbj}).$$

From the symmetry of g_{ijkl} it follows that the Hartree-Fock operator is Hermitian. Assuming the diagonal form of h_{ij}^{HF} is qualified,⁴

$$h_{ij}^{\text{HF}} = \varepsilon_i \delta_{ij},$$

it is seen that Eq. (E.10)—that is, $h_{ra}^{\text{HF}} = 0$ —is trivially satisfied. This equation has the simple form of an eigenvalue equation,

$$h^{\text{HF}}(\xi)\phi_i(\xi) = \varepsilon_i\phi_i(\xi), \quad (\text{E.11})$$

where the eigenfunctions represent the so-called Hartree-Fock orbitals.

The simplicity of the eigenvalue expression, Eq. (E.11), is deceptive. The Hartree-Fock operator presupposes knowledge of the occupied orbitals; thus this is a non-linear equation requiring an iterative solution. The evaluation is aided by the introduction

⁴In Ref. [34] this assumption is shown to be valid for the restricted (i.e., spherically symmetric) Dirac-Hartree-Fock equations for a closed-shell atomic system; this will ultimately be the application of the Hartree-Fock equations derived here.

of the Hartree-Fock potential, $u^{\text{HF}}(\xi)$,

$$\begin{aligned} h_{ij}^{\text{HF}} &\equiv f_{ij} + u_{ij}^{\text{HF}}, \\ u_{ij}^{\text{HF}} &\equiv \sum_b (g_{ibjb} - g_{ibbj}). \end{aligned}$$

In practice, an educated “guess” is initially made for the form of the occupied orbitals; these orbitals in turn are used to determine the Hartree-Fock potential. With this potential the eigenvalue equation, Eq. (E.11), is solved to find a new set of orbitals, from which point the process is repeated until the orbitals converge.

The expectation value of the Hamiltonian for the Hartree-Fock Slater determinant is then

$$\begin{aligned} \langle \alpha | H | \alpha \rangle &= \sum_a f_{aa} + \frac{1}{2} \sum_{ab} (g_{abab} - g_{abba}) \\ &= \sum_a h_{aa}^{\text{HF}} - \frac{1}{2} \sum_{ab} (g_{abab} - g_{abba}) \\ &= \sum_a \varepsilon_a - \frac{1}{2} \sum_{ab} (g_{abab} - g_{abba}). \end{aligned} \tag{E.12}$$

E.5 The Dirac Equation

The relativistic motion of an electron in the static electromagnetic potentials $\{\Phi(\mathbf{r}), \mathbf{A}(\mathbf{r})\}$ is governed by the Dirac equation, which in its standard form is given by

$$h(\mathbf{r})\phi(\mathbf{r}) = \varepsilon\phi(\mathbf{r}),$$

where the (single-particle) Dirac Hamiltonian is (see, for example, Ref. [53])

$$h(\mathbf{r}) = c\boldsymbol{\alpha} \cdot \left[-i\nabla + \frac{1}{c}\mathbf{A}(\mathbf{r}) \right] - \Phi(\mathbf{r}) + \beta c^2.$$

The quantities $\alpha_{x,y,z}$ and β are 4×4 Dirac matrices, given by

$$\boldsymbol{\alpha} = \begin{pmatrix} 0 & \boldsymbol{\sigma} \\ \boldsymbol{\sigma} & 0 \end{pmatrix}, \quad \beta = \begin{pmatrix} I & 0 \\ 0 & -I \end{pmatrix}, \quad (\text{E.13})$$

with underlying 2×2 matrices $\sigma_{x,y,z}$ and I being the Pauli matrices, Eq. (B.3), and the identity matrix, respectively. The eigenfunctions of the Dirac Hamiltonian, $\phi(\mathbf{r})$, are themselves four-component column matrices (spinors). Furthermore, in this formalism the spin angular momentum operator is represented by

$$\mathbf{S} = \frac{1}{2} \begin{pmatrix} \boldsymbol{\sigma} & 0 \\ 0 & \boldsymbol{\sigma} \end{pmatrix}, \quad (\text{E.14})$$

and the parity operator by

$$\mathcal{P} = \begin{pmatrix} I & 0 \\ 0 & -I \end{pmatrix} \mathcal{I},$$

where $\mathcal{I}f(\mathbf{r}) = f(-\mathbf{r})$.

This problem is considerably simplified for the case of a spherically symmetric electrostatic potential, $\{\Phi(\mathbf{r}) = \Phi(r), \mathbf{A}(\mathbf{r}) = 0\}$. Given this restriction, the Dirac Hamiltonian is written

$$h(\mathbf{r}) = -ic\boldsymbol{\alpha} \cdot \boldsymbol{\nabla} + \beta c^2 + v(r), \quad (\text{E.15})$$

where $v(r)$ is the potential energy (the proportionality constant between the *electrostatic* potential and the *energy* potential is the charge of the electron, -1 a.u.). This Dirac Hamiltonian can be shown to commute with the operator for the total angular momentum $\mathbf{J} = \mathbf{L} + \mathbf{S}$ and the parity operator P . With these considerations, the

eigenspinors may be cast in the form

$$\phi_{n\kappa m}(\mathbf{r}) = \frac{1}{r} \begin{pmatrix} iG_{n\kappa}(r)\Omega_{\kappa m}(\theta, \phi) \\ F_{n\kappa}(r)\Omega_{-\kappa m}(\theta, \phi) \end{pmatrix}, \quad (\text{E.16})$$

where $\Omega_{\kappa m}(\theta, \phi)$ are the spinor spherical harmonics introduced in Appendix B. The spinors $\phi_{n\kappa m}(\mathbf{r})$ satisfy the eigenvalue equations

$$\begin{aligned} J^2 \phi_{n\kappa m}(\mathbf{r}) &= j_\kappa(j_\kappa + 1) \phi_{n\kappa m}, \\ J_z \phi_{n\kappa m}(\mathbf{r}) &= m \phi_{n\kappa m}, \\ P \phi_{n\kappa m}(\mathbf{r}) &= (-1)^{l_\kappa} \phi_{n\kappa m}, \end{aligned}$$

where j_κ and l_κ are given by Eq. (B.4).⁵ The additional quantum number n in Eq. (E.16) encapsulates all remaining quantum numbers needed to specify the state.

With these $\phi_{n\kappa m}(\mathbf{r})$, the Dirac Hamiltonian, Eq. (E.15), reduces to the two coupled radial equations

$$[v(r) + c^2] G_{n\kappa}(r) + c \left[\frac{d}{dr} - \frac{\kappa}{r} \right] F_{n\kappa}(r) = \varepsilon_{n\kappa} G_{n\kappa}(r), \quad (\text{E.17})$$

$$-c \left[\frac{d}{dr} + \frac{\kappa}{r} \right] G_{n\kappa}(r) + [v(r) - c^2] F_{n\kappa}(r) = \varepsilon_{n\kappa} F_{n\kappa}(r). \quad (\text{E.18})$$

These equations allow for both positive and negative eigenvalues, $\varepsilon_{n\kappa}$. The positive eigenvalues correspond to energies of the appropriate electron state (note that the Dirac Hamiltonian incorporates the electron rest energy c^2 ; as an example, the ground

⁵One should be warned that the Dirac Hamiltonian does not commute with the operator L^2 , and therefore the spinors $\phi_{n\kappa m}(\mathbf{r})$ do *not* represent eigenspinors of L^2 . However, in the non-relativistic limit $F(r) \ll G(r)$ and consequently $L^2 \phi_{n\kappa m}(\mathbf{r}) \simeq l_\kappa(l_\kappa + 1) \phi_{n\kappa m}(\mathbf{r})$ as expected. On the other hand, S^2 does commute with the Dirac Hamiltonian. Indeed from Eq. (E.14) it is found that $S^2 = 3/4$, which is a consequence of the inherent spin-1/2 character of the Dirac relativistic electron theory.

state of the hydrogen atom is $\varepsilon_{1s_{1/2}} \simeq (137)^2 - 1/2 > 0$). The negative eigenvalues, on the other hand, are associated with positron states. These “negative energy states” will not be considered here; however they will be discussed briefly in Appendix F in the context of finite basis set solutions to the Dirac equation. Considering bound states (i.e., $0 < \varepsilon_{n\kappa} < c^2$), $G_{n\kappa}(r)$ and $F_{n\kappa}(r)$ may be taken simultaneously as real and, for a given κ , the solutions may always be chosen such that

$$\int_0^\infty [G_{n'\kappa}(r)G_{n\kappa}(r) + F_{n'\kappa}(r)F_{n\kappa}(r)] dr = \delta_{n'n}.$$

It will be assumed that this choice is always made. Along with the normalization condition of the spherical spinors, Eq. (B.5), this choice further implies normalization of the eigenspinors

$$\int \phi_{n'\kappa'm'}^\dagger(\mathbf{r})\phi_{n\kappa m}(\mathbf{r})d^3\mathbf{r} = \delta_{n'n}\delta_{\kappa'\kappa}\delta_{m'm},$$

where the integration ranges over the entire coordinate space of \mathbf{r} .

It is now worthwhile to consider the non-relativistic limit, wherein $|\varepsilon_{n\kappa} - c^2| \ll c^2$. Within this regime, Eq. (E.18) reduces to the approximate relation (the appropriate assumption $|v(r)| \ll c^2$ is also used)

$$F_{n\kappa}(r) \simeq \frac{1}{2c} \left[\frac{d}{dr} + \frac{\kappa}{r} \right] G_{n\kappa}(r).$$

This expression shows that the radial wavefunction $F_{n\kappa}(r)$ is suppressed by a factor of c^{-1} relative to the radial wavefunction $G_{n\kappa}(r)$. Because of this imbalance, the respective parts of $\phi_{n\kappa m}$ associated with $G_{n\kappa}(r)$ and $F_{n\kappa}(r)$ are aptly referred to as the large and small components, respectively. The approximation for $F_{n\kappa}(r)$ may be

substituted into Eq. (E.17) to obtain an approximate differential equation for $G_{n\kappa}(r)$

$$\begin{aligned} -\frac{1}{2} \left[\frac{d}{dr} - \frac{\kappa}{r} \right] \left[\frac{d}{dr} + \frac{\kappa}{r} \right] G_{n\kappa}(r) + v(r)G_{n\kappa}(r) &\simeq (\varepsilon_{n\kappa} - c^2) G_{n\kappa}(r), \\ -\frac{1}{2} \left[\frac{d^2}{dr^2} - \frac{\kappa(\kappa+1)}{r^2} \right] G_{n\kappa}(r) + v(r)G_{n\kappa}(r) &\simeq (\varepsilon_{n\kappa} - c^2) G_{n\kappa}(r), \\ \left[-\frac{1}{2} \frac{d^2}{dr^2} + \frac{l_\kappa(l_\kappa+1)}{2r^2} + v(r) \right] G_{n\kappa}(r) &\simeq (\varepsilon_{n\kappa} - c^2) G_{n\kappa}(r). \end{aligned}$$

This last expression is immediately recognizable as the radial eigenvalue equation of the non-relativistic Schrödinger equation for an electron with orbital angular momentum l_κ in a spherically symmetric potential. Thus it is expected that the radial wavefunction $G_{n\kappa}(r)$ for an electron in a bound state will show resemblance to the corresponding non-relativistic radial wavefunction.

E.6 The Dirac-Hartree-Fock Approximation

The Dirac Hamiltonian, Eq. (E.15), describes the relativistic motion of a single electron in a spherically symmetric electrostatic potential. In particular, for the pure Coulomb potential $v(r) = -Z/r$ this describes the motion of an electron around a point-like, infinitely massive nucleus of atomic charge Z . For such hydrogen-like atoms, the coupled differential equations, Eqs. (E.17, E.18), have analytic solutions. However, for more complicated atomic systems (i.e., $N > 1$), the interactions between electrons spoils hopes for an analytic solution and approximate methods must be pursued. Such methods usually begin with the Dirac-Hartree-Fock (DHF) approximation. Beginning with the Dirac Hamiltonian extended to many electrons, this approximation follows the general formalism of Section E.4.

A suitable Hamiltonian describing the relativistic motion of the N electrons is the starting point. In particular, the hydrogen-like Dirac Hamiltonians (for each electron)

are supplemented with terms representing the dominant electron-electron interaction, namely the Coulomb repulsion

$$H(\mathbf{r}_1, \mathbf{r}_2, \dots, \mathbf{r}_N) = \sum_q [-ic\boldsymbol{\alpha}_q \cdot \nabla_q + \beta_q c^2 + v_{\text{nuc}}(r_q)] + \sum_{p < q} v_{ee}(\mathbf{r}_p, \mathbf{r}_q), \quad (\text{E.19})$$

where the energy associated with the Coulomb repulsion between two electrons is

$$v_{ee}(\mathbf{r}, \mathbf{r}') = \frac{1}{|\mathbf{r} - \mathbf{r}'|},$$

and the nuclear potential is given by $v_{\text{nuc}}(r) = -Z/r$ for a point-like nucleus, although in practice a nucleus of finite extent is typically implemented. It is assumed that additional effects neglected here (e.g., Breit, hyperfine, recoil) may be treated perturbatively at a later stage.

Of course, the troublesome term in Eq. (E.19) is the Coulomb repulsion term. This interaction may be approximated by the DHF potential. The problem then reduces to solving the single-particle eigenvalue equation

$$h_{\text{DHF}}(\mathbf{r})\phi_i(\mathbf{r}) = \varepsilon_i\phi_i(\mathbf{r}),$$

where the single-particle DHF Hamiltonian is

$$h_{\text{DHF}}(\mathbf{r}) = -ic\boldsymbol{\alpha} \cdot \nabla + \beta c^2 + v_{\text{nuc}}(r) + v_{\text{DHF}}(\mathbf{r}).$$

The DHF potential is defined by its action on the DHF eigenspinors

$$v_{\text{DHF}}(\mathbf{r})\phi_j(\mathbf{r}) = \sum_i (v_{\text{DHF}})_{ij} \phi_i(\mathbf{r}),$$

where

$$(v_{\text{DHF}})_{ij} = \sum_b (g_{ibjb} - g_{ibbj}),$$

and the g_{ijkl} are given by

$$g_{ijkl} = \iint \frac{1}{|\mathbf{r} - \mathbf{r}'|} [\phi_i^\dagger(\mathbf{r})\phi_k(\mathbf{r})] [\phi_j^\dagger(\mathbf{r}')\phi_l(\mathbf{r}')] d^3\mathbf{r}d^3\mathbf{r}'.$$

In accordance with the earlier notation, the summation over index b is limited to occupied orbitals (spinors) only.

The DHF expressions are based upon the variational constraint that the overall wavefunction is represented by a Slater determinant composed of single-particle spinors. In atomic physics, it is typically advantageous to further constrain the spinors to the form of Eq. (E.16) and only allow variations in the radial wavefunctions (the *restricted* DHF method). Given this form for the DHF eigenspinors, one may find (note that now i specifies the quantum numbers $i = (n_i, \kappa_i, m_i) = (n_i, j_i, l_i, m_i)$)

$$\begin{aligned} (v_{\text{DHF}})_{ij} &= \sum_b (g_{ibjb} - g_{ibbj}) \\ &= \delta_{\kappa_i \kappa_j} \delta_{m_i m_j} \sum_{n_b \kappa_b} (2j_b + 1) \left\{ \int_0^\infty [G_i(r)G_j(r) + F_i(r)F_j(r)] v_0(b, b, r) dr \right. \\ &\quad \left. - \sum_k \Lambda_{\kappa_i k \kappa_b} \int_0^\infty [G_i(r)G_b(r) + F_i(r)F_b(r)] v_k(b, j, r) dr \right\}, \end{aligned} \tag{E.20}$$

where

$$\begin{aligned} \Lambda_{\kappa_i k \kappa_j} &= \frac{|\langle \kappa_i || C_k || \kappa_j \rangle|^2}{(2j_i + 1)(2j_j + 1)}, \\ v_k(i, j, r) &= \int_0^\infty \frac{r_{<}^k}{r_{>}^{k+1}} [G_i(r')G_j(r') + F_i(r')F_j(r')] dr'. \end{aligned}$$

Here $\langle \kappa_i || C_k || \kappa_j \rangle$ is the reduced matrix element given by Eq. (B.7) and $r_<$ ($r_>$) is the lesser (greater) of r and r' . Note that $v_k(i, j, r)$ does not depend on the quantum numbers m_i and m_j . It is also noted that Eq. (E.20) assumes a closed-shell system. A shell is defined by the quantum numbers n and κ ; a closed shell system is one in which the m states are either all occupied or all unoccupied (virtual) for any give shell.

As shown above, the DHF potential $v_{\text{DHF}}(r)$ is properly defined by its action on the DHF eigenspinors. However, it is often given the association

$$v_{\text{DHF}}(r) \frac{1}{r} \begin{pmatrix} iG_{n\kappa}(r)\Omega_{\kappa m}(\theta, \phi) \\ F_{n\kappa}(r)\Omega_{-\kappa m}(\theta, \phi) \end{pmatrix} = \frac{1}{r} \begin{pmatrix} i[v_{\text{DHF}}(r)G_{n\kappa}(r)]\Omega_{\kappa m}(\theta, \phi) \\ [v_{\text{DHF}}(r)F_{n\kappa}(r)]\Omega_{-\kappa m}(\theta, \phi) \end{pmatrix},$$

from which it further follows

$$(v_{\text{DHF}})_{ij} = \delta_{\kappa_i \kappa_j} \delta_{m_i m_j} \int_0^\infty [G_{n_i \kappa_i}(r)v_{\text{DHF}}(r)G_{n_j \kappa_j}(r) + F_{n_i \kappa_i}(r)v_{\text{DHF}}(r)F_{n_j \kappa_j}(r)] dr. \quad (\text{E.21})$$

With this association, the DHF eigenspinors can be regarded as solutions of the coupled differential equations

$$\begin{aligned} [v_{\text{nuc}}(r) + v_{\text{DHF}}(r) + c^2] G_{n\kappa}(r) + c \left[\frac{d}{dr} - \frac{\kappa}{r} \right] F_{n\kappa}(r) &= \varepsilon_{n\kappa} G_{n\kappa}(r), \\ -c \left[\frac{d}{dr} + \frac{\kappa}{r} \right] G_{n\kappa}(r) + [v_{\text{nuc}}(r) + v_{\text{DHF}}(r) - c^2] F_{n\kappa}(r) &= \varepsilon_{n\kappa} F_{n\kappa}(r). \end{aligned}$$

Comparing Eqs. (E.20, E.21), $v_{\text{DHF}}(r)$ can be defined in terms of its action on large

and small component radial wavefunctions of the DHF eigenspinors according to

$$v_{\text{DHF}}(r) \begin{pmatrix} G_i(r) \\ F_i(r) \end{pmatrix} = \sum_{n_b \kappa_b} (2j_b + 1) \left[v_0(b, b, r) \begin{pmatrix} G_i(r) \\ F_i(r) \end{pmatrix} - \sum_k \Lambda_{\kappa_i k \kappa_b} v_k(b, i, r) \begin{pmatrix} G_b(r) \\ F_b(r) \end{pmatrix} \right]. \quad (\text{E.22})$$

This, of course, can be used to determine the action of $v_{\text{DHF}}(r)$ on any general spinor as the DHF eigenspinors form a complete set. It should be clarified that the two-component column matrices appearing here are not Dirac spinors.

E.7 Non-Locality and Asymptotic Behavior of the DHF Potential

The DHF potential is a non-local potential; its effect on a spinor at a given radial position r depends on the occupied spinors at radial positions other than r . However, in the limit $r \rightarrow \infty$ the DHF potential takes on the character of a local potential which can be written as a simple function of r . To explore this, the limit of the multipolar potentials $v_k(i, j, r)$ is first examined; $v_k(i, j, r)$ (along with an extra factor of r) is split into two contributions

$$r v_k(i, j, r) = \frac{p_k(i, j, r)}{r^k} + \frac{q_k(i, j, r)}{r^{-(k+1)}},$$

where

$$\begin{aligned} p_k(i, j, r) &= \int_0^r (r')^k [G_i(r')G_j(r') + F_i(r')F_j(r')] dr', \\ q_k(i, j, r) &= \int_r^\infty (r')^{-(k+1)} [G_i(r')G_j(r') + F_i(r')F_j(r')] dr'. \end{aligned}$$

The limit of $p_k(i, j, r)$ with $k = 0$ is easily found to be

$$\lim_{r \rightarrow \infty} p_0(i, j, r) = \delta_{n_i n_j} \delta_{\kappa_i \kappa_j}.$$

For $k > 0$, the corresponding limit may or may not be finite. For $q_k(i, j, r)$ the limit is seen to be

$$\lim_{r \rightarrow \infty} q_k(i, j, r) = 0.$$

Evaluation of the respective terms of $rv_k(i, j, r)$ in the limit $r \rightarrow \infty$ then requires l'Hôpital's rule; the first term (for $k > 0$) is

$$\lim_{r \rightarrow \infty} \frac{p_k(i, j, r)}{r^k} = \lim_{r \rightarrow \infty} \frac{\frac{d}{dr} p_k(i, j, r)}{\frac{d}{dr} r^k} = \lim_{r \rightarrow \infty} \frac{1}{k} r [G_i(r)G_j(r) + F_i(r)F_j(r)] = 0 \quad (k > 0),$$

where the last equality holds due to the requirement that the radial wavefunctions be square-integrable (i.e., physically acceptable solutions to the radial Dirac equation).

The second term is evaluated similarly

$$\lim_{r \rightarrow \infty} \frac{q_k(i, j, r)}{r^{-(k+1)}} = \lim_{r \rightarrow \infty} \frac{\frac{d}{dr} q_k(i, j, r)}{\frac{d}{dr} r^{-(k+1)}} = \lim_{r \rightarrow \infty} \frac{1}{k+1} r [G_i(r)G_j(r) + F_i(r)F_j(r)] = 0,$$

Together these results imply

$$\lim_{r \rightarrow \infty} rv_k(i, j, r) = \delta_{n_i n_j} \delta_{\kappa_i \kappa_j} \delta_{k0}.$$

With Eq. (E.22), it is then found that in the limit $r \rightarrow \infty$ the DHF potential has the following action on the radial wavefunctions

$$\begin{aligned} v_{\text{DHF}}(r) \begin{pmatrix} G_i(r) \\ F_i(r) \end{pmatrix} &\rightarrow \sum_{n_b \kappa_b} (2j_b + 1) (1 - \Lambda_{\kappa_i 0 \kappa_b} \delta_{n_i n_b} \delta_{\kappa_i \kappa_b}) \frac{1}{r} \begin{pmatrix} G_i(r) \\ F_i(r) \end{pmatrix} \\ &= \left(N_{\text{occ}} - \sum_{n_b \kappa_b} \delta_{n_i n_b} \delta_{\kappa_i \kappa_b} \right) \frac{1}{r} \begin{pmatrix} G_i(r) \\ F_i(r) \end{pmatrix}, \end{aligned} \quad (\text{E.23})$$

where

$$N_{\text{occ}} = \sum_{n_b \kappa_b} (2j_b + 1) = \sum_{n_b \kappa_b m_b} 1 = \sum_b 1,$$

is the total number of electrons in the atom (the relation $\Lambda_{\kappa_i 0 \kappa_b} = (2j_b + 1)^{-1} \delta_{\kappa_i \kappa_b}$ for the angular factor was employed here). The summation over occupied orbitals combined with the delta symbols in Eq. (E.23) reveals two possible scenarios

$$v_{\text{DHF}}(r) \begin{pmatrix} G_i(r) \\ F_i(r) \end{pmatrix} \rightarrow \begin{cases} \frac{N_{\text{occ}} - 1}{r} \begin{pmatrix} G_i(r) \\ F_i(r) \end{pmatrix} & \text{if } i \text{ is an occupied orbital} \\ \frac{N_{\text{occ}}}{r} \begin{pmatrix} G_i(r) \\ F_i(r) \end{pmatrix} & \text{if } i \text{ is a virtual orbital} \end{cases} \quad (\text{E.24})$$

For the case in which i represents an occupied orbital the DHF potential is seen here to give the proper asymptotic result—as $r \rightarrow \infty$ a given electron “feels” the Coulomb repulsion from the remaining $N - 1$ electrons in the atom. It is apparent from the second case in Eq. (E.24) that the virtual orbitals obtained from the DHF method are not expected to provide an accurate representations of electron states (at least in the limit $r \rightarrow \infty$).

The non-local character of the DHF potential can be attributed to the exchange part of the electron-electron interaction (which in turn is attributed to the antisymmetrization requirement for the fermion system). The fact that the DHF potential has the local character at $r \rightarrow \infty$ reflects the physical characteristic of the exchange interaction that it tends to zero at large separation distances⁶

E.8 Single-Valence Systems and the V^{N-1} DHF Potential

The atomic systems dealt with in Chapters 4 and 5—namely cesium, aluminum, and gallium—are single-valence systems. The relative “stiffness” of the atomic core is a key feature to which allows an effective description of these many-body systems. This section discusses an appropriate lowest-order description of the single-valence systems rooted in the DHF approximation.

To begin the discussion, a specific application is considered. Suppose that one is interested in calculating the static Stark effect (i.e., interaction of an atom with a static external field) for the ground state of lithium. Lithium represents the simplest univalent system, having a single electron outside of the closed $1s$ core. With the assumption that the electric field points along the z -axis, the second order energy

⁶Following through the derivation above to get the factor $(N_{\text{occ}} - 1)$ it is found that the term N_{occ} is obtained from direct term and -1 is obtained from the exchange term. The -1 just reflects the cancellation of exchange terms g_{abba} with the direct terms g_{abab} for which $a = b$. Formally there is no need to ever include such terms in the theory, and they consequently do not have any physical significance (their inclusion is a matter of convenience). It is in this context that the exchange interaction “tends to zero”.

shift is given by

$$\begin{aligned} \delta E_{1s^2 2s_{1/2}}^{(2)} = & \mathcal{E}^2 \sum_n \frac{\langle 1s^2 2s_{1/2} | D_z | 1s^2 n p_{1/2} \rangle \langle 1s^2 n p_{1/2} | D_z | 1s^2 2s_{1/2} \rangle}{E_{1s^2 2s_{1/2}} - E_{1s^2 2p_{1/2}}} \\ & + \mathcal{E}^2 \sum_n \frac{\langle 1s^2 2s_{1/2} | D_z | 1s^2 n p_{3/2} \rangle \langle 1s^2 n p_{3/2} | D_z | 1s^2 2s_{1/2} \rangle}{E_{1s^2 2s_{1/2}} - E_{1s^2 2p_{3/2}}}, \end{aligned} \quad (\text{E.25})$$

where $D_z = -(z_1 + z_2 + z_3)$ is the z -component of the electric dipole operator (the subscripts 1, 2, 3 here corresponding to the three electrons of the system).⁷ This expression omits highly suppressed contributions from intermediate states which have a core-excited character (i.e., those which do not have a $1s^2(n\kappa)$ configuration).

Numerical evaluation of Eq. (E.25) requires approximate atomic states and energies. An initial choice may be to use the DHF method for the ground state, in which case one obtains the the set of occupied and virtual orbitals

$$\begin{aligned} & \{ \phi_{1s_{1/2}}, \phi_{2s_{1/2}} \} \quad (\text{occupied}), \\ & \left. \begin{aligned} & \{ \phi_{3s_{1/2}}, \phi_{4s_{1/2}}, \dots \} \\ & \{ \phi_{2p_{1/2}}, \phi_{3p_{1/2}}, \dots \} \\ & \{ \phi_{2p_{3/2}}, \phi_{3p_{3/2}}, \dots \} \\ & \quad \vdots \end{aligned} \right\} \quad (\text{virtual}), \end{aligned}$$

and the wavefunctions appearing in Eq. (E.25) then being approximated by the appropriate Slater determinants built from this orbital set. The corresponding approximate energies are then given by Eq. (E.12). From Eq. (E.24) of the previous section, however, it can be seen that the DHF potential acting on a virtual orbital has the

⁷Note that the m -quantum numbers are suppressed here and in the following expressions for clarity.

improper asymptotic behavior as $r \rightarrow \infty$ (being an $N_{\text{occ}}/r = 3/r$ Coulomb potential as opposed to a $2/r$ Coulomb potential) and, consequently, it is expected that these virtual orbitals do not appropriately represent the valence electron states as desired.

An alternative may be to calculate the DHF orbitals separately for each state involved in Eq. (E.12). Each separate wavefunction would be a Slater determinant built from the occupied orbitals of the resulting distinct sets. The previous expressions for the matrix elements of one- and two-particle operators between Slater determinants, Eqs. (E.7—E.9), would not be applicable in this case, and one would have to include extra terms to account for the non-orthogonality of the orbitals of the separate sets. Furthermore, the resulting approximate wavefunctions would then all be eigenfunctions of a different Hamiltonian (as the DHF potentials for each would be different), which is inconsistent with the perturbation theory formalism.⁸

For a moment it is worthwhile to consider the ground state of the Li^+ ion—that is, the $1s^2$ core with the valence electron removed. Qualitatively speaking, the closed core is typically quite “stiff”, which is to say that it is relatively insusceptible to external fields (this qualitative feature is why the core-excited contributions were omitted from Eq. (E.25)). With this in mind, the lithium core is not expected to be perturbed extensively by the additional presence of a valence electron, and in particular, by which state it is in. Following this reasoning, the core states may be assumed to be represented sufficiently well by the DHF orbitals of the Li^+ ion. Solving the DHF equations for the Li^+ ion, one obtains the following set of occupied

⁸Furthermore, the approaches laid out in this paragraph and the previous paragraph involve the DHF method applied to an open-shell system, which requires some additional considerations.

and virtual orbitals

$$\begin{array}{l} \{\phi_{1s_{1/2}}\} \quad (\text{occupied}) \\ \\ \left. \begin{array}{l} \{\phi_{2s_{1/2}}, \phi_{3s_{1/2}}, \dots\} \\ \{\phi_{2p_{1/2}}, \phi_{3p_{1/2}}, \dots\} \\ \{\phi_{2p_{3/2}}, \phi_{3p_{3/2}}, \dots\} \\ \vdots \end{array} \right\} \quad (\text{virtual}) \end{array}$$

The action of the DHF potential on the virtual orbitals in this case has the asymptotic behavior corresponding to an $N_{\text{occ}}/r = 2/r$ Coulomb potential, which is desired for these orbitals to accurately represent valence electron states. Furthermore, the Slater determinants built from these orbitals are orthonormal, making them a suitable basis for a consistent perturbative treatment. The expressions for the matrix elements of one- and two-particle operators between Slater determinants (Eqs. (E.7—E.9)) are applicable (though one has to consider footnote 3 of Section E.3) and may be used to reduce Eq. (E.25) in terms of single-particle matrix elements and energies,

$$\begin{aligned} \delta E_{1s^2 2s_{1/2}}^{(2)} = & \mathcal{E}^2 \sum_n \frac{\langle 2s_{1/2}|z|np_{1/2}\rangle \langle np_{1/2}|z|2s_{1/2}\rangle}{\varepsilon_{2s_{1/2}} - \varepsilon_{np_{1/2}}} \\ & + \mathcal{E}^2 \sum_n \frac{\langle 2s_{1/2}|z|np_{3/2}\rangle \langle np_{3/2}|z|2s_{1/2}\rangle}{\varepsilon_{2s_{1/2}} - \varepsilon_{np_{3/2}}}. \end{aligned}$$

As the representation of the atomic state $|1s^2 2s_{1/2}\rangle$ includes more than the two “occupied” orbitals, the terminology “core” orbitals is now preferred to describe the $1s$ orbitals and “valence” orbital to describe the $2s$ orbital. In the context of perturbation theory, it is still useful to refer to the remaining orbitals as “virtual” orbitals.

The arguments of this section extend to other single-valence systems as well. The method described here, in which the atomic states are built from the DHF orbitals of

the ionic core in the absence of the valence electron is referred to as the V^{N-1} DHF method. The V^{N-1} DHF orbitals provide a particularly efficient starting point from which further corrections to the atomic structure may be calculated; this is the topic of the following section.

E.9 Beyond the V^{N-1} DHF Approximation: Correlation Corrections

The V^{N-1} DHF approximation as described above is capable of providing a good description of the gross structure of many-electron atomic systems. However, when atomic calculations of reasonable accuracy are desired, it is typically found that the DHF approximation alone will not suffice. In this section, corrections to the atomic structure beyond the DHF approximation will be discussed. As atomic structure theory diverges in many directions at this point, this discussion will be kept brief and will emphasize only the general motives.

In the preceding sections the (V^{N-1}) DHF method was introduced as a method for finding approximate energies and wavefunctions (eigenspinors) for a single-valence atomic system described by the Hamiltonian, Eq. (E.19),

$$H = \sum_q [-ic\boldsymbol{\alpha}_q \cdot \boldsymbol{\nabla}_q + \beta_q c^2 + v_{\text{nuc}}(r_q)] + \sum_{p < q} v_{ee}(\mathbf{r}_p, \mathbf{r}_q). \quad (\text{E.26})$$

The resulting approximate wavefunction—the DHF wavefunction Ψ_v^{DHF} —is a Slater determinant composed of the single-particle DHF core orbitals and valence orbital v ; this wavefunction is an eigenfunction of the DHF Hamiltonian

$$H^{\text{DHF}} = \sum_q [-ic\boldsymbol{\alpha}_q \cdot \boldsymbol{\nabla}_q + \beta_q c^2 + v_{\text{nuc}}(r_q) + v_{\text{DHF}}(r_q)], \quad (\text{E.27})$$

with eigenvalues (DHF energies)

$$E_v^{\text{DHF}} = \sum_a \varepsilon_a + \varepsilon_v.$$

The exact Hamiltonian, Eq. (E.26), may be written in terms of the DHF Hamiltonian, Eq. (E.27), as

$$H = H^{\text{DHF}} + V,$$

where

$$V = \sum_{p < q} v_{ec}(\mathbf{r}_p, \mathbf{r}_q) - \sum_q v_{\text{DHF}}(r_q).$$

Here it is plain to see that V may be regarded as a perturbation to the DHF system. One may expand the exact wavefunctions and energies in orders of the perturbation in the usual way,

$$\begin{aligned} \Psi_v &= \Psi_v^{(0)} + \Psi_v^{(1)} + \Psi_v^{(2)} + \dots, \\ E_v &= E_v^{(0)} + E_v^{(1)} + E_v^{(2)} + \dots, \end{aligned}$$

given the associations $\Psi_v^{(0)} = \Psi_v^{\text{DHF}}$ and $E_v^{(0)} = E_v^{\text{DHF}}$. The higher order corrections beyond the DHF approximation are referred to as *correlation corrections*. Correlation corrections, in principle, may be determined by commencing with the standard order-by-order perturbation evaluation seeded from the V^{DHF} approximation. For accurate calculations, however, the standard perturbation theory is usually augmented by some means such that dominant higher order effects are included. In Chapter 5, for example, the potential v_{DHF} is replaced with $v_{\text{DHF}} + \Sigma$ (Σ being the non-local “correlation potential”) to obtain a new set of single-particle orbitals, the so-called Brueckner orbitals. Qualitatively, the Brueckner orbitals provide a better representation of the physical state than the DHF orbitals (namely for the valence orbital).

As a different example, in Chapter 4 high-accuracy experimental data is employed to account for important correlation corrections. Furthermore, high-accuracy ab initio matrix elements obtained from a coupled cluster approach were also used. The coupled-cluster method will be discussed briefly in the following paragraphs.

The so-called correlation operator, χ , has the effect of producing the exact wavefunction when acting on the zeroth order (DHF) state,

$$\Psi_v = (1 + \chi) \Psi_v^{(0)}.$$

The correlation operator may be expanded in orders of the perturbation—i.e., $\chi = \chi^{(1)} + \chi^{(2)} + \dots$ —in which case the following relation is realized (for $n > 0$),

$$\Psi_v^{(n)} = \chi^{(n)} \Psi_v^{(0)}.$$

To solve the conventional perturbation equations through a given order is to effectively solve the correlation operator through that order (actually to obtain the energy to a given order n only requires the correlation operator through the order $n - 1$). Alternatively, one may choose to expand the correlation operator in terms of the number of electron “excitations” from the DHF state, $\chi = \chi^{[1]} + \chi^{[2]} + \dots + \chi^{[N]}$, where $\chi^{[1]} \Psi_v^{\text{DHF}}$, for instance, encapsulates the part of the exact wavefunction Ψ_v which is a linear combination of all Slater determinants in which the valence *or one* core orbital in Ψ_v^{DHF} is replaced with a virtual orbital. Similarly, $\chi^{[N]} \Psi_v^{\text{DHF}}$ encapsulates the part of the exact wavefunction Ψ_v which is a linear combination of all Slater determinants in which the valence *and all* core orbitals are replaced with virtual orbitals. Note the difference between $\chi^{(n)}$ and $\chi^{[n]}$: $\chi^{(n)} \Psi_v^{\text{DHF}}$ is the correction to Ψ_v^{DHF} which is n -th order in the perturbation (and includes all possible excitations), whereas $\chi^{[n]} \Psi_v^{\text{DHF}}$ is the correction to Ψ_v^{DHF} which involves n -electron excitations (and includes all orders

of the perturbation).

In practice it is necessary (for all but the lightest atomic systems) to truncate the expansion at some reasonable excitation-level, $\chi = \chi^{[1]} + \chi^{[2]} + \dots + \chi^{[n]}$, with $n < N$. As an example, taking the expansion $\chi = \chi^{[1]} + \chi^{[2]}$ results in the linearized coupled-cluster singles-doubles (LCCSD) method.⁹ To numerically solve for $\chi^{[1]}$ and $\chi^{[2]}$ requires an iterative procedure which is typically computationally-intensive. However, the result is a correlation operator which takes single and double excitations into account through all orders of perturbation theory, and it is known that the single and double excitations account for the bulk of the correlation effects in single-valence systems (see, e.g., Ref. [43]).

E.10 Matrix Elements of the Electric Dipole and Hyperfine Interaction Operators

The ac Stark effect on the hyperfine structure, as derived in Chapter 3, depends on matrix elements of the electric dipole operator \mathbf{D} and (electronic) hyperfine interaction operator \mathcal{T} . In this section, expressions for matrix elements of the underlying single-particle operators between the Dirac spinors of the form of Eq. (E.16) are derived.

⁹The coupled-cluster method is formulated from the ansatz $\chi = \{\exp(S)\}_{\text{Normal}}$, where it is the cluster operator $S = S^{[1]} + S^{[2]} + \dots$ which is truncated. The exponential expansion includes non-linear terms in S . The linearized coupled-cluster method neglects these non-linear terms, in which case $\chi^{[n]} = S^{[n]}$ follows. The $\{\}_{\text{Normal}}$ here indicates that the normal form of the operator in braces is to be taken.

The operators \mathbf{D} and \mathcal{T} are one-particle vector operators and may be written as

$$\begin{aligned}\mathbf{D} &= -\sum_{p=1}^N \mathbf{r}_p, \\ \mathcal{T} &= \sum_{p=1}^N \mathbf{t}(\mathbf{r}_p).\end{aligned}\quad (\text{E.28})$$

The spherical components of the single-particle operators \mathbf{r} (the position vector) and \mathbf{t} may be written in terms of the rank-1 C -tensor components (Section B.3) as

$$\begin{aligned}r_\lambda &= rC_{1\lambda}(\theta, \phi) \\ t_\lambda &= -\frac{i}{r^2} [\boldsymbol{\alpha} \cdot \mathbf{L}C_{1\lambda}(\theta, \phi)],\end{aligned}\quad (\text{E.29})$$

where again $\boldsymbol{\alpha}$ represents the Dirac matrices (Eq. (E.13)) and \mathbf{L} is the orbital angular momentum operator. The brackets around $\boldsymbol{\alpha} \cdot \mathbf{L}C_{1\lambda}(\theta, \phi)$ indicate that the orbital angular momentum operator does not act beyond the C -tensor. (It is worth clarifying that in Eqs. (E.28) the index p labels the electron number and in Eqs. (E.29) the index λ corresponds to the spherical components $(-1, 0, 1)$ of the vectors.)

Considering \mathbf{r} first, the matrix elements between Dirac spinors $\phi_{n\kappa m}(\mathbf{r})$ are given by

$$\begin{aligned}\langle n' \kappa' m' | r_\lambda | n \kappa m \rangle = \\ \int \begin{pmatrix} iG_{n'\kappa'}(r)\Omega_{\kappa'm'}(\theta, \phi) \\ F_{n'\kappa'}(r)\Omega_{-\kappa'm'}(\theta, \phi) \end{pmatrix}^\dagger rC_{1\lambda}(\theta, \phi) \begin{pmatrix} iG_{n\kappa}(r)\Omega_{\kappa m}(\theta, \phi) \\ F_{n\kappa}(r)\Omega_{-\kappa m}(\theta, \phi) \end{pmatrix} d^3\mathbf{r}.\end{aligned}\quad (\text{E.30})$$

Upon expanding the integrand, the following angular integrals may be evaluated

directly with the Wigner-Eckart theorem, Eq. (C.4),

$$\int_0^{2\pi} \int_0^\pi \Omega_{\pm\kappa'm'}(\theta, \phi) C_{1\lambda}(\theta, \phi) \Omega_{\pm\kappa m}(\theta, \phi) \sin\theta d\theta d\phi = (-1)^{j'-m'} \begin{pmatrix} j' & 1 & j \\ -m' & \lambda & m \end{pmatrix} \langle \kappa' || C_1 || \kappa \rangle, \quad (\text{E.31})$$

where $j = j_\kappa = j_{-\kappa}$ (and similar for j') and $\langle \kappa' || C_k || \kappa \rangle = \langle -\kappa' || C_k || -\kappa \rangle$ are the reduced matrix elements of the C -tensor given by Eq. (B.7). With the phase factor and 3- j symbol factored out, the remaining part of Eq. (E.30) represents the reduced matrix element of \mathbf{r} . Explicitly, this is

$$\langle n' \kappa' || \mathbf{r} || n \kappa \rangle = \langle \kappa' || C_1 || \kappa \rangle \int_0^\infty r [G_{n'\kappa'}(r) G_{n\kappa}(r) + F_{n'\kappa'}(r) F_{n\kappa}(r)] dr.$$

Selection rules of this matrix element follow from the selection rules of the matrix element of the C -tensor—namely, $l'+l = \text{odd integer}$ (parity) and $|j' - j| \leq 1$ (angular momentum).

Now considering \mathbf{t} , the matrix elements are given by (here the integrand has been expanded)

$$\langle n' \kappa' m' | t_\lambda | n \kappa m \rangle = \int \frac{1}{r^2} \left\{ F_{n'\kappa'}(r) G_{n\kappa}(r) \Omega_{-\kappa'm'}^\dagger(\theta, \phi) [\boldsymbol{\sigma} \cdot \mathbf{L} C_{1\lambda}(\theta, \phi)] \Omega_{\kappa m}(\theta, \phi) - G_{n'\kappa'}(r) F_{n\kappa}(r) \Omega_{\kappa'm'}^\dagger(\theta, \phi) [\boldsymbol{\sigma} \cdot \mathbf{L} C_{1\lambda}(\theta, \phi)] \Omega_{-\kappa m}(\theta, \phi) \right\} d^3\mathbf{r}.$$

Attention will initially be focused on the angular integrals

$$\int_0^{2\pi} \int_0^\pi \Omega_{\mp\kappa'm'}^\dagger(\theta, \phi) [\boldsymbol{\sigma} \cdot \mathbf{L} C_{k\lambda}(\theta, \phi)] \Omega_{\pm\kappa m}(\theta, \phi) \sin\theta d\theta d\phi.$$

To analyze this, it is first worthwhile to consider the action of the orbital angular

momentum operator on arbitrary (normalizable) functions $f(\theta, \phi)$ and $g(\theta, \phi)$ (here the θ and ϕ dependence is made implicit for clarity)

$$\mathbf{L}(fg) = -i\mathbf{r} \times \nabla(fg) = -i\mathbf{r} \times [(\nabla f)g + f(\nabla g)] = (\mathbf{L}f)g + f(\mathbf{L}g),$$

where the explicit form $\mathbf{L} = -i\mathbf{r} \times \nabla$ was used to emphasize the derivative character of \mathbf{L} . Following from this general result is the relation

$$[\boldsymbol{\sigma} \cdot \mathbf{L}C_{k\lambda}(\theta, \phi)]\Omega_{\pm\kappa m}(\theta, \phi) = \boldsymbol{\sigma} \cdot \mathbf{L}[C_{k\lambda}(\theta, \phi)\Omega_{\pm\kappa m}(\theta, \phi)] - C_{k\lambda}(\theta, \phi)[\boldsymbol{\sigma} \cdot \mathbf{L}\Omega_{\pm\kappa m}(\theta, \phi)].$$

It is also useful to emphasize that $\boldsymbol{\sigma} \cdot \mathbf{L}$ is a Hermitian operator, which has the implication

$$\int_0^{2\pi} \int_0^\pi f^\dagger(\theta, \phi) [\boldsymbol{\sigma} \cdot \mathbf{L}g(\theta, \phi)] \sin\theta d\theta d\phi = \int_0^{2\pi} \int_0^\pi [\boldsymbol{\sigma} \cdot \mathbf{L}f(\theta, \phi)]^\dagger g(\theta, \phi) \sin\theta d\theta d\phi.$$

With these considerations, the angular integrals may be written

$$\begin{aligned} \int_0^{2\pi} \int_0^\pi \Omega_{\mp\kappa' m'}^\dagger(\theta, \phi) [\boldsymbol{\sigma} \cdot \mathbf{L}C_{k\lambda}(\theta, \phi)] \Omega_{\pm\kappa m}(\theta, \phi) \sin\theta d\theta d\phi = \\ \int_0^{2\pi} \int_0^\pi [\boldsymbol{\sigma} \cdot \mathbf{L}\Omega_{\mp\kappa' m'}(\theta, \phi)]^\dagger C_{k\lambda}(\theta, \phi) \Omega_{\pm\kappa m}(\theta, \phi) \sin\theta d\theta d\phi \\ - \int_0^{2\pi} \int_0^\pi \Omega_{\mp\kappa' m'}^\dagger(\theta, \phi) C_{k\lambda}(\theta, \phi) [\boldsymbol{\sigma} \cdot \mathbf{L}\Omega_{\pm\kappa m}(\theta, \phi)] \sin\theta d\theta d\phi \end{aligned}$$

In Eq. (B.6) it was shown that the spinor spherical harmonics $\Omega_{\kappa m}(\theta, \phi)$ are eigen-spinors of $\boldsymbol{\sigma} \cdot \mathbf{L}$ with the eigenvalues $-(\kappa + 1)$. Making use of this result, the angular

integrals are found to be

$$\int_0^{2\pi} \int_0^\pi \Omega_{\mp\kappa'm'}^\dagger(\theta, \phi) [\boldsymbol{\sigma} \cdot \mathbf{L}C_{k\lambda}(\theta, \phi)] \Omega_{\pm\kappa m}(\theta, \phi) \sin\theta d\theta d\phi =$$

$$\pm (-1)^{j'-m'} \begin{pmatrix} j' & k & j \\ -m' & \lambda & m \end{pmatrix} (\kappa' + \kappa) \langle -\kappa' || C_k || \kappa \rangle.$$

And it then follows that the reduced matrix element of \mathbf{t} is given by

$$\langle n'\kappa' || \mathbf{t} || n\kappa \rangle = (\kappa' + \kappa) \langle -\kappa' || C_1 || \kappa \rangle \int_0^\infty \frac{1}{r^2} [G_{n'\kappa'}(r)F_{n\kappa}(r) + F_{n'\kappa'}(r)G_{n\kappa}(r)] dr.$$

Again the selection rules follow from the selection rules of the matrix element of the C -tensor—namely, $l'+l = \text{even integer (parity)}$ and $|j' - j| \leq 1$ (angular momentum).

Appendix F

Finite Basis Sets Composed of B-Splines

F.1 Introducing B-Splines

This appendix describes the role of B-splines in numerical evaluation of atomic many-body problems. The discussion begins with an introduction of B-splines. A complete description of B-splines is given in Refs. [18, 5].

A B-spline set consists of piecewise polynomial functions of order k ,¹

$$\{B_1^{(k)}(x), B_2^{(k)}(x), \dots, B_n^{(k)}(x)\},$$

where an individual $B_i^{(k)}(x)$ is referred to as a B-spline. Aside from k , a particular B-spline set also depends on the so-called knot sequence $\{t_1, t_2, \dots, t_m\}$, where the m

¹A polynomial $p^{(k)}(x)$ of order k has the form $p^{(k)}(x) = a_0 + a_1x + \dots + a_{k-1}x^{k-1}$, where the a_i are constants. Piecewise polynomials of order k have the above form, but with “constants” a_i which depend on the particular interval (for B-splines the intervals are determined by the values of the knots in the knot sequence).

“knots” satisfy

$$t_1 \leq t_2 \leq \cdots \leq t_m. \quad (\text{F.1})$$

For a given knot sequence, the B-spline set of order 1 is defined by

$$B_i^{(1)}(x) = \begin{cases} 1 & \text{for } t_i \leq x < t_{i+1} \\ 0 & \text{otherwise} \end{cases}, \quad \text{where } i = 1, 2, \dots, m-1.$$

B-spline sets of higher orders are then defined by the recursion relation

$$B_i^{(k)}(x) = \frac{x - t_i}{t_{i+k-1} - t_i} B_i^{(k-1)}(x) + \frac{t_{i+k} - x}{t_{i+k} - t_{i+1}} B_{i+1}^{(k-1)}(x), \quad \text{where } i = 1, 2, \dots, m-k. \quad (\text{F.2})$$

Note that the order k and number of knots m determine the number of B-splines n in the set according to $n = m - k$ ($k < m$ is required). From this point the discussion will be limited to a B-spline set of a given order k ; as a consequence the notation $B_i(x)$ will suffice.

Each B-spline is non-negative; moreover each B-spline is non-zero only within an interval spanning k knots. In particular,

$$\begin{aligned} B_i(x) &> 0 && \text{for } t_i < x < t_{i+k}, \\ B_i(x) &= 0 && \text{for } x < t_i \text{ or } x > t_{i+k}, \end{aligned} \quad (\text{F.3})$$

(the value at points $x = t_i$ and $x = t_{i+k}$ may be either 0 or 1 and is determined by the multiplicity of knots at those values; this is to be discussed below). Essentially, the B-spline $B_i(x)$ “starts” at the knot t_i and “ends” at the knot t_{i+k} , with a positive-definite value between.

Following from Eq. (F.3), it is noted that only the B-splines $B_{i-k+1}(x)$, $B_{i-k+2}(x)$, \dots , $B_i(x)$ are non-zero within the interval $t_i \leq x < t_{i+1}$. These B-splines have the

property

$$\sum_{j=i-k+1}^i B_j(x) = 1 \quad \text{for } t_i \leq x < t_{i+1},$$

where $k \leq i \leq n$ is assumed (such that the index j is not less than 1 or greater than n). One is free to extend the summation to include all other B-splines (which do not contribute within the given interval anyhow); subsequently generalizing to the interval $t_k \leq x < t_{n+1}$ gives

$$\sum_{j=1}^n B_j(x) = 1 \quad \text{for } t_k \leq x < t_{n+1}.$$

It is apparent from Eq. (F.1) that the knots are not required to have distinct values. The multiplicity of knots (that is, the number of knots) associated with a particular value x_0 is directly connected to the continuity properties of the B-splines at the point $x = x_0$. To begin the discussion a useful terminology is introduced: a function regarded as class C^n has continuous derivatives up to the order n . In particular, C^{-1} refers to functions which themselves are discontinuous, C^0 refers to functions which are continuous but whose first derivatives are discontinuous, etcetera.² Now suppose a given B-spline $B_l(x)$ “straddles” the point x_0 (i.e., it is non-zero in the vicinity x_0). If μ represents the multiplicity of knots at x_0 ($\mu \leq k$ will be assumed³), then it can be shown that $B_l(x)$ is of continuity class $C^{k-\mu-1}$ at x_0 . Now suppose that $B_l(x)$ “starts” on one of the knots at x_0 (i.e., $t_l = x_0$); in this case $B_l(x)$ effectively “sees” only the knots t_i with $i \geq l$ and its continuity properties follow accordingly. The case

²Within a region $t_i < x < t_{i+1}$, the B-splines are simple polynomials and are of class $C^{(\infty)}$; thus the discussion here is focused on continuity properties *at* the knot values.

³Strictly speaking, one may have $\mu > k$; however, including “extra” knots beyond $\mu = k$ is to simply include extra B-splines which are equivalent to zero. The expressions following Eq. (F.2) assume that the knot-multiplicity at any point is limited to k .

in which B_l “ends” on one of the knots at x_0 is analogous. As an example, consider the specific case

$$t_1 = t_2 = \cdots = t_k = 0,$$

corresponding to maximum multiplicity at $x = 0$. As the first B-spline, $B_1(x)$, starts at t_1 , it effectively sees all k knots at $x = 0$ and is thus of class C^{-1} at $x = 0$ (i.e., it is discontinuous); $B_2(x)$ effectively sees $k - 1$ knots and is of class C^0 at the $x = 0$; \dots ; and $B_k(x)$ effectively sees 1 knot and is of class C^{k-2} at $x = 0$. It is noted here that for $k \geq 3$ and knots having distinct values, the B-splines are continuous and furthermore have continuous first derivatives.

Because of the general features associated with B-splines—such that they are piecewise polynomials, they are non-negative, they are non-zero only over short intervals, and they overlap only with nearby B-splines—they constitute both a convenient and numerically efficient set of basis functions to work with (the “B” actually stands for “basis”). With parameters chosen appropriately for a given problem, the B-spline set may be regarded as a quasi-complete set of functions. That is, any appropriate function may be suitably represented by an expansion over the B-splines.

F.2 Finite Basis Set Solutions to the Radial Dirac Equation

The radial Dirac equation, Eqs. (E.17, E.18), for a given angular symmetry κ may be written⁴

$$\begin{pmatrix} [v(r) + c^2] & c[d/dr - \kappa/r] \\ -c[d/dr + \kappa/r] & [v(r) - c^2] \end{pmatrix} \begin{pmatrix} G(r) \\ F(r) \end{pmatrix} = \varepsilon \begin{pmatrix} G(r) \\ F(r) \end{pmatrix}. \quad (\text{F.4})$$

For the atomic many-body problem, which is of interest for this dissertation, the potential is taken as $v(r) = v_{\text{nuc}}(r) + v_{\text{DHF}}(r)$. The requirement that the solutions represent physically acceptable states is encapsulated in the boundary conditions

$$G(r)|_{0,\infty} = F(r)|_{0,\infty} = 0. \quad (\text{F.5})$$

This radial Dirac equation may be derived from a variational theory, beginning with the action S ,

$$\begin{aligned} S = \frac{1}{2} \int_0^\infty \left\{ G(r)c \left[\frac{d}{dr} - \frac{\kappa}{r} \right] F(r) - F(r)c \left[\frac{d}{dr} + \frac{\kappa}{r} \right] G(r) \right. \\ \left. + G^2(r) [v(r) + c^2] + F^2(r) [v(r) - c^2] \right. \\ \left. - \varepsilon [G^2(r) + F^2(r)] \right\} dr, \end{aligned}$$

One then seeks an extremum of S with respect to small variations in the radial wavefunctions. From the variational perspective, ε is a Lagrange multiplier which serves to ensure the variational constraint of normalization—i.e., $\delta N = 0$, where

⁴The consideration here is limited to bound state solutions and so $G(r)$ and $F(r)$ may be assumed real.

$N = \int_0^\infty [G^2(r) + F^2(r)] dr$. The (lowest-order) variation of S is

$$\begin{aligned} \delta S = & \int_0^\infty \left(\delta G(r) \left\{ [v(r) + c^2] G(r) + c \left[\frac{d}{dr} - \frac{\kappa}{r} \right] F(r) - \varepsilon G(r) \right\} \right. \\ & \left. + \delta F(r) \left\{ -c \left[\frac{d}{dr} + \frac{\kappa}{r} \right] G(r) + [v(r) - c^2] F(r) - \varepsilon F(r) \right\} \right) dr \\ & + \frac{1}{2} [G(r)\delta F(r) - F(r)\delta G(r)] \Big|_0^\infty. \end{aligned} \quad (\text{F.6})$$

The boundary conditions, Eqs. (F.5), are to be treated as another variational constraint, which is to say $\delta G(r)|_{0,\infty} = \delta F(r)|_{0,\infty} = 0$. As a consequence, the last line of Eq. (F.6) vanishes. To be an extremum, the variation δS must equal zero for all possible variations $\delta G(r)$ and $\delta F(r)$ (subject to the constraints, of course). It follows from Eq. (F.6) that this condition is satisfied only for

$$\begin{aligned} [v(r) + c^2] G(r) + c \left[\frac{d}{dr} - \frac{\kappa}{r} \right] F(r) - \varepsilon G(r) &= 0, \\ -c \left[\frac{d}{dr} + \frac{\kappa}{r} \right] G(r) + [v(r) - c^2] F(r) - \varepsilon F(r) &= 0. \end{aligned}$$

Together, these two differential equations constitute the radial Dirac equation, Eq. (F.4).

One may attempt to solve the radial Dirac equation numerically by employing a finite basis set. This method begins by expanding the large and small radial wavefunctions in terms of basis functions $\{l_i(r), s_i(r)\}$,

$$\begin{pmatrix} G(r) \\ F(r) \end{pmatrix} = \sum_{i=1}^{2n} p_i \begin{pmatrix} l_i(r) \\ s_i(r) \end{pmatrix}, \quad (\text{F.7})$$

where the p_i are expansion coefficients to be determined and the $l_i(r)$ and $s_i(r)$ are real functions. For the radial wavefunctions to represent physically acceptable states

the basis functions should satisfy

$$\left(\begin{array}{c} l_i(r) \\ s_i(r) \end{array} \right) \Big|_{0,\infty} = 0.$$

It is further assumed that $l_i(r)$, $s_i(r)$, $dl_i(r)/dr$, and $ds_i(r)/dr$ are continuous (from $r = 0_+$ on). Following from these assumptions and integration by parts, the functions $l_i(r)$ and $s_i(r)$ can be seen to satisfy

$$\int_0^\infty l_i(r) \frac{ds_j(r)}{dr} dr + \int_0^\infty \frac{dl_i(r)}{dr} s_j(r) dr = l_i(r) s_j(r) \Big|_0^\infty = 0. \quad (\text{F.8})$$

Furthermore, it is assumed that the basis functions $\{l_i(r), s_i(r)\}$ are linearly independent.

The action associated with the “trial function” $\{G(r), F(r)\}$ of Eq. (F.7) is

$$S = \frac{1}{2} \sum_{i=1}^{2n} \sum_{j=1}^{2n} p_i p_j (D + V + M - \varepsilon N)_{ij},$$

where D , V , M , and N are real $2n \times 2n$ matrices with elements⁵

$$\begin{aligned} D_{ij} &= c \int_0^\infty l_i(r) \left[\frac{d}{dr} - \frac{\kappa}{r} \right] s_j(r) dr - c \int_0^\infty s_i(r) \left[\frac{d}{dr} + \frac{\kappa}{r} \right] l_j(r) dr, \\ V_{ij} &= \int_0^\infty v(r) [l_i(r)l_j(r) + s_i(r)s_j(r)] dr, \\ M_{ij} &= c^2 \int_0^\infty [l_i(r)l_j(r) - s_i(r)s_j(r)] dr, \\ N_{ij} &= \int_0^\infty [l_i(r)l_j(r) + s_i(r)s_j(r)] dr. \end{aligned}$$

With Eq. (F.8) it can be seen that D is a symmetric matrix—i.e., $D_{ji} = D_{ij}$. It is plain to see that V , M , and N are also symmetric. Furthermore, as the basis functions are assumed to be linearly independent, the matrix N is non-singular and the inverse matrix N^{-1} exists (and is symmetric as well). Note that if orthonormal basis functions are chosen, N is simply the $2n \times 2n$ identity matrix; this is by no means a requirement though.

The next step in the finite basis set approach is to seek an extremum of S with respect to small variations in the expansion coefficients; mathematically this is done

⁵It should be noted that the DHF potential $v_{\text{DHF}}(r)$ is a non-local potential and cannot be written as simple function of r . Thus $(V_{\text{DHF}})_{ij} = \int_0^\infty v_{\text{DHF}}(r) [l_i(r)l_j(r) + s_i(r)s_j(r)] dr$ would really be an improper representation of the matrix element. A more appropriate representation would be

$$(V_{\text{DHF}})_{ij} = \int_0^\infty (l_i(r) \ s_i(r)) v_{\text{DHF}}(r) \begin{pmatrix} l_j(r) \\ s_j(r) \end{pmatrix} dr.$$

It is also noted that the potential $v_{\text{DHF}}(r)$ must be known; it is typically found by solving DHF equation by means of a finite difference method. One may then question the need for a finite basis set solution; this is discussed in Section F.4.

by demanding $dS/dp_k = 0$ for all $k = 1, \dots, 2n$. Explicitly, this requirement is

$$\begin{aligned} \frac{dS}{dp_k} &= \frac{1}{2} \sum_{i=1}^{2n} \sum_{j=1}^{2n} (p_i \delta_{kj} + p_j \delta_{ki}) (D + V + M - \varepsilon N)_{ij} \\ &= \sum_{j=1}^{2n} p_j (D + V + M - \varepsilon N)_{kj} = 0. \end{aligned}$$

As this last relation must hold for all $k = 1, \dots, 2n$, one is free to multiply by $(N^{-1})_{ik}$ and sum over k . With the additional matrix definition $H = N^{-1}(D + V + M)$, the requirement that $dS/dp_k = 0$ for all $k = 1, \dots, 2n$ can now be written as a standard matrix eigenvalue equation

$$H\bar{p} = \varepsilon\bar{p},$$

where the eigenvector \bar{p} is the column matrix containing the expansion coefficients, $\bar{p} = \{p_1, p_2, \dots, p_{2n}\}$. As H is a $2n \times 2n$ matrix, there will be $2n$ eigenvectors \bar{p} (which may be chosen orthonormal) with $2n$ associated eigenvalues ε .

In practice, one chooses appropriate basis functions to compose the finite basis set, calculates the matrix elements of D , V , M , and N , and then solves the eigenvalue equation to obtain the $2n$ eigenvalues and eigenvectors.

F.3 B-spline Basis Sets for the Radial Dirac Wavefunctions

With the exception of a few basic mathematical requirements, the basis functions $\{l_i(r), s_i(r)\}$ of the previous section were kept completely general. Basis functions composed of B-splines have proven to be a numerically effective choice for the atomic relativistic many-body problem and will be discussed here.

Consider the B-spline set of order $k \geq 3$ with knot sequence

$$\begin{aligned} t_1 &= \cdots = t_k = 0, \\ t_k &< t_{k+1} < \cdots < t_{n-1} < t_n, \\ t_{n+1} &= \cdots = t_{n+k} = R. \end{aligned}$$

The basis functions $\{l_i(r), s_i(r)\}$ may be built up from this B-spline set as

$$\begin{pmatrix} l_i(r) \\ s_i(r) \end{pmatrix} = \begin{cases} \begin{pmatrix} B_i(r) \\ 0 \end{pmatrix} & \text{for } 1 \leq i \leq n \\ \begin{pmatrix} 0 \\ B_{i-n}(r) \end{pmatrix} & \text{for } n+1 \leq i \leq 2n \end{cases}. \quad (\text{F.9})$$

Not all of the the basis functions here satisfy the assumptions made in the previous section. Strictly speaking, one should omit basis functions $\{l_i(r), s_i(r)\}$ with $i = 1, n+1$ (the first B-spline is non-zero at $r = 0$) and $i = n, 2n$ (the last B-spline is not continuous at $r = R$). It will temporarily be assumed that these basis functions have been properly omitted.⁶

All of the B-splines are zero for $r > R$. Thus, this choice of basis set can be regarded as an implementation of a variational constraint appropriate to the boundary condition

$$G(r)|_R = F(r)|_R = 0.$$

⁶Being even more strict, the basis functions with $i = n-1, 2n-1$ should also be omitted as the second to last B-spline has a discontinuous derivative at $r = R$. However if one is to follow the interpretation that there is an infinite potential wall at $r = R$ (as discussed in the following paragraph), then such a discontinuity in the derivative is allowed. Mathematically, the integrals should then be taken to have upper limit R_- in place of ∞ .

This boundary condition is fitting for a potential $v(r)$ which is infinite for $r > R$. Thus one may speak of the finite basis set solutions as (approximate) solutions for an electron (or atom) confined to a cavity of radius R . Evidently for the a finite basis set solution to resemble an actual solution for the unconfined electron, a sufficiently large radius R must chosen.

It is well-known that a variational finite basis set method applied to the Schrödinger equation (i.e., the Rayleigh-Ritz method) yields eigenvalues that are bounded from below by the lowest exact eigenvalue solutions (see, e.g., Ref. [53]). Subsequently adding more basis functions (i.e., making the basis set more complete), can only cause the eigenvalues to decrease in value (and, hence, become closer to the exact value). In stark contrast to the Schrödinger equation, the Dirac equation allows a continuum of negative-energy eigenvalue solutions ($\varepsilon < -c^2$) corresponding to positron states. It would be detrimental to the current relativistic variational method if the eigenvalues approached the lowest exact eigenvalue (i.e., $\varepsilon \rightarrow -\infty$). Fortunately, this is not the case, and the B-spline basis set (Eq. (F.9)) returns n negative energy eigenvalues (with $\varepsilon \sim -c^2$) and n positive energy eigenvalues (with $\varepsilon \sim c^2$).⁷ The positive energy solutions approximate the exact solutions for the electron in the cavity of radius R , as desired.

A peculiarity which arises in the application of the B-spline basis set (Eq. (F.9)) is the appearance of so-called spurious states in the resulting positive energy spectrum.⁸ Spurious states appear as the lowest positive-energy solutions for $\kappa > 0$ angular symmetries. Such solutions do not correspond to any actual physical state

⁷A discussion regarding the bounds of the eigenvalues may be found in Ref. [56].

⁸The appearance of spurious states is not a peculiarity necessarily associated B-splines, but rather with the particular form of the basis set of Eq. (F.9); see Ref. [72].

(generally their radial wavefunctions oscillate “wildly”). One may choose to simply ignore such solutions—i.e., to throw these spurious states away. An alternative method of handling this problem is to include the improper basis functions (i.e., the ones with $i = 1, n + 1$ and $i = n, 2n$) and instead enforce the boundary conditions by supplementing the action S with a boundary term S_{bound} [35].⁹ This method effectively “pushes” the spurious states to the end of the spectrum where they are then essentially unnoticed. (This is the method used for the numerical evaluations presented in Chapters 4 and 5.) A third, more robust method, is to employ the so-called dual kinetic balance B-spline basis set [72, 8]. This method replaces the zeros in Eq. (F.9) with small “kinetically balanced” functions (such that $s_i(r) \sim l_i(r)/2c$ or $l_i(r) \sim s_i(r)/2c$). The resulting spectrum is then completely devoid of spurious states.

F.4 Quasi-Completeness of the B-spline Basis Sets

To exemplify the utility of the B-spline basis set it is useful to consider, as in Section E.8, the specific example of the static Stark effect. Here the ground state of the hydrogen atom will be considered, although the arguments of this section apply equally well to the many-body systems. The second-order energy shift is given by¹⁰

$$\delta E_{1s_{1/2}}^{(2)} = \mathcal{E}^2 \sum_{i\kappa} \frac{\langle \phi_{1s_{1/2}} | z | \phi_{i\kappa} \rangle \langle \phi_{i\kappa} | z | \phi_{1s_{1/2}} \rangle}{\varepsilon_{1s_{1/2}} - \varepsilon_{i\kappa}}, \quad (\text{F.10})$$

⁹ S_{bound} , numerically speaking, serves more as an encouragement for the boundary conditions than an enforcement. Furthermore, this method actually relies on numerical inaccuracies in the evaluation of the matrix elements $D_{1,1}$ and $D_{n+1,n+1}$, as these matrix elements are not actually finite; see Ref. [8].

¹⁰Here i is used to represent the radial quantum number $i = n - l_\kappa$, where n is the principal quantum number (for the numerable bound states). Note that the lower limit on i is always 1. It should also be noted that the angular quantum number m is suppressed in Eq. (F.10) for clarity.

where the electric field has been taken in the z -direction. A fundamental tool used in the derivation of the second-order perturbation expression is the closure relation

$$\sum_{i\kappa} |\phi_{i\kappa}\rangle \langle \phi_{i\kappa}| = 1.$$

This closure relation expresses the fact that the states $|\phi_{i\kappa}\rangle$ (the true eigenstates of the Hamiltonian) form a complete basis set. This basis set includes the bound states associated with energies $\varepsilon < c^2$ (these are infinite in number given atomic potentials) as well as the innumerable continuum states associated with energies $\varepsilon \geq c^2$. In principle, a numerical evaluation of Eq. (F.10) involves calculating the matrix elements and performing a direct summation over the entire basis. In several applications of perturbation theory, the majority of the entire summation is accounted for by only a handful of terms and a truncation of the summation at the lowest few bound states does not concede much in terms of accuracy. For other applications, such as the present example, such a truncation omits important effects of the remaining bound and continuous spectrum. In these cases, the direct summation method becomes problematic due to the infinite number of bound and innumerable continuum intermediate states.

With an appropriate choice of parameters, the B-spline basis set is quasi-complete and provides an effective means to overcome this dilemma. With the variational method described above, the B-spline basis set yields n positive energy solutions to the Hamiltonian for each angular symmetry κ (tildes are now used to distinguish the

B-spline basis set solutions from the exact solutions)¹¹

$$|\tilde{\phi}_{i\kappa}\rangle, \quad \tilde{\varepsilon}_{i\kappa} \quad \text{where } i = 1, \dots, n. \quad (\text{F.11})$$

If R is chosen large enough (such that it is effectively infinity) and n is chosen large enough (such that the B-spline basis set is indeed essentially complete), then the lowest positive-energy solutions will closely match the corresponding exact bound state solutions (i.e., $|\tilde{\phi}_{i\kappa}\rangle \simeq |\phi_{i\kappa}\rangle$ and $\tilde{\varepsilon}_{i\kappa} \simeq \varepsilon_{i\kappa}$).¹² Progressing towards the higher-energy end of the spectrum, one notices that the states begin to lose resemblance with the exact states. In particular, the energy spectrum remains quantized and well-separated, even into the region $\tilde{\varepsilon}_{i\kappa} \geq c^2$ (after all, these can be thought of as solutions to the atom in a cavity, which has only bound states).

The states $|\tilde{\phi}_{i\kappa}\rangle$ themselves form a quasi-complete basis set and can be used in Eq. (F.10) in place of the exact eigenstates (likewise the energies $\tilde{\varepsilon}_{i\kappa}$ are to be used in place of the exact energies). Thus, the summation over an innumerable spectrum is replaced with a summation over just n states for each angular symmetry κ ,

$$\delta E_{1s_{1/2}}^{(2)} = \mathcal{E}^2 \sum_{\kappa} \sum_{i=1}^n \frac{\langle \tilde{\phi}_{1s_{1/2}} | z | \tilde{\phi}_{i\kappa} \rangle \langle \tilde{\phi}_{i\kappa} | z | \tilde{\phi}_{1s_{1/2}} \rangle}{\tilde{\varepsilon}_{1s_{1/2}} - \tilde{\varepsilon}_{i\kappa}}.$$

In this particular case, the summation over κ is limited by angular and parity selection rules to only $\kappa = 1, -2$ symmetries (i.e., $p_{1/2,3/2}$); in the general case, however, it is often necessary to truncate κ appropriately. As the Dirac equation is angularly-

¹¹There may be less than n positive energy solutions if the first and last B-splines are omitted from the set and if a spurious state is thrown out as described in the previous section.

¹²The particular choice of knot sequence also has a significant impact on the efficiency of the B-spline basis set. In particular, the knots are usually “bunched” up nearer to the origin as this is where the radial wavefunctions (of the lowest energy states) oscillate the most.

decoupled, a different B-spline basis set may be employed for each κ (in particular, n could be different for each κ).

Thus, the true power of the B-spline basis set is that it is capable of providing an accurate representation of the true low-energy bound spectrum (eigenstates as well as energies) with a one-to-one correspondence while simultaneously forming a quasi-complete basis set which accounts for the entire true spectrum, both bound and continuous.

Appendix G

The Zeeman Effect and the Quantizing Magnetic Field

G.1 The Zeeman Effect

This appendix considers the Zeeman effect, which describes the perturbation of an atom in a static uniform magnetic field. With the magnetic field assumed to be in the z -direction—i.e., $\mathbf{B} = B\hat{\mathbf{e}}_z$ —this perturbation is given by

$$V_{\text{Zee}} = -\mathbf{B} \cdot (\boldsymbol{\mu} + \mathbf{M}) = -B(\mu_z + M_z),$$

where $\boldsymbol{\mu}$ is the magnetic dipole operator acting in the nuclear subspace (introduced in Chapter 2) and \mathbf{M} is the magnetic dipole operator acting in the electronic subspace. What will be of interest here are the matrix elements of V_{Zee} between the states $|FM\rangle$ of the model space (see Chapter 2; throughout this appendix, the quantum numbers γIJ associated with the model space are explicit only where necessary). Employing

relations from Appendix C, these matrix elements may be written

$$\begin{aligned}
\langle F'M'|V_{Zee}|FM\rangle &= -B(-1)^{F'-M'} \begin{pmatrix} F' & 1 & F \\ -M' & 0 & M \end{pmatrix} \langle F' || (\boldsymbol{\mu} + \mathbf{M}) || F \rangle \\
&= -B(-1)^{F'-M'} \begin{pmatrix} F' & 1 & F \\ -M' & 0 & M \end{pmatrix} \sqrt{(2F'+1)(2F+1)} \\
&\quad \times \left[(-1)^{I+J+F+1} \begin{Bmatrix} F' & 1 & F \\ I & J & I \end{Bmatrix} \langle I || \boldsymbol{\mu} || I \rangle \right. \\
&\quad \left. + (-1)^{I+J+F'+1} \begin{Bmatrix} F' & 1 & F \\ J & I & J \end{Bmatrix} \langle J || \mathbf{M} || J \rangle \right]. \tag{G.1}
\end{aligned}$$

The reduced matrix element $\langle I || \boldsymbol{\mu} || I \rangle$ appearing above was expressed in terms of the nuclear gyromagnetic ratio g_I and the nuclear magneton μ_N ($\mu_N = e\hbar/2m_p c = \alpha/2m_p$) in Eq. (2.4); that expression is repeated here:

$$\langle I || \boldsymbol{\mu} || I \rangle = \sqrt{I(I+1)(2I+1)} g_I \mu_N. \tag{G.2}$$

In a similar spirit, the reduced matrix element $\langle J || \mathbf{M} || J \rangle$ may be expressed in terms of the electronic gyromagnetic ratio g_J and the Bohr magneton μ_B

$$\langle J || \mathbf{M} || J \rangle = -\sqrt{J(J+1)(2J+1)} g_J \mu_B, \tag{G.3}$$

where the difference in sign is conventional.¹ (The Bohr magneton is given by $\mu_B =$

¹Actually, there is some discrepancy between authors in defining the nuclear gyromagnetic ratio g_I . Some include a negative sign or even use the Bohr magneton in favor of nuclear magneton in Eq. (G.2). On the other hand, Eqs. (G.3, G.4) are the accepted relation for the gyromagnetic ratios g_J and g_F .

$e\hbar/2m_e c = \alpha/2$; note that the Bohr magneton is defined with the electron mass in the denominator whereas the nuclear magneton is defined with the proton mass in the denominator.) The *diagonal* reduced matrix elements $\langle F || (\boldsymbol{\mu} + \mathbf{M}) || F \rangle$ can also be given an appropriate expression in terms of gyromagnetic ratio g_F and μ_B

$$\langle F || (\boldsymbol{\mu} + \mathbf{M}) || F \rangle = -\sqrt{F(F+1)(2F+1)}g_F\mu_B. \quad (\text{G.4})$$

From the expressions above, it can be seen that g_F can be written in terms of g_I and g_J as

$$g_F = (-1)^{I+J+F} \sqrt{\frac{(2F+1)}{F(F+1)}} \left[\left\{ \begin{matrix} F & 1 & F \\ I & J & I \end{matrix} \right\} \sqrt{I(I+1)(2I+1)}g_I \left(\frac{\mu_N}{\mu_B} \right) - \left\{ \begin{matrix} F & 1 & F \\ J & I & J \end{matrix} \right\} \sqrt{J(J+1)(2J+1)}g_J \right].$$

Evaluation of the 6- j symbols here give the simplified result

$$g_F = -\frac{F(F+1) + I(I+1) - J(J+1)}{2F(F+1)}g_I \left(\frac{\mu_N}{\mu_B} \right) + \frac{F(F+1) + J(J+1) - I(I+1)}{2F(F+1)}g_J \quad (\text{G.5})$$

It is found that the diagonal matrix elements can be expressed as

$$\langle FM | V_{Zee} | FM \rangle = Bg_F\mu_B M.$$

It may also be noted that if the Zeeman interaction V_{Zee} is only to be considered within the model space (in which case it is defined completely by the matrix elements

of Eq. (G.1)), then the V_{Zee} may be written²

$$V_{Zee} = -g_I\mu_N\mathbf{I} \cdot \mathbf{B} + g_J\mu_B\mathbf{J} \cdot \mathbf{B}.$$

The factor μ_N/μ_B appearing in Eq. (G.5) is equivalent to the electron-to-proton mass ratio, $\mu_N/\mu_B = m_e/m_p \sim 10^{-4}$. Thus the contribution from the nuclear magnetic dipole moment is highly suppressed compared to the contribution from the electronic magnetic dipole moment. Furthermore, if the states $|FM\rangle$ are approximately eigenfunctions of L^2 and S^2 , then in the non-relativistic limit (in which $\mathbf{M} \rightarrow -\alpha/2(\mathbf{L} + 2\mathbf{S})$) g_J takes the simple form

$$g_J = 1 + \frac{J(J+1) - L(L+1) + S(S+1)}{2J(J+1)}.$$

In particular, for a state with ${}^2S_{1/2}$ symmetry ($L = 0, S = 1/2, J = 1/2$) $g_J = 2$, and for a state with ${}^2P_{1/2}$ symmetry ($L = 1, S = 1/2, J = 1/2$) $g_J = 2/3$.

As $\boldsymbol{\mu}$ and \mathbf{M} are spherical tensor (vector) operators, the z -component of each, and therefore V_{Zee} as well, commute with F_z . As a consequence, the matrix elements $\langle F'M'|V_{Zee}|FM\rangle$ are diagonal in the M quantum numbers; this is ensured by the selection rule $-M' + M = 0$ associated with the 3- j symbol of Eq. (G.1). However,

²This follows from the Wigner-Eckart theorem specific to vectors, in which one may find that (here \mathbf{M} may represent *any* vector operator acting in the \mathbf{J} -space)

$$\langle JM'_J|\mathbf{M}|JM_J\rangle = \frac{\langle J||\mathbf{M}||J\rangle}{\sqrt{J(J+1)(2J+1)}}\langle JM'_J|\mathbf{J}|JM_J\rangle.$$

If one is only interested in matrix elements which are also diagonal in F , then V_{Zee} may further be written $V_{Zee} = g_F\mu_B\mathbf{F} \cdot \mathbf{B}$. With this, it is noted that the factors appearing in Eq. (G.5) may be regarded as arising from the operators

$$\frac{F^2 + I^2 - J^2}{2F^2} = \frac{\mathbf{I} \cdot \mathbf{F}}{F^2}, \quad \frac{F^2 + J^2 - I^2}{2F^2} = \frac{\mathbf{J} \cdot \mathbf{F}}{F^2},$$

which qualitatively represent the projections of \mathbf{I} and \mathbf{J} onto the axis of \mathbf{F} .

V_{Zee} does not commute with F^2 , and therefore $\langle F'M|V_{\text{Zee}}|FM\rangle$ are generally non-zero for $F' \neq F$. An order-of-magnitude estimate of the matrix elements is given by

$$|\langle F'M'|V_{\text{Zee}}|FM\rangle| \sim B\mu_{\text{B}}\delta_{M'M}.$$

G.2 The Quantizing Magnetic Field

In Chapter 2 it was argued that, due to the fact that \mathbf{F} commutes with V_{hfi} as well as H_{elec} , the states $|FM\rangle$ spanning the degenerate model space represent the good zeroth order states to be used in the perturbative analysis. However, in the presence of the plane electromagnetic wave (V_{E1}), the total Hamiltonian $H = H_{\text{elec}} + V_{\text{hfi}} + V_{E1}$ no longer commutes with \mathbf{F} ; this is evident by the appearance of geometrical parameters θ_k and θ_p (as well as associated axial and tensor polarizabilities) in Eq. (3.22), which indicate a dependence of the system on a particular orientation in space. If the perturbation due to the electromagnetic wave is much smaller than the perturbation due to the hyperfine interaction ($V_{\text{hfi}} \gg V_{E1}$), then F is approximately a good quantum number. However, as V_{hfi} itself does not split the degeneracy in the M substates, M in general does not remain a good quantum number the presence of V_{E1} . In practice, however, an external uniform magnetic field may be applied in the z -direction to effectively ensure that M may indeed be treated as a good quantum number. The perturbation associated with this magnetic field, V_{Zee} , is an intermediate perturbation ($V_{\text{hfi}} \gg V_{\text{Zee}} \gg V_{E1}$) such that F still remains a good quantum number. As in the previous section, it is assumed that the magnetic field is in the z -direction.

In the absence of the magnetic field and the plane electromagnetic wave, the degenerate energy level E is split by the hyperfine interaction into distinct hyperfine levels $E + [\delta E_F]_{\text{hfi}}$ given by the quantum number F , with each F -level being $(2F + 1)$ -

fold degenerate. Turning on the static magnetic field lifts this degeneracy, and the subsequent level shifts may be taken as perturbations on top of the hyperfine levels. As $[F_z, V_{Zee}] = 0$, the states $|FM\rangle$ are taken as the good states, and the leading effects are given by the usual first and second order perturbation expressions³

$$[\delta E_{FM}]_{Zee} = \langle FM|V_{Zee}|FM\rangle + \sum_{F' \neq F} \frac{\langle FM|V_{Zee}|F'M\rangle \langle F'M|V_{Zee}|FM\rangle}{[\delta E_F]_{\text{hfi}} - [\delta E_{F'}]_{\text{hfi}}},$$

where, for the second order effect, only dominant terms involving the relatively small hyperfine energy intervals in the denominator are considered. The first order term here is given by Eq. (G.4), namely

$$\langle FM|V_{Zee}|FM\rangle = Bg_F\mu_B M.$$

The second order terms incorporate “mixing” of the various hyperfine levels, and therefore effectively give the degree to which F remains a good quantum number. The degree of this mixing can be estimated by $B\mu_B/|A_{\text{hfi}}|$, where A_{hfi} is the hyperfine structure constant giving the scale of the hyperfine energy splittings. If $B\mu_B/|A_{\text{hfi}}| \ll 1$, then F may be treated as a good quantum number.

In a similar fashion, the effect of the plane electromagnetic wave can then be taken as a perturbation on top of the Zeeman-split hyperfine levels. The lowest order

³There is a subtlety here. For this perturbation expression the “zeroth” order energies (appearing in the denominator) are taken as the hyperfine-shifted energies, whereas the zeroth order states (appearing in the numerator) are the unperturbed states (i.e., *not* the true hyperfine states). For the estimates of this section, this inconsistency is acceptable; the perturbation formalism of Chapter 3, however, is more consistent.

expressions are

$$[\delta E_{FM}]_{E1} = \langle FM|H^{(0,2)}|FM\rangle + \sum_{M' \neq M} \frac{\langle FM|H^{(0,2)}|FM'\rangle \langle FM'|H^{(0,2)}|FM\rangle}{[\delta E_{FM}]_{\text{Zee}} - [\delta E_{FM'}]_{\text{Zee}}}, \quad (\text{G.6})$$

where only dominant terms which include the small Zeeman energy intervals in the denominator are considered. The operator $H^{(0,2)}$ is defined by Eq. (3.7) and has matrix elements given by Eq. (3.9). In a similar fashion as for quantum number F above, the second term here can be used to gauge the degree to which M remains a good quantum number. In particular, if $\mathcal{E}^2 |\alpha_F^{\text{a},\text{T}}| / B\mu_{\text{B}} \ll 1$, then M remains a good quantum number. Note that the scalar polarizability is not considered in this ratio, as the scalar part does not mix states of different M -quantum numbers.